Imp, a key regulator of transposable elements, cell growth, and differentiation genes during embryogenesis

Paula Vazquez-Pianzola[1,6], Dirk Beuchle[1], Peter M'Angale [2], Gimena Alegre[2], Greco Hernández [3, 4], Simon L. Bullock[5], Travis Thomson[2,6] and Beat Suter[1, 6]

1) Institute of Cell Biology, University of Bern, 3012 Bern, Switzerland.
2) Department of Neurobiology, University of Massachusetts Chan Medical School, Worcester, Massachusetts, United States of America.
3) mRNA and Cancer Laboratory, Instituto Nacional de Cancerología (INCan; National Institute of Cancer). Mexico City 14080, Mexico.
4) Tecnologico de Monterrey, Escuela de Medicina y Ciencias de la Salud. Mexico.
5) Division of Cell Biology, MRC Laboratory of Molecular Biology, Cambridge, UK.
6) Communicating authors

ABSTRACT

Imps are a highly conserved family of RNA-binding proteins involved in embryonic development, cancer progression, and neurogenesis. However, the molecular pathways and RNAs regulated by Imp to control these processes remain poorly understood. Embryos derived from *Imp* mutant germline clones arrest development, and transcriptome analysis revealed significant dysregulation of genes involved in cell growth, differentiation, tube morphogenesis, neuronal projection development, and RNA metabolism, along with de-repression of transposable element (TE) RNAs. Consistent with these findings, *Imp* mutant embryos display TE-overexpression phenotypes, are smaller in size, and exhibit defective organ development, including impaired tracheal branching and gastrulation. Reduced levels of Imp at the larval neuromuscular junction (NMJ) impair synaptic bouton formation and decrease adult longevity. RIP-seq experiments showed that Imp-associated RNAs are enriched for TE RNAs. Proteomic analyses confirmed that several TE-encoded proteins are upregulated in *Imp* mutant embryos. Specifically, the Ty1 family retrotransposon *Copia* was derepressed. Consistent with recent findings that *Copia* is a potent inhibitor of synaptogenesis, its upregulation likely contributes to the impaired NMJ formation and broader embryonic defects observed in *Imp* mutants. Moreover, Imp associates with piRNA pathway proteins, ensures Piwi nuclear localization, and—like *piwi* mutants—its loss disrupts TE silencing and causes position-effect variegation (PEV) defects. The analysis of Imp complexes further points to potential mechanisms by which Imp may regulate TE expression. Overall, these results indicate that Imp maintains genome

stability and ensures proper developmental progression and neuronal activity by regulating post-transcriptional processes and suppressing transposons.

INTRODUCTION

Imps (IGF2 mRNA-binding proteins), originally named for their ability to bind insulin-like growth factor 2 (IGF2) mRNA, are a family of highly conserved RNA-binding proteins known to regulate a broad set of transcripts involved in development and disease. Roles in RNA localization, translation, and stability of specific RNAs have been described for the different Imp orthologs (Degrauwe et al., 2016; Vazquez-Pianzola and Suter, 2012). Mammals express three Imp paralogs (Imp1-3) and *Drosophila* codes for only one *Imp* gene, which is more closely related to Imp1 (Vazquez-Pianzola and Suter, 2012). The expression pattern of the mammalian Imp1 and Imp3 paralogs is oncofetal, whereas Imp2 expression persists in some normal adult tissues. Imp1 and Imp3 are also overexpressed in several cancer types (Degrauwe et al., 2016; Mancarella and Scotlandi, 2020). Like mammalian orthologs, *Drosophila Imp* is expressed throughout embryogenesis and has also been implicated in cancer progression, where it is required to sustain neuroblast tumor growth (Narbonne-Reveau et al., 2016; Nielsen et al., 2000).

The embryonic expression of Imp protein paralogs correlates with their essential role during embryogenesis (Xu et al., 2022). In zebrafish, depletion of maternal Imp3 destabilizes maternal mRNAs before the maternal-to-zygotic transition (MZT), leading to abnormal cytoskeletal organization, cell cycle defects, and impaired embryonic development(Ren et al., 2020). Conversely, overexpression of Imp3 inhibits MZT, resulting in developmental delay (Ren et al., 2020). In mice, depletion of Imp2 also causes early embryonic arrest by targeting CCAR1 and RPS14, and by stabilizing IGF2 mRNA during zygotic genome activation (ZGA) (Liu et al., 2019; Xu et al., 2022). A similar effect on IGF2 regulation has been reported in human embryos. Loss of *Imp1* in mice causes dwarfism and impaired gut development, with only 50% of the *Imp1* mutant progeny reaching the third day of life (Hansen et al., 2004). Mutant mice are 40% smaller than the wild type, with most organs hypoplastic. Vg1 RBP, the *Xenopus* ortholog, is essential for cell migration in early neural development and for maintaining epithelial integrity (Shoshkes et al., 2015; Yaniv et al., 2003). *Drosophila Imp* is also an essential gene during embryogenesis (Boylan et al., 2008; Munro et al., 2006). Females lacking maternal *Imp* exhibit normal ovarian development; however, they produce non-viable

embryos, with the majority dying during early development and only a few surviving until late larval or early pupal stages (Boylan et al., 2008; Munro et al., 2006).

Imp protein orthologs have essential roles in RNA metabolism, principally in the transport and local translation of specific RNAs. *Xenopus* Imp (also referred to as Vg1RBP or Vera) binds *Vg1* mRNA and localizes with it to the vegetal pole of *Xenopus* oocytes during maturation (Deshler et al., 1998; Havin et al., 1998). Vg1RBP and chicken Imp1, also known as zipcode-binding protein 1 (ZBP-1), are required for the localization and translational repression of β-actin mRNA during its transport to the leading edge of motile fibroblasts and neurons (Hüttelmaier et al., 2005; Oleynikov and Singer, 2003; Yaniv et al., 2003). Proper localization of β-actin mRNA supports axon guidance, dendritic branching, and growth in developing neurons (Buxbaum et al., 2014; Lepelletier et al., 2017; Leung et al., 2006; Sasaki et al., 2010). In *Drosophila* brains, Imp assembles into neuronal RNP granules that include *Profilin* mRNA, which encodes an actin regulator (Medioni et al., 2014). The prion-like domain (PLD) of Imp, a motif associated with the neurodegenerative progression of other neuronal RNA-binding proteins, is essential for the developmentally regulated localization of Imp RNP granules to axons and for Imp's role in axon remodeling (Vijayakumar et al., 2019). *Drosophila* Imp also binds RNAs critical for embryonic patterning, such as *osk* and *grk*. However, although these sequences are essential for the localization of these RNAs in oocytes and embryos, their localization and translation are unaffected in *Imp* mutant ovaries and early embryos (Boylan et al., 2008; Munro et al., 2006). These and other mRNAs essential for oocyte determination, differentiation, establishment of anterior-posterior, dorsal-ventral and apical-basal polarity are transported by a general RNA transport machinery in *Drosophila.* This machinery includes Bicaudal-D (BicD) and the RNA-binding protein Egalitarian (Egl), which interact with cytoplasmic microtubule motors—Dynein and Dynactin—to move mRNA cargo along microtubules to distinct cellular compartments (Bullock and Ish-Horowicz, 2001; Dienstbier et al., 2009; Vazquez-Pianzola et al., 2017).

The role of Imp, if any, within the BicD/Egl/Dynein localization machinery has not been investigated. Moreover, the molecular mechanisms underlying the essential maternal function of *Imp* in embryonic development, as well as the regulatory networks in which Imp operates, remain unclear. Imp RNA targets have been systematically identified in larval brains, cultured cells, and in other biological systems (Hansen et al., 2004; Hansen et al., 2015; Lee et al., 2025). However, the embryonic RNA targets regulated by *Imp* in *Drosophila*, and particularly those that could explain the developmental arrest observed in embryos lacking maternal Imp, have yet to be comprehensively defined.

104 In this study, we identify RNAs bound by Imp and characterize the transcriptomic and
105 proteomic differences between wild-type and *Imp* mutant embryos. We show that loss of
106 maternal *Imp* leads to widespread gene dysregulation, affecting genes involved in growth,
107 differentiation, morphogenesis, and RNA metabolism. Notably, *Imp* mutant embryos exhibit
108 strong de-repression of transposable element (TE) RNAs and proteins, particularly those of the
109 Ty1/Copia retrotransposon family, which are known to impair synaptogenesis. These embryos
110 are smaller in size, display defective gastrulation and tracheal development. Furthermore,
111 larvae with reduced Imp levels at the neuromuscular junction (NMJ) show impaired synaptic
112 bouton formation and a reduced adult lifespan. All these phenotypes are consistent with known
113 consequences of TE misregulation. Mechanistically, Imp binds TE transcripts, interacts with
114 components of the piRNA pathway, and is required for the nuclear localization of Piwi.
115 Furthermore, *Imp* mutants exhibit defects in position-effect variegation (PEV), linking Imp to
116 the regulation of heterochromatin and transposon silencing. Together, these findings suggest
117 that Imp safeguards genome integrity and supports normal developmental progression by
118 coordinating post-transcriptional regulation and transposon repression.

119

120 **RESULTS**

121

122 ***Drosophila* Imp makes a complex with the BicD/dynein transport machinery**

123 Previous mass spectrometry analyses identified Imp in BicD immunoprecipitates (Vazquez-
124 Pianzola et al., 2011, reproduced in Fig. S1A). The presence of Imp in BicD/Egl complexes
125 was further confirmed by reverse immunoprecipitation experiments (Fig. 1A). Antibodies
126 targeting GFP co-immunoprecipitated Imp-GFP along with BicD, Egl and poly-A binding
127 protein (PABP), in Imp-GFP^{G080} embryo extracts expressing a functional Imp-GFP trap protein
128 (Fig. 1A, Fig. S2). Imp was also specifically pulled down using anti-GFP antibodies from
129 extracts expressing Egl::GFP (Fig. 1A). These findings show that Imp is a constituent of the
130 BicD/Egl complex. Antibodies targeting BicD co-immunoprecipitated Imp, Egl and PABP.
131 Treatment with RNase reduced the BicD/Imp interaction by 84 % (Fig. S1B, Vazquez-Pianzola
132 et al., 2011). The Egl/BicD interaction was not affected, as expected for a known direct
133 interaction between these two proteins (Fig. S1B, (Dienstbier et al., 2009; Vazquez-Pianzola et
134 al., 2011). This suggests that the presence of Imp in the BicD-RNP is at least in part dependent
135 on or stabilized by the associated RNAs. To test for additional direct interaction between BicD

136 and Imp, we performed a yeast two-hybrid assay. We observed a weak but consistent direct
137 interaction between the carboxy terminus of BicD and Imp proteins (Fig. 1B).
138
139 **Identification of novel Imp interactors**
140 To identify novel proteins that associate with Imp that could give us an insight into the essential
141 roles of maternal IMP during embryo development, we conducted immunoprecipitation (IP)
142 experiments using embryo extracts expressing the Imp-GFP^{G080} trap protein followed by mass
143 spectrometry analysis (Morin et al., 2001). As a mock control for the immunoprecipitation
144 experiments, we generated a mutant version of the functional *Imp-GFP*^{G080} chromosome, using
145 a CRISPR-Cas9 mutagenesis screen. The selected mutant chromosome has an 8-nucleotide
146 deletion after the GFP insertion site, leading to a frameshift in the open reading and the
147 introduction of a premature stop codon (Fig. S2, see methods). This results in the production
148 of the fusion protein Imp$^{1-31}$ -GFP- Imp$^{32-95}$- XX^{18aa}- Stop protein expressed under the same
149 regulatory domains as the *Imp-GFP*^{G080} line (Fig. S2B). This mutant allele is lethal in flies. We
150 refer to this fly line as *Imp-GFP*^{Stop} and use it as a mock control for the immunoprecipitations
151 (Fig. S2A,B). Thus, extracts from embryos expressing either Imp-GFP^{G080}, Imp-GFP^{Stop}, or
152 wild-type embryos were subjected to immunoprecipitation (IP) with anti-GFP antibodies
153 followed by mass spectrometry analysis of the immunoprecipitated material (Fig. S3, raw data
154 in Tables S1-2).
155 The IPs were performed in the presence and absence of RNase A to identify factors that
156 bind independently of the presence of RNA in the complex. Fig. S3 shows the top 100
157 interactors, and Tables S1-2 show the raw data. Gene Ontology (GO) analyses of the identified
158 Imp interactors revealed enrichment of proteins involved in several RNA metabolic pathways,
159 including RNA localization, translation, gene expression regulation by silencing, and splicing
160 (Fig. 1C, Fig. S4A). Proteins involved in oogenesis, regionalization, and cell maturation,
161 processes that also depend on RNA localization, translational control, and tight regulation of
162 gene expression, were also enriched among the GO terms associated with Imp interactors (Fig.
163 1C, Fig. S4A). The top 100 interactors include many RNA-binding proteins, and their
164 association with Imp was affected by RNase treatment, suggesting that they may be part of
165 BicD complexes through shared RNA targets (Fig. S3A-C). GO analysis also revealed that
166 interactors whose presence in the Imp complex was reduced by RNase treatment were primarily
167 enriched in RNA metabolic processes (Fig. S4B). Among the top 100 interactors, only the
168 presence of Fmr1 and CG5726 was clearly not reduced in Imp complexes in the presence of
169 RNase, suggesting a direct interaction with Imp (Fig. S3C). CG5726 is the *Drosophila* ortholog

170 of human CTIF, a cap-binding complex-dependent translation initiation factor with no
171 previously described function in *Drosophila*. Fmr1, which displayed slightly increased
172 association with Imp in the presence of RNase, is an RNA-binding protein involved in RNA
173 trafficking, translation, and neuronal excitability. In *Drosophila*, Fmr1 acts as a component of
174 BicD/dynein transport complexes in neurons (Bianco et al., 2010), and its loss in humans
175 causes the Fragile X syndrome.
176 Notably, several other BicD-interacting proteins, including Egl, Fmr1, PABP, Dhc,
177 alongside the proteins involved in RNA localization in oogenesis, Stau and Sqd, were enriched
178 in the Imp-GFP immunoprecipitations compared to the peptides detected in the Imp-GFP^{Stop}
179 immunoprecipitations (Fig. 1D). These results confirm that Imp associates with BicD and
180 BicD-associated proteins involved in RNA transport. We have previously shown that aside
181 from its role in RNA transport, BicD also has a role in meiotic progression through interacting
182 and properly localizing clathrin heavy chain (Chc) to meiotic spindles (Vazquez-Pianzola et
183 al., 2022). Remarkably, Chc showed an enrichment in the presence of RNase in the Imp-GFP
184 pull-downs (Fig. 1D). Furthermore, GO analysis revealed that in the absence of RNA, Imp is
185 associated with factors involved in mitotic and meiotic cell cycle processes, chromosome
186 segregation, spindle organization (Fig. S4C, D). These results further point to novel
187 moonlighting functions of Imp in these processes.
188
189 **Imp is recruited to apically localizing RNAs in blastoderm embryos, but is redundant for**
190 **RNA localization**
191 Imp overexpression during oogenesis affects dorsoventral polarity and the localization of *grk*
192 and *osk* maternal RNAs (Boylan et al., 2008; Geng and Macdonald, 2006). Furthermore, the
193 Imp-binding sequences in *osk* mRNA are required for *osk* RNA anchoring, localization, and
194 translational regulation (Munro et al., 2006). Nevertheless, *Imp* mutant germline clones do not
195 block maternal mRNA localization during oogenesis, indicating a redundant role for Imp in
196 mRNA localization in the ovarian germline (Boylan et al., 2008; Geng and Macdonald, 2006;
197 Munro et al., 2006). Its involvement in the mRNA localization of BicD targets in early
198 embryogenesis was not investigated and could be a potential cause for embryonic lethality. To
199 test if Imp associates with mRNAs that are transported by BicD and Egl in the embryo, we
200 injected a fluorescently labeled variant of the *hairy* (*h*) mRNA *(hSL1x3)*, which contains
201 multiple copies of the Egl-BicD binding site and monitored Imp localization through the
202 fluorescence of the Imp-GFP trap protein or antibodies against Imp. Once injected into the
203 basal side of wild-type blastoderm embryos, these *h* transcripts are transported in a

204 BicD/Egl/dynein-dependent manner to the cytoplasm apical to the nuclei (Bullock and Ish-
205 Horowicz, 2001). Consistent with the presence of Imp in BicD complexes, we found that Imp
206 co-localized with *hSL1x3* and BicD at the apical sites (Fig. 2Aa-b). Like BicD, Imp-GFP is
207 seen apically of the nuclei (Fig. 2Ac) and upon basal injection of localizing RNAs, it
208 hyperaccumulates with the injected RNAs apically of the nuclei (Fig. 2A.c-d, (Bullock and Ish-
209 Horowicz, 2001)). Furthermore, inhibition of Imp activity by pre-injection of anti-Imp
210 antibodies in wild-type embryos, as well as pre-injection of anti-GFP antibodies in Imp-GFP
211 expressing embryos before injection of localizing *h* and *fushi tarazu* (*ftz*) RNAs, disrupted their
212 apical transport (Fig. 2B-C). However, the localization of endogenous *ftz* and *h* RNAs remained
213 unaffected in *Imp* mutant embryos generated by inducing mutant germline clones (GLCs) (Fig.
214 2D, Fig. S5A for information on *Imp* mutant alleles). Nevertheless, the inhibition of apical
215 localization of injected mRNAs by preinjecting anti-Imp and anti-GFP antibodies suggests a
216 mechanism where these antibodies sequester Imp-associated proteins necessary for the
217 formation of a functional ribonucleoprotein transport complex. The finding that Imp interactors
218 were enriched for RNA-binding proteins involved in RNA transport, stability, and translation
219 control supports this notion (Fig. 1C-D, Fig. S3-4).
220 These observations collectively suggest that while Imp–RNP complexes are crucial for
221 proper RNA transport, Imp itself is not an essential component, or adaptation to the loss of Imp
222 begins early in development, indicating functional redundancy of Imp during early stages.
223
224 **Transcriptomes of *Imp* mutant embryos display dysregulation in stem cell versus**
225 **differentiation pathways.**
226 Embryos devoid of maternal *Imp* during early development showed no defects in pair-rule
227 mRNA localization (Fig. 2D). However, cuticle preparations of embryos devoid of maternal
228 Imp (derived from *Imp* germline clones (GLCs)) revealed predominant defects in anterior
229 development, consistent with previous reports (Boylan et al., 2008)(Fig. S5B). These defects
230 resulted in defective dorsal closure and seem to happen during germband retraction or head
231 involution (Fig. S5C).
232 To deepen our understanding of the role of maternal *Imp* throughout embryogenesis,
233 we conducted a detailed RNA transcriptome analysis comparing Imp^{+} embryos (*y w*) with
234 embryos derived from induced germline clones of two distinct *Imp* null mutant alleles, namely
235 Imp^{2} and Imp^{8} (refer to Fig. S5A and the methods for allele descriptions). Our study involved
236 total RNA sequencing of embryos aged 0-4 hours (before visible phenotypes emerged) and 0-

237 8 hours (when defects in germband retraction started to appear) for *Imp* mutants and control
238 *Imp*$^{+}$ embryos. RNA sequencing was performed on biological triplicates. Both *Imp* mutants
239 exhibited similar disparities in gene expression compared to *Imp*$^{+}$ embryos, causing them to
240 cluster together in the heat map of gene plots (Fig. 3, raw differential expression (DE) counts
241 data in Tables S3-S6). Among the top misregulated genes in the absence of *Imp,* we observed
242 a significant prevalence of upregulated genes over downregulated ones, suggesting that Imp
243 primarily functions as a repressor of gene expression (Fig. 3). Additionally, GO analysis of
244 the most differentially expressed genes in 0-4-hour embryos revealed downregulation of genes
245 associated with translation, RNA metabolism, RNA splicing, and cell growth. Whole embryo
246 immunostaining and cuticle preparations revealed that *Imp* embryos are smaller compared to
247 wild-type embryos (Fig. S5B-C), reinforcing the role of *Imp* in embryo growth. Interestingly,
248 this size reduction is reminiscent of the ~40% smaller size observed in *Imp1*-deficient mice,
249 and it indicates a proportional decrease in most organ sizes (Hansen et al., 2004). In contrast,
250 genes linked to morphogenesis, tube morphogenesis, muscle development, differentiation, and
251 negative regulation of cellular biosynthesis and transcription were upregulated (Fig. 4A).
252 Similarly, 0-8-hour embryos displayed upregulation of genes linked to tube morphogenesis and
253 neuronal projection development and abnormally branched trachea, indicative of defects in
254 morphogenesis, particularly during tube formation and branching (Fig. 4C, C'). The roles of
255 *Imp* in activating genes involved in cell growth and repressing genes involved in differentiation
256 suggest that premature differentiation causes the defects in gastrulation and differentiation. *Imp*
257 may thus play a role in coordinating cell numbers with differentiation—potentially by
258 repressing differentiation until normal cell numbers are achieved.
259
260 **Imp associates with mRNAs involved in pathways governing cell growth, cell cycle, stem**
261 **cell regulation, and differentiation.**
262 We then conducted RIP-seq analyses to pinpoint RNAs interacting with Imp particles.
263 Immunopurification of Imp-RNA complexes was performed using *Imp-GFP*^{G080} embryo
264 extracts and anti-GFP antibodies. As a mock control, we also sequenced RNAs
265 immunoprecipitated with anti-GFP antibodies from extracts of embryos expressing the non-
266 functional N-terminal version of Imp fused to GFP (*Imp-GFP*^{Stop}) (Fig. 5; raw data in Table S7;
267 Fig. S2). Additionally, total RNA sequencing was performed on the input extract utilized for
268 the Imp::GFP pulldown as an additional control (Fig. 5A-B; raw data in Table S8). A high
269 overlap was observed for transcripts enriched in the Imp-GFP^{G080} IPs compared to the input
270 RNA control and the same IP compared to the compared to the *Imp-GFP*^{Stop} mock IP control

271 (Venn diagram, Fig. 5A). The heat map illustrating the top RNAs enriched in the Imp::GFP^{G080}
272 IP vs Imp::GFP^{G080} input RNA and the *Imp-GFP^{Stop}* mock IP control show that many of these
273 RNAs encode ribosomal proteins, long non-coding RNAs (lncRNAs) and TE RNAs (Fig. 5B).
274 Further analysis of Imp-associated RNAs (from the genes in the overlap in Fig. 5A) through
275 GO enrichment highlighted terms closely aligned with those RNAs differentially expressed in
276 the *Imp* mutants (Fig. 5C-Fig.4A-B). This included genes linked to translation, RNA splicing,
277 and genes involved in regulation of tube size, the tracheal system and embryonic development.
278

279 **Imp associates with TE mRNAs and represses them**

280 Unexpectedly, in both 0-8- and 0-4-hour-old *Imp* mutant embryos, a substantial increase in
281 RNAs originating from transposable elements (TE) was evident (Fig. 3B-D, raw data in Tables
282 S3-S6). TE RNAs were prominently overrepresented in the *Imp* mutants compared to wild-
283 type controls, and the increase was even more pronounced in the 0-8-hour embryo collections,
284 indicating that TEs were derepressed in the mutant embryos (Fig. 6A). Our standard RNA
285 sequencing pipeline captured this difference in expression, likely due to polymorphisms across
286 various transposon insertions. Subsequent utilization of a specialized RNA sequencing
287 pipeline, targeting transposable element expression, further validated and strengthened the
288 observed transposon de-repression in *Imp* mutant embryos (Fig. 6B, B') (Pogorelcnik et al.,
289 2018). Several transposons were highly upregulated in the *Imp* mutant embryos. Furthermore,
290 the top list of RNAs that co-immunoprecipitated with Imp-GFP^{G080} was also notably enriched
291 with TE RNAs and non-coding RNAs (Fig. 6C). These enrichments are real since the
292 representation of these biotypes was increased only in the list of RNAs enriched in the Imp-
293 GFP^{G080} IP and not in the RNAs not found enriched in the IPs (Fig. 6C). TE RNA sequencing
294 mapping also identified specific TE enriched in the Imp-GFP ^{G080} IPs (Fig. 6D). This correlates
295 with biotypes overrepresented in the RNAs found to be upregulated in *Imp* mutant embryos in
296 the transcriptome analysis (Fig. 6A). Accordingly, a proteomic analysis of 0-4-hour-old
297 embryos unveiled the presence of peptides specific to TE-encoded proteins solely in *Imp*
298 mutant embryos. Peptides corresponding to *roo* elements (|Q8I7Q1), Envelop (Env, Q5K600)
299 protein from the *Tirant* transposon, and the Gag protein (O01350) from the *Burdock*
300 transposable element were specifically detected in *Imp^{8}* and *Imp^{2}* embryos but were absent in
301 their *Imp*$^{+}$ counterparts (Table 1).

302 Staining *Imp* mutant embryos with an antibody against the Gag/pol protein encoded by
303 the Copia transposable element detected distinct signals in specific cells or groups of cells (Fig.
304 7A). Conversely, no or only minimal positive signals were observed in wild-type embryos.

305 Copia^{gag} expression emerged as early as stage 12 of embryogenesis in *Imp* mutants, becoming
306 notably prevalent in yolk cells by stage 14. Western blot analysis confirmed Copia
307 overexpression in *Imp* mutant embryos (Fig. 7B).
308 The observed misregulation of genes involved in the development of neuronal
309 projections, led us to examine the larval neuromuscular junction (NMJ). Knocking down *Imp*
310 at the larval NMJ by expressing *Imp* RNAi under the control of the motor neuron-specific
311 driver C380 reduced the number of synaptic boutons (Fig. 7C, C'). Although these flies survive
312 to adulthood, they show a reduced lifespan, confirming a critical role for *Imp* in neurogenesis
313 and its importance for fly survival (Fig. 7D). We found that this phenotype correlated with
314 increased expression of Copia, which appeared condensed in and around the larval NMJs
315 following *Imp* RNAi knockdown (Fig. 7E-E'). Altogether, this points to a role for Imp in
316 repressing Copia expression at larval synapses and during embryogenesis.
317
318 **Loss of *Imp* neither impairs nuclear export of piRNA precursors nor piRNA production**
319 Because TEs were de-repressed in *Imp* mutants, we investigated whether *Imp* affects the
320 piRNA pathway, the primary defense against transposons. The regulation of transposon
321 families expressed during early development depends on maternally deposited piRNAs and
322 Piwi proteins (Fabry et al., 2021). piRNA precursors, originating from the *Flam* and *42AB* loci,
323 are pivotal in suppressing transposable elements in both the soma and germline of *Drosophila*,
324 particularly targeting retrotransposons like the *gypsy* family, which exhibited heightened
325 expression in *Imp* mutants. Although Imp's orthologs have suggested roles in nuclear RNA
326 export (Oleynikov and Singer, 2003; Pan et al., 2007), we found no evidence indicating that
327 *Imp* is needed for the production or nuclear export of these piRNA precursors (Fig. S6A-B).
328 We further investigated whether *piwi* RNA production was compromised in *Imp* mutant
329 embryos by sequencing the small RNAs in control and *Imp* mutant embryos (Fig. S6C-D). The
330 percentage of total small RNAs mapping to TEs was not affected in embryos devoid of
331 maternal *Imp* (Fig. S6C). Although the levels of piRNAs mapping specifically to some de-
332 repressed TEs were slightly reduced in the *Imp* mutants (Tirant, HET-A, Stalker-2,
333 microcopia), this expected inverse correlation did not generalize to the other TEs de-repressed
334 in *Imp* mutants (such as Copia) (Fig. S6D). We next investigated whether the ping-pong
335 amplification cycle was affected by *Imp* loss by quantifying the fraction of piRNA read pairs
336 with 10-nt 5′ overlaps between sense and antisense reads. Across all samples, we found only a
337 small subset of transposon-mapping piRNAs with such 5' overlaps (Fig. S6E). For these
338 piRNAs, the percentage of sense and antisense pairs with a 10-nt overlap did not differ between

339 wild-type and *Imp* mutant samples. These observations suggest that *Imp* does not influence the
340 ping-pong amplification pathway and piRNA production. However, since the number of piwi
341 RNA reads detected in embryos was very low, they may have masked the role of *Imp* in *piwi*
342 RNA production if it functions earlier during oogenesis.
343
344 **Imp associates with proteins involved in gene silencing.**
345 Finding no effects on piRNAs, we closely examined the proteins present in complex with Imp
346 to learn more about the mechanism of TE regulation by *Imp* in embryos (Fig. S3, Fig. 1C). GO
347 analyses of Imp interactors revealed a strong association with proteins involved in negative
348 regulation of gene expression and gene silencing (Fig. 1C, S3A). Notably, in the Imp-GFP^{G080}
349 immunoprecipitates, several components of the RNA processing machinery involved in mRNA
350 and transposon silencing were enriched (Fig. 8A). Key players in the piRNA production and
351 amplification pathway—such as Piwi, Spn-E, Tdrd3, Hop, Aub, Ago3, and Cbp80—were
352 identified (Fig. 8A).
353 Other factors involved in heterochromatin formation and transposon silencing remained
354 associated with Imp even in the presence of RNase during the immunoprecipitation
355 experiments, namely Fmr1, Top3beta, Tdrd3, Su(var)205/HP1, Aub, and His2A, indicating a
356 direct binding of Imp with some of them, regardless of shared RNA or TE mRNA targets (Fig.
357 8A). However, the pattern of histone H3 lysine 9 trimethylation (H3K9me3) and Hp1
358 localization in *Imp* mutant embryos did not show any clear visible disruption (Fig. S7A).
359
360 **Piwi protein is not properly localized to the nuclei of *Imp* mutant nurse cells**
361 Our proteomic analysis of *Imp* mutants revealed that Piwi, a key regulator protein of TE
362 expression, was upregulated (Table 1). In *Imp* mutants, Piwi appears to be present during
363 embryogenesis and enriched in all blastoderm nuclei from early embryogenesis on (Fig. S7B).
364 Aside from its enrichment inside all blastoderm nuclei, Piwi appeared concentrated in dot-like
365 structures in the heterochromatin. This pattern was not as strong in some *Imp* embryos derived
366 from *Imp* GLCs, but the differences were subtle and below our threshold of detection (Fig.
367 S7B). However, examination of the maternal germline revealed a striking mislocalization of
368 Piwi protein in *Imp* mutant ovaries (Fig. 9A). In wild-type ovaries, Piwi protein localizes to the
369 nuclei of both nurse cells and follicle cells, showing higher expression in the nurse cells
370 compared to a lower signal observed in the follicle cells. In contrast, in most *Imp* mutant egg
371 chambers, Piwi accumulates at lower levels in the nurse cells than in the follicle cells or fails
372 to accumulate at all in the nurse cell nuclei (see Fig. Legend for quantification), while Piwi still

373 showed nuclear localization in the surrounding follicle cells, which retained normal Imp
374 expression (Fig. 9A). The strong phenotype in the germline, compared to the subtle one in
375 embryos, may be because zygotic expression of other factors in the embryo partially
376 compensates for or masks the maternal defect. Localization of Ago1, a regulator of the miRNA
377 pathway, was not affected in *Imp* mutants, consistent with Imp having a specific role in the
378 piRNA pathway independent of the miRNA pathway (Fig. 9B).
379
380 ***Imp* mutants are defective in transcriptional silencing by position-effect variegation**
381 **(PEV)**
382 In *Drosophila,* components of the RNA-induced silencing complex (RISC) and the piRNA
383 pathway, including Piwi, act as heterochromatin regulators and are implicated in Position
384 Effect Variegation (PEV) (Lee et al., 2018). Therefore, we investigated whether Imp functions
385 similarly using a standard PEV assay in the eye, a somatic tissue (Fig. 9C). In this assay, a
386 reporter encoding the *white* gene inserted near heterochromatin (*wm4h*), results in variegated
387 red eyes due to heterochromatin spreading and subsequent transcriptional silencing in some
388 cells but not others. Like *piwi* mutants, females carrying the *wm4h* reporter but displaying
389 reduced Imp levels due to heterozygosity for *Imp* alleles (*Imp7/+*, *ImpH44/+*, or *ImpH149/+*)
390 showed an increased *mini-white* gene expression in their eyes compared to females with normal
391 Imp levels (*Imp* ±/+ background) (Fig. 9C-C', Fig. S8). This suggests that like Piwi, Imp
392 regulates transcriptional silencing by position-effect variegation (PEV).
393
394 **DISCUSSION**
395
396 This study provides insights into the molecular mechanisms by which maternal Imp
397 (IGF2BP) influences early embryonic development in *D. melanogaster*. Females with mutant
398 *Imp* germline clones display normal ovaries, but their embryos do not develop, highlighting
399 the critical role of maternal *Imp* for embryogenesis. Previous research suggested a role for Imp
400 in mRNA localization during oogenesis, though this role appeared redundant (Boylan et al.,
401 2008; Munro et al., 2006). Imp is also involved in neuronal RNP assembly and granule
402 dynamics, regulating axonal remodeling (Vijayakumar et al., 2019). Immunoprecipitation,
403 mass spectrometry, and yeast two-hybrid analyses identified Imp as part of BicD complexes,
404 linking Imp to the BicD/dynein transport machinery in embryo extracts. Notably, BicD
405 interacted with the Imp carboxy terminus which contains the Prion Like Domain (PLD),
406 identified as critical for promoting the motility of axonal Imp granules (Vijayakumar et al.,

407 2019). This domain is also essential for efficient Imp localization to axons and appears to be
408 responsible for recruiting molecular motors. Despite Imp's recruitment to apically localizing
409 RNAs in blastoderm embryos, endogenous mRNA localization remained unaffected in *Imp*
410 mutants. These observations support the notion that germline *Imp* is not essential for the apical
411 localization of these mRNAs, and it might be redundant during *Drosophila* oogenesis and early
412 embryogenesis for RNA transport, a conclusion that was also reached by others (Geng and
413 Macdonald, 2006b; Munro et al., 2006) However, inhibition of Imp by pre-injection of anti-
414 Imp antibodies disrupted the apical transport of injected mRNAs, suggesting that antibodies
415 against Imp may prevent the localization of RNAs by blocking the formation of functional RNP
416 localizing particles containing Imp and Imp-binding proteins. Indeed, Gene Ontology (GO)
417 analysis of the identified Imp interactors showed an enrichment of proteins involved in RNA
418 localization. Imp appears to interact directly with Fmr1, a protein known to associate with BicD
419 (Bianco et al., 2010) and be involved in RNA transport and translational control (Prashad and
420 Gopal, 2021). GO analysis revealed that many Imp interactors, which do not depend on RNA
421 for their interaction, are factors involved in mitotic cell cycle processes, chromosome
422 segregation, spindle organization, and nucleocytoplasmic transport. For example, Chc, a
423 known BicD interactor involved in cell cycle regulation, was associated with Imp when RNA
424 was depleted in the extracts. Remarkably, although the role of the Imp paralogs in
425 nucleocytoplasmic transport has been demonstrated (Hüttelmaier et al., 2005; Oleynikov and
426 Singer, 2003; Pan et al., 2007) their potential moonlighting role in cell cycle regulation requires
427 further investigation.

428 Transcriptome analysis of *Imp* mutant embryos revealed significant dysregulation of genes
429 associated with cell growth, differentiation, and RNA metabolism, along with upregulated TE
430 RNAs. Genes involved in translation, RNA metabolism, RNA splicing, and cell growth were
431 downregulated in *Imp* mutant embryos, suggesting that *Imp* positively regulates the expression
432 or stability of these transcripts. In contrast, genes associated with morphogenesis, tube
433 development, muscle development, neurogenesis, and differentiation were upregulated,
434 indicating that *Imp* normally represses their expression at this stage of embryogenesis. The
435 RNAs present in the purified Imp-RNP complexes displayed similar GO terms. Several of the
436 phenotypes observed in *Imp* mutant embryos—such as smaller size compared to their Imp^+
437 counterparts, defects in tracheal branching, incomplete dorsal closure in embryos, and
438 defective larval NMJ formation—correlate with the role of *Imp* in controlling the expression
439 of genes involved in molecular pathways that regulate stem cell function and differentiation.

440 TE-encoding mRNAs were also detected in Imp-RNP complexes, and both proteomic
441 analysis and immunostaining confirmed the upregulation of TE-encoded proteins in *Imp*
442 mutant embryos. We previously demonstrated that reducing Copia levels at the NMJ increases
443 bouton formation, indicating that *Copia* acts as an inhibitor of synaptic plasticity (M'Angale et
444 al., 2025). *Copia* protein levels are elevated in *Imp* mutant embryos and at the larval NMJ
445 following *Imp* knockdown. Consistent with this upregulation, NMJs with reduced *Imp* levels
446 exhibit fewer boutons compared to wild-type NMJs. Our findings suggest that loss of Imp may
447 impair NMJ plasticity and potentially affect embryo survival through its regulatory role in
448 controlling the expression of Copia and other transposons. It remains to be determined whether
449 reducing *Copia* expression or the expression of other misregulated transposons can rescue the
450 NMJ phenotype or mitigate age-related defects caused by *Imp* loss. We also found that *Profilin*
451 mRNA, a regulator of the actin cytoskeleton and a previously described Imp target, is enriched
452 in Imp-RNP complexes in embryos. In the brain, overexpression of *Profilin* mRNA can rescue
453 the axonal remodeling defects observed in *Imp* mutants (Medioni et al., 2014). Whether
454 *Profilin* mRNA influences axonal growth at the NMJ or interacts with *Copia* remains unclear
455 but represents a highly interesting direction for future investigations.
456 The intricate regulation of TEs encompasses various mechanisms crucial for controlling
457 their activity and preventing genomic instability. The piRNA (Piwi-interacting RNA) pathway
458 is a primary and conserved mechanism governing TE expression in metazoans. In the
459 cytoplasm, Piwi proteins and piRNAs cleave TE transcripts, suppressing their further
460 transcription, expression, and transposition. The piRNA/Piwi machinery also operates within
461 the nucleus, inducing histone H3 lysine 9 trimethylation (H3K9me3), ultimately driving
462 transcriptional silencing of TEs. Several key players in the piRNA pathway—such as Piwi,
463 Spn-E, Tdrd3, Hop, Aub, Ago3, and Cbp80—were enriched in the Imp-RNP complexes. Loss
464 of *Imp* did not impair nuclear RNA export of piRNA precursors in oogenesis, and small RNA
465 sequencing indicated that piRNA levels were not significantly altered in *Imp* mutant embryos,
466 suggesting that *Imp*'s role in TE silencing might involve mechanisms independent of, or
467 downstream from piRNA synthesis. However, we observed a strong effect on Piwi nuclear
468 localization in the nurse cells of *Imp* mutant egg chambers, and Piwi protein was enriched in
469 Imp IPs. Though the strong effect on Piwi localization observed in the absence of *Imp* in the
470 germline contrasts with the lack of strong effects on Piwi localization during embryogenesis,
471 zygotic transcription might mask the role of maternal Imp. Our results suggest that *Imp* may
472 influence transposon silencing independently of piRNA production, potentially by ensuring the

473 proper maternal deposition of Piwi or functional Piwi/piRNA complexes into early eggs, a
474 hypothesis that requires further investigation.

475 The Imp interactions also point to another pathway. A complex comprising *Drosophila*
476 Top3B, Tdrd3, and the RNAi-induced silencing complex (RISC)—housing Ago2, the p68
477 RNA helicase, and Fmr1—selectively associates with specific nascent RNAs featuring
478 intricate tertiary structures. This complex contributes to resolving RNA topological challenges
479 and recruits the heterochromatin components Su(var)3-9 and Su(var)205/HP1 (Lee et al.,
480 2018). Together, they recruit methyltransferases pivotal for heterochromatin formation and
481 transposon silencing. Interestingly, Fmr1, Top3B, Tdrd3, Su(Var)205/HP1, Aub, and His2A
482 were associated with Imp in RNase-treated extracts, indicating direct binding of Imp to
483 components of this transposon silencing complex, regardless of shared RNA or TE mRNA
484 targets.

485 PSI (P-element somatic inhibitor), Hp48 (also known as Hrb27C), Hrp36 (Hrb87F),
486 Hrp38 (Hrb98DE), and PABP were also enriched in Imp complexes. The presence of PSI in
487 Imp complexes was specific, as point mutations in Imp's dual KH domains, which lead to
488 lethality similar to Imp^2, Imp^7, and Imp^8 mutants, also disrupted PSI binding (Fig. 8B). This
489 complex functionally assembles on P-element pre-mRNAs, blocking splicing of the third intron
490 (IVS3), preventing the production of fully spliced transposase mRNA, and the translation into
491 an active transposase (Ghanim et al., 2020; Horan et al., 2015; Siebel et al., 1994; Siebel et al.,
492 1995). This mechanism prevents transposition of P-elements in somatic cells. Recent research
493 has shown that piRNAs regulate P elements and transposable elements, particularly the Gypsy
494 retrovirus-like element, by controlling transposon alternative splicing (Ghanim et al., 2020;
495 Karam Teixeira et al., 2017). This suggests that splicing regulation between P-elements and
496 transposons may share similar mechanisms. An intriguing hypothesis is that Imp/PSI
497 complexes may regulate transposon levels by controlling TE splicing. Moreover, Piwi protein
498 and PSI levels were elevated in *Imp* mutant embryos (Table 1), suggesting that these embryos
499 upregulate mechanisms to inhibit TE expression and to counteract the misexpression of genes
500 involved in growth and development as an essential compensatory mechanism for embryo
501 survival. Thus, *Imp* seems to impact embryo survival by affecting various RNA targets and
502 controlling different RNA metabolic pathways.

503 The question of why Imp's role in localizing certain developmental mRNAs appears
504 redundant while its role in TE silencing is essential is intriguing. One possibility is functional
505 compensation. Other RNA-binding proteins may be able to substitute for Imp in the BicD/Egl
506 transport machinery for a subset of cargoes, ensuring robust developmental progression.

However, its role in the piRNA pathway may be more specialized, perhaps involving specific protein-protein interactions or recognition of TE-associated RNA features that other proteins cannot replicate. This would make Imp an indispensable node in the TE silencing network, while being a more dispensable component of a broader RNA transport system.

A central finding of this study is the strong correlation between the loss of maternal Imp, the de-repression of TEs, and severe embryonic defects. While we propose that the uncontrolled activity of TEs is a primary driver of the developmental failure, we cannot formally exclude the possibility that TE de-repression is a secondary consequence of general cellular stress in a dying embryo. Disentangling cause and effect is a critical next step. A definitive experiment would be to perform a genetic rescue. If the developmental phenotypes of *Imp* mutant embryos could be partially or fully rescued by simultaneously silencing the most highly de-repressed transposons (e.g., using a multi-target RNAi approach), it would provide powerful evidence that TE activity is indeed the primary cause of lethality.

Our findings underscore the essential role of maternal Imp in early *Drosophila* development, likely through its roles in RNP complexes that regulate cell growth and differentiation, and by controlling transposon silencing. These processes contribute to a deeper understanding of the molecular pathways that govern embryogenesis and maintain genomic stability.

METHODS

Drosophila stocks

FRT lines Imp^2, Imp^8, and the original Imp^7 stock were kindly provided by Daniel S. Johnston (Munro et al., 2006). These lines were sequenced to confirm the nature of the mutations. Imp^2 carries a deletion of a region spanning the two putative AUGs, along with a 20Kb intronic insertion after the Imp start codons, which makes this line lethal. Although the deletion was as previously described, the additional insertion had not been reported before. Imp^8 contains a 6Kb insertion and a 16 bp short insertion, as well as a deletion of a region that removes the first KH domain. This contrasts with previously reported data, where the entire ORF was described as deleted. This line is also lethal. The Imp^7 line carries a deletion that starts after the two putative AUGs and extends through the rest of the ORF, deleting all KH domains and the PLD. This deletion extends further into the 3′ UTR as previously described, removing part of the 3′ UTR. A schematic representation of the mutant genes is shown in Fig. S5A. *Imp* germline clones were induced using the FLP/FRT OvoD technique. The Imp^7 line was recombined with

541 the FRT chromosome *y,w,v,P{FRT(w{hs})}101* obtained from Bloomington (BL1844).
542 Germline clones were then generated by crossing females bearing the *Imp*^{2}, *Imp*^{8} or *Imp*^{7} FRT
543 recombined chromosome *to w,ovoD1,v,P{FRT(w[hs])}101/C(1)DX,y,f/Y; P{hsFLP}38* males
544 (Bloomington, BL1813). The progeny was heat-shocked twice a day for two days upon
545 reaching the late L2 or early L3 stages. Females bearing both the *Imp* mutant chromosome and
546 the *OvoD* chromosome were then used to collect embryos or ovaries lacking *Imp.*
547 *Imp-GFP*^{G080} was kindly provided by William Chia and Xavier Morin (Morin et al., 2021).
548 *Piwi*^{2} and variegating white reporters P[w^{var}], embedded in the fourth chromosome pericentric
549 region (stock: *yw; P{hsp26-pt-T}* at *118E-10*, BL84108), the fourth chromosome
550 heterochromatin (*P{hsp26-pt-T}39C-12 at 102B5*, BL84110), or the X chromosome (+w^{m4h},
551 BL76618), were obtained from Bloomington. *Imp*^{H44} and *Imp*^{H149} flies were generously
552 provided by T. Hays (Boylan et al., 2008). Cas9 fly stocks were obtained from Bloomington
553 (BL78782 and BL54591). Transgenic flies were generated using the attP/attB system.(Bischof
554 et al., 2007)
555
556 **Adult Drosophila aging assay**
557 Adult fly aging was assayed with the previously described survival analysis (M'Angale and
558 Staveley, 2016). In brief, single-vial matings with virgin females and males of the appropriate
559 genotypes were performed at room temperature (RT) in fly rearing bottles. Age-matched
560 cohorts of at least 200 F1 male flies were collected. The flies were pushed to new food every
561 other day and scored for survival, with flies determined dead when they did not display
562 movement upon agitation. Survival curves were graphed using GraphPad Prism software, and
563 the curves were compared using the log-rank (Mantel-Cox) test.
564
565 **DNA constructs for RNA injections**
566 DNA constructs used as templates to prepare RNA for injection experiments *hairy (h*^{SL1x3}*), ftz*
567 and *grk* were previously described (Bullock and Ish-Horowicz, 2001; Bullock et al., 2006) To
568 generate the template to transcribe the *hairy (h*^{SL1x3}*)* RNA containing a poly-(A)$_{71}$ tail, a
569 BamHI/HindIII fragment from the *h*^{SL1x3} cDNA was subcloned into the NcoI/ BglII site of the
570 FLuc-cassette plasmid (Hernández et al., 2004) by fill-in reaction to generate the - *h*^{SL1x3} *-(A)*$_{71}$
571 cDNA.
572
573
574

575 **DNA constructs for two-hybrid screens**

576 The plasmids BicD carboxy-terminal (534-782)-BD, BicD full-length-AD, Egl full-length-AD
577 and Egl full-length-BD were described (Vazquez-Pianzola et al., 2022). DNA fragments
578 encoding *D. melanogaster* IMP were cloned in-frame with the Gal4 cDNA into the vector
579 pOAD (activator domain, AD) to create the "bait" constructs (Cagney et al., 2000). Full-length
580 *IMP1* was cloned as a EcoRI-NcoI fragment to create the construct IMP1 FL-AD. IMP1 amino-
581 terminal (amino acids 1-234) was cloned as a EcoRI-PstI fragment to create the construct IMP1
582 (1-234)-AD. IMP2 amino-terminal (amino acids 1-242) was cloned as a EcoRI-PstI fragment
583 to create the construct IMP2 (1-242)-AD, and IMP1 and IMP2 carboxy-terminal (amino acids
584 242-573 of IMP1, amino acids 235-566 of IMP2) were cloned as a EcoRI-NcoI to create the
585 construct IMP1/2 (carboxy)-AD

586

587 **DNA constructs for generating the *Imp-GFP^{Stop}* and *Imp^{KH}* mutants**

588 DNA constructs to generate the *Imp-GFP* plasmids for making the mutations in different KH
589 domains were constructed as follows. The *Imp-GFP* region was amplified by PCR using
590 genomic DNA obtained from *Imp-GFP* expressing flies and primers containing EcoRI and
591 XhoI restriction sites (called IMP-rec-F and IMP-rec-R). The resulting fragments were cloned
592 into the corresponding sites in pBluescript (pBSK). Primer sequences are listed in Table S9.
593 The KH domains in the generated plasmid were then mutated by replacing the conserved
594 GXXG motifs with GDDG sequences. These mutant protein versions have been shown to fold
595 properly but impair *Imp* ortholog RNA binding (Hollingworth et al., 2012). These mutations
596 were introduced either as single KH mutants or as double mutations in KH1 and KH2 (KH1-
597 2), or in KH3 and KH4 (KH3-4), using site-directed mutagenesis with the corresponding
598 primers listed in Table S9. Double mutants were generated by sequential mutations. The PAM
599 sites corresponding to the gRNAs were also mutated in the donor DNAs.

600 Genomic sequences were scanned for suitable sgRNA target sites using FlyBase Jbrowse
601 DNA oligos for cloning of the *gRNA* genes were ordered from Microsynth (Balgach,
602 Switzerland) and cloned into pCFD5 following the protocols on the website:
603 http://crisprflydesign.org/. Table S9 shows the primers used for cloning the different *gRNA*
604 genes used in this study. gRNA-1 was used to generate the Imp-GFP^{Stop} mutant stock. Mid2
605 gRNA was used to generate the single KH mutations and the Mid1 gRNA for the generation of
606 KH1-2 and KH3-4 double mutants.

607

608

609 **Generation of *Imp-GFP^{Stop}* and *Imp^{KH}* mutant flies.**

610 The *Imp-GFP^{G080}* trap chromosome encodes a fusion of *Imp* with *GFP*, where the *GFP* is
611 inserted in-frame after the 32nd amino acid of the Imp-RA isoform (Fig. S2) (Morin et al.,
612 2001). Other isoforms could also be translated, differing only in the sequence of this short N-
613 terminal region. After the GFP insertion site, both isoforms share the same sequences,
614 including all the functional regions of the protein: the four KH domains and the conserved PLD
615 domain. Moreover, homozygous *Imp-GFP^{G080}* flies are viable and fertile (Boylan et al., 2008;
616 Munro et al., 2006). The gRNA transgenes are described in the cloning section of the methods,
617 and the sequences are shown in Table S9.

618 To generate a mutant version of the *Imp-GFP^{G080}* chromosome, we performed a CRISPR-
619 Cas9 mutagenesis screen using a gRNA targeting a site downstream of the GFP insertion in the
620 Imp coding region (gRNA-1). The nos-Cas9 stock (BL54591) was used. This resulted in a
621 mutant version of the *Imp-GFP* chromosome with an 8-nucleotide deletion (sequence:
622 GACAGGGC), leading to a frameshift in the open reading frame and the introduction of a
623 premature stop codon. The frameshift occurs after the 17th amino acid of the KH1 domain.
624 This mutation was lethal in flies and resulted in the production of a GFP protein under the same
625 regulatory elements as Imp expression. This fly line, referred to as *Imp-GFP^{Stop,}* was used as a
626 mock control for protein and RNA immunoprecipitations (Fig. S2A-B).

627 To generate *Imp-GFP^{KH}* mutants in single KH domains, females bearing the Imp-GFP
628 chromosome and the gRNA *Mid2* transgene were crossed with *nos-Cas9*-bearing males
629 (BL54591). For the generation of double KH mutant stocks, females carrying the *Mid1,*
630 gRNAs were crossed to males bearing the *Cas9* from the BL 78782 stock. The corresponding
631 Imp-GFP mutated plasmids were injected into their embryo progeny. Single flies were then
632 screened for the presence of the required mutations. Flies with single mutations, referred to as
633 *Imp^{KH1}*, *Imp^{KH2}*, *Imp^{KH3}*, and *Imp^{KH4}*, as well as double mutant flies *Imp^{KH1-2}* and *Imp^{KH3-4}*, were
634 generated by injecting the corresponding donor DNA *Imp-GFP* mutated templates. The donor
635 plasmids were mutated in the corresponding KH domain as well as in the PAM site recognized
636 by the gRNA used. Single mutant flies turned out to be viable and fertile, while flies bearing
637 the double mutations were lethal.

638

639 **Yeast two-hybrid assays**

640 Interactions between prey and bait proteins were tested in a yeast two-hybrid system using the
641 haploid strains PJ69-4a and PJ69-4alpha (Cagney et al., 2000). Diploid cells containing both
642 bait and prey plasmids were grown on selective media (—W(tryptophan), —L (leucine)) and

643 are shown as growth controls. Protein interactions were detected by replica-plating diploid cells
644 onto the selective media (—W, —L, —H (histidine) + 5 mM 3-amino-1,2,4-triazole (3AT)).
645 Growth was scored after 6 days of incubation at 30 °C.
646
647 **Protein Immunoprecipitations (IPs) and Western blot analysis**
648 The immunoprecipitations (IPs), followed by mass spectrometry and Western blotting used to
649 identify Imp in the BicD complexes, (depicted in Fig.s 1A-B) were previously partially
650 described (Vazquez-Pianzola et al., 2011). Additionally, to detect Imp in the
651 immunoprecipitates, anti-IMP antibodies (1:3,000 , (Munro et al., 2006)) were used.
652 To identify novel Imp interactors, the IPs were performed essentially as described in
653 (Vazquez-Pianzola et al., 2011) with some modifications. *Imp-GFP* and *Imp-GFP*^{Stop} 0-8 h-old
654 embryos were used. Dechorionated 0-8 h-old embryos were homogenized on ice in
655 homogenization buffer (HB; 25 mM Hepes pH 7.4, 50 mM KCl, 1 mM MgCl2, 1 mM DTT,
656 0.5% NP-40, and EDTA-free protease inhibitor cocktail Complete™ (Roche Diagnostics)). 2
657 mL of HB was used per gram of embryos. The supernatants were centrifuged at 16,000 x g for
658 45 minutes at 4°C, and the resulting supernatant was transferred and centrifuged again at
659 16,000 x g for 25 minutes at 4°C. 2 mL of anti-GFP IDJ42 monoclonal antibody supernatant
660 were incubated with 62.5 µL of protein-G Mag Sepharose magnetic beads (Cytiva) for 3 hours
661 at room temperature. After extensive washing with PBS, the bead-antibody complexes were
662 incubated overnight at 4°C on a rotating wheel with 1.7 mL of embryo extract per IP. The
663 unbound material was washed off 7 times with 1 mL of homogenization buffer (HB) without
664 detergents, and the beads were transferred to new tubes during the first and last washes. For
665 Western blot analysis, a 100 µL aliquot of the resuspended beads was taken after the final wash
666 and resuspended in 40 µL of sample buffer to confirm successful Imp pull-down. The
667 remaining IP material was subjected to mass spectrometry analysis.
668 For Western blot analysis of Imp-GFP complexes, small-scale IPs were performed using
669 30-40 µL of beads and 1 mL of embryo extract. Blots were performed using the following
670 primary antibodies: rabbit anti-Pabp (1:5,000 dilution), anti-Imp (1:3,000, (Munro et al., 2006),
671 Fig. 1), anti-Imp (1:1,000,(Geng and Macdonald, 2006) ; Fig. 8), and mouse anti-BicD (a mix
672 of 1B11 and 4C2, 1:10 dilution).
673 To detect Copia isoforms in Imp embryos, dechorionated embryos were homogenized in
674 loading buffer containing 0.1 M DTT and 2% SDS, and the Copia isoforms were detected using
675 anti-Copia antibodies (1:1,000, (M'Angale et al., 2025)). Horseradish peroxidase-conjugated
676 antibodies were obtained from GE Healthcare.

677 **Whole embryo and IP mass spectrometry**

678 For the preparation of whole embryo extracts for mass spectrometry analysis, 0-4 h-old
679 dechorionated embryos were homogenized with a pestle in a buffer containing 8M Urea and
680 100 mM Tris-HCl (pH 8). The extract was centrifuged at 16,000 x g for 40 minutes at 4°C.
681 Protein concentration was measured using the Bradford assay (BioRad). The supernatant was
682 then subjected to mass spectrometry analysis. For the mass spectrometry identification of Imp
683 interactors, IP beads were also subjected to mass spectrometry analysis. Mass spectrometry
684 analysis was performed by the Proteomics and Mass Spectrometry Core Facility of the
685 University of Bern. The proteins bound to the magnetic beads were resuspended in 8M Urea /
686 50 mM Tris-HCl (pH8), reduced for 30 min at 37^0C with 0.1M DTT / 100 mM Tris-HCl pH8,
687 alkylated for 30 min at 37^0C in the dark with IAA 0.5M / 100 mM Tris-HCl (pH8) and diluted
688 with 4 volumes of 20 mM Tris-HCl pH8 / 2 mM CaCl2 before overnight digestion at room
689 temperature with 100 ng sequencing grade trypsin (Promega). Samples were centrifuged, and
690 a magnet holder trapped the magnetic beads to extract the peptides in the supernatant. The
691 digested proteins were analyzed by liquid chromatography. (LC)-MS/MS (PROXEON coupled
692 to a QExactive mass spectrometer, ThermoFisher Scientific) with three injections of 5 µl
693 digested proteins. Peptides were trapped on a µPrecolumn C18 PepMap100 (5 µm, 100 Å pore
694 size, 300 µm x 5 mm, ThermoFisher Scientific, Reinach, Switzerland) and separated by
695 backflush onto an analytical C18 column (5 µm, 100 Å, 75 µm x 15 cm, C18). Separation was
696 performed using a 60 min gradient from 5% acetonitrile to 40% in water, 0.1% formic acid, at
697 a flow rate of 350 ml/min. The Full Scan MS was acquired at a resolution of 70,000 with an
698 automatic gain control (AGC) target of $1x10^6$ and a maximum ion injection time of 50 ms. The
699 data-dependent method for precursor ion fragmentation was applied with the following
700 settings: resolution 17,500, AGC of 1E05, maximum ion time of 110 milliseconds, mass
701 window 2 m/z, collision energy 27, underfill ratio 1%, charge exclusion of unassigned and 1+
702 ions, and peptide match preferred, respectively. The data were then processed with the software
703 MaxQuant (Cox and Mann, 2008), version 1.6.14.0, against the UniProtKB (Bateman,
704 2019)Drosophila 7228 database (release 2021_02) containing canonical and isoform entries, to
705 which common contaminants were added. The following parameters were set: digestion by
706 strict trypsin (maximum three missed cleavages), first search peptide tolerance of 15 ppm,
707 MS/MS match tolerance of 20 ppm, PSM and protein FDR set to 0.01, and a minimum of 2
708 peptides requested per group. Carbamidomethylation on cysteine was selected as a fixed
709 modification; the following variable modifications were allowed: methionine oxidation,

710 deamidation of asparagines and glutamines, and protein N-terminal acetylation; a maximum of
711 3 modifications per peptide was allowed. Match between runs was turned on (match time
712 windows 0.7 min) but only allowed within replicates of the same kind. Peptides were
713 normalized by variance stabilization (Huber et al., 2002), imputed, and combined to form Top3
714 intensities (Silva et al., 2006) and considered alongside MaxQuant's Label-Free Quantification
715 (LFQ) values. Missing peptides, respectively LFQ intensities, were imputed by drawing values
716 from a Gaussian distribution of width 0.3 centered at the sample distribution mean minus 2.5x
717 the sample standard deviation, provided there were at most 1 non-zero value in the group;
718 otherwise, the Maximum Likelihood Estimation (Silver et al., 2009) was used. Differential
719 expression was performed by applying the empirical Bayes test (Kammers et al., 2015) between
720 groups; significance testing was performed as described (Uldry et al., 2022).

721 **Immunostaining and RNA *in-situ* hybridization in embryos and ovaries**

722 Immunostaining experiments were performed as described in previous studies (Rashpa et al.,
723 2017; Vazquez-Pianzola et al., 2014; Vazquez-Pianzola et al., 2022). Immunostaining of
724 whole-mount embryos and ovaries was conducted using the following primary antibodies:
725 mouse anti-BicD (a mix of 1B11 and 4C2, 1:10 dilution), rabbit anti-Imp (1:1,500, (Geng and
726 Macdonald, 2006)), rabbit anti-Imp (1:500, (Munro et al., 2006)), rabbit anti-Copia (1:500
727 (M'Angale et al., 2025)), mouse anti-Piwi P3G11 (1:1,000; (Saito et al., 2006)), mouse anti-
728 Ago1 (1:500, (Miyoshi et al., 2005)), mouse anti-Hp1 (1:20, C1A9-S, Developmental Studies
729 Hybridoma Bank), anti-H3K9m3 (1:600, AbCam 176916), anti-lamin ADL84 (1:500–1:300;
730 Developmental Studies Hybridoma Bank), and anti-Serp (1:1,000; (Luschnig et al., 2006)).
731 Secondary antibodies were obtained from Jackson ImmunoResearch or Molecular Probes.
732 Where necessary, nuclei were stained with 2.5 µg/mL Hoechst 33258 (Molecular Probes) for
733 20 minutes during the final washing steps. Images were analyzed using a Leica TCS-SP8
734 confocal microscope. RNA *in situ* hybridization using Stellaris probes to detect piRNA
735 precursors was performed essentially as described (Mohn et al., 2014; Rashpa et al., 2017).
736 However, following hybridization, samples were subjected to immunostaining to reveal Imp
737 and Lamin proteins. Stellaris probes for detecting the 42AB sense transcripts (probe 42AB-RS
738 labeled with CalFluor 590) and probes against the 20A transcripts (labeled with Quasar 670)
739 were also previously described in (Mohn et al., 2014). *In situ* hybridization experiments to
740 detect mRNA expression were performed as described (Vazquez-Pianzola et al., 2017).
741 Linearized *Osi9*, containing the *Osi9* cDNA, was used as a template to generate digoxigenin-

742 labeled RNA antisense probes. Images were analyzed using a Leica TCS-SP8 confocal
743 microscope and processed with Leica software, Photoshop, and ImageJ.
744
745 **NMJ immunostaining and protein intensity quantification**
746 *Drosophila* larvae were dissected in HL3 media and fixed in 4% paraformaldehyde. Washes
747 and permeabilization were performed in 0.1M PBS supplemented with 0.2% Triton X-100.
748 Larval fillets were incubated overnight in primary and secondary antibodies at 4˚C followed
749 by 2 hours at RT. After this, they were mounted. Laser scanning confocal microscopy and
750 intensity measurements were as previously described (M'Angale et al., 2025).
751
752 **Fluorescent RNA synthesis and injections**
753 RNA for injections was synthesized in the presence of either Alexa-488-UTP (Molecular
754 Probes) or Cy3-UTP (NE Life Sciences) as described (Bullock et al., 2006). *hairy* RNA was
755 synthesized using linearized h^{SL1x3} cDNA in pBSK[(1)] or $h\text{-}(A)_{71}$ cDNA, *ftz* using *ftz*-
756 pCRIITOPO and *grk* using pBSK-*grk* as templates. For blocking experiments, affinity-purified
757 anti-Imp antibody (Munro et al., 2006) and anti-GFP (Roche or AMS Biotechnology) were pre-
758 injected at 1 μg μl^{-1}, 10-12 min before injecting the fluorescently labeled RNAs. Fluorescently
759 labeled RNAs were used at 0.4 μg μl^{-1}. Fixing and immunofluorescent stainings of injected
760 embryos were done as described (Bullock and Ish-Horowicz, 2001; Vazquez-Pianzola et al.,
761 2017). Images were analyzed with a Leica TCS-SP2 confocal microscope. Localization was
762 designated as strong (most of the RNA was in the apical cytoplasm), weak (most of the RNA
763 remained basal, but there were some apical caps of RNA) or unlocalized (no apical
764 concentration of RNA).
765
766 **Pigment determination**
767 Pigment quantification was performed as described in (Rabinow et al., 1991). The heads of 22
768 flies of the appropriate genotypes were dissected and frozen on dry ice. The heads were
769 homogenized with a pestle in 550 μL of methanol acidified with 0.1% HCl, followed by the
770 addition of another 550 μL of acidified methanol. The extract was briefly centrifuged for 1
771 minute at 16,000 x g, and the supernatant was used to measure absorbance at 480 nm.

772 **Isolation of Imp-bound RNAs**
773 RNA immunoprecipitation (RNA-IP) was essentially performed as described in (Vazquez-
774 Pianzola et al., 2017) with the following modifications. Flies of the desired genotypes (*Imp*-

775 *GFP^{G80}, Imp-GFP^{Stop}/Fm7c*) were reared in population cages. For each IP, 1.2 mL of 0-8 h-old
776 embryo extract (dechorionated embryos homogenized at a ratio of 1 g embryos to 2 mL of
777 homogenization buffer) of the corresponding genotype was mixed with 646 µL of adjusting
778 buffer. The IPs were performed in triplicates, using embryos from different collections. For
779 each IP, 80 µL of magnetic beads (Protein G Mag Sepharose, Cytiva) were used. A detailed
780 protocol is available upon request.
781
782 **RNA purification, Library Preparation, RNA sequencing and analysis**
783 Total RNA was isolated using TRIzol® Reagent (Invitrogen) following the manufacturer's
784 instructions. For transcriptome and small RNA analysis, 0-4 or 0-8 h-old embryos were
785 collected, dechorionated, and homogenized directly in the indicated amount of TRIzol reagent.
786 For RIP-Seq, TRIzol reagent was added directly to the RNA bound to the magnetic beads.
787 RNA concentration was measured using a Qubit RNA BR or HS Assay Kit (Thermo Fisher
788 Scientific, Q10211 or Q32855, respectively) in a Thermo Fisher Scientific Qubit 4.0
789 fluorometer. RNA quality was assessed using the Agilent Advanced Analytical Fragment
790 Analyzer System with a Fragment Analyzer RNA Kit (Agilent, DNF-471).
791 For RIP-Seq and transcriptome analysis, library preparation and RNA sequencing were
792 performed at the Next Generation Sequencing Platform of the Vetsuisse Faculty in Bern.
793 Libraries for RNA-seq were prepared using Lexogen's CORALL Total RNA-Seq Library Prep
794 Kit with RiboCop (Lexogen, 117.96). The libraries were paired-end sequenced with a read
795 length of 100 bp on an Illumina NovaSeq 6000 instrument (100 cycles; Illumina).
796 The quality of the RNA-seq data was assessed using fastqc
797 v.0.11.9 (http://www.bioinformatics.babraham.ac.uk/projects/fastqc/) and RSeQC v.4.0.0
798 (Wang et al., 2012). The reads were mapped to the reference genome using HiSat2
799 v.2.2.1 (Kim et al., 2015). FeatureCounts v.2.0.1 (Liao et al., 2014) was used to count the
800 number of reads overlapping with each gene as specified in the genome annotation
801 (Drosophila_melanogaster.BDGP6.32.103) The Bioconductor package DESeq2
802 v1.38.3 (Love et al., 2014) was used to test for differential gene expression between the
803 experimental groups. ClusterProfiler v4.7.1 (Wu et al., 2021) was used to identify gene
804 ontology terms containing unusually many differentially expressed genes. An interactive
805 Shiny application v1.6.0 (Chang et al. 2022) was set up to facilitate the exploration and
806 visualization of the RNA-seq results. All analyses were run in R version 4.2.1 (2022-06-23)
807 (R Core Team 2022). The small RNA libraries were prepared and sequenced by a Novogene
808 sequencing platform. Single-end 50 bp sequencing strategy was used to sequence the samples.

809 The sRNAPipe in Galaxy was used for small RNA analysis (Pogorelcnik et al., 2018). The
810 mapping was done, allowing either 1 or 2 mismatches. The small RNAs were mapped to the
811 *Drosophila melanogaster* BDGP6.46 version.
812

813 **ACKNOWLEDGEMENTS**

814 We thank Drs. Daniel St Johnston, Thomas Hays, Fabio Mohn, Mikiko C. Siomi, and Nicola
815 Iovino for providing antibodies, probes, constructs, and fly stocks. We also thank Alexander
816 Nater, Geert van Geest, and Rémy Bruggmann from the Interfaculty Bioinformatics Unit for
817 their assistance with the RNA-seq differential expression analysis. Additionally, we express
818 our gratitude to Dr. Pamela Nicholson from the NGS Platform for her advice on RNA-seq
819 protocols. We acknowledge the Developmental Studies Hybridoma Bank (DSHB, University
820 of Iowa) for antibodies, the Bloomington Stock Center (University of Indiana) for fly stocks,
821 and FlyBase for invaluable support.
822

823 **FUNDING STATEMENT**
824 This work was supported by the Swiss National Science Foundation project grants
825 31003A_173188 and 310030_205075, and by the Equipment grant 316030_150824 to BS.
826 Support also came from the University of Bern to BS, an equal opportunity grant from the
827 University of Bern (to PVP), and an MVUB grant from the Phil.-nat. Fakultät
828 (http://www.philnat.unibe.ch) to PVP. Work in the group of SLB is supported by the Medical
829 Research Council as part of UK Research and Innovation (MC_U105178790). The funders had
830 no role in study design, data collection, and interpretation, or the decision to submit the work
831 for publication."
832
833

REFERENCES

Bateman, A. (2019). UniProt: A worldwide hub of protein knowledge. *Nucleic Acids Res* **47**, D506–D515.

Bianco, A., Dienstbier, M., Salter, H. K., Gatto, G. and Bullock, S. L. (2010). Report Bicaudal-D Regulates Fragile X Mental Retardation Protein Levels, Motility, and Function during Neuronal Morphogenesis. *Current Biology* **20**, 1487–1492.

Bischof, J., Maeda, R. K., Hediger, M., Karch, F. and Basler, K. (2007). An optimized transgenesis system for Drosophila using germ-line-specific C31 integrases. *Proc Natl Acad Sci U S A* **104**, 3312–3317.

Boylan, K. L. M., Mische, S., Li, M., Marqué, G., Morin, X., Chia, W. and Hays, T. S. (2008). Motility Screen Identifies Drosophila IGF-II mRNA-Binding Protein-Zipcode-Binding Protein Acting in Oogenesis and Synaptogenesis. *PLoS Genet* **4**, e36.

Bullock, S. L. and Ish-Horowicz, D. (2001). Conserved signals and machinery for RNA transport in Drosophila oogenesis and embryogenesis. *Nature* **414**, 611–616.

Bullock, S. L., Nicol, A., Gross, S. P. and Zicha, D. (2006). Guidance of Bidirectional Motor Complexes by mRNA Cargoes through Control of Dynein Number and Activity. *Current Biology* **16**, 1447–1452.

Buxbaum, A. R., Wu, B. and Singer, R. H. (2014). Single β-actin mRNA detection in neurons reveals a mechanism for regulating its translatability. *Science (1979)* **343**, 419–422.

Cagney, G., Uetz, P. and Fields, S. (2000). High-throughput screening for protein-protein interactions using two-hybrid assay. *Methods Enzymol* **328**, 3–14.

Cox, J. and Mann, M. (2008). MaxQuant enables high peptide identification rates, individualized p.p.b.-range mass accuracies and proteome-wide protein quantification. *Nat Biotechnol* **26**, 1367–1372.

Degrauwe, N., Suvà, M.-L., Janiszewska, M., Riggi, N. and Stamenkovic, I. (2016). IMPs: an RNA-binding protein family that provides a link between stem cell maintenance in normal development and cancer. *Genes Dev* **30**, 2459–2474.

Deshler, J. O., Highett, M. I., Abramson, T. and Schnapp, B. J. (1998). A highly conserved RNA-binding protein for cytoplasmic mRNA localization in vertebrates. *Current Biology* **8**, 489–496.

Dienstbier, M., Boehl, F., Li, X. and Bullock, S. L. (2009). Egalitarian is a selective RNA-binding protein linking mRNA localization signals to the dynein motor. *Genes Dev* **23**, 1546–1558.

Fabry, M. H., Falconio, F. A., Joud, F., Lythgoe, E. K., Czech, B. and Hannon, G. J. (2021). Maternally inherited piRNAs direct transient heterochromatin formation at active transposons during early Drosophila embryogenesis. *Elife* **10**, e68573.

Geng, C. and Macdonald, P. M. (2006). Imp Associates with Squid and Hrp48 and Contributes to Localized Expression of gurken in the Oocyte . *Mol Cell Biol* **26**, 9508–9516.

Ghanim, G. E., Rio, D. C. and Teixeira, F. K. (2020). Mechanism and regulation of P element transposition. *Open Biol* **10**, 200244.

Hansen, T. V. O., Hammer, N. A., Nielsen, J., Madsen, M., Dalbaeck, C., Wewer, U. M., Christiansen, J. and Nielsen, F. C. (2004). Dwarfism and Impaired Gut Development in Insulin-Like Growth Factor II mRNA-Binding Protein 1-Deficient Mice. *Mol Cell Biol* **24**, 4448–4464.

Hansen, H. T., Rasmussen, S. H., Adolph, S. K., Plass, M., Krogh, A., Sanford, J., Nielsen, F. C. and Christiansen, J. (2015). Drosophila Imp iCLIP identifies an RNA assemblage coordinating F-actin formation. *Genome Biol* **16:123**,.

Havin, L., Git, A., Elisha, Z., Oberman, F., Yaniv, K., Schwartz, S. P., Standart, N. and Yisraeli, J. K. (1998). RNA-binding protein conserved in both microtubule- and microfilament-based RNA localization. *Genes Dev* **12**, 1593–1598.

Hernández, G., Vázquez-Pianzola, P., Sierra, J. M. and Rivera-Pomar, R. (2004). Internal ribosome entry site drives cap-independent translation of reaper and heat shock protein 70 mRNAs in Drosophila embryos. *RNA* **10**, 1783–1797.

Hollingworth, D., Candel, A. M., Nicastro, G., Martin, S. R., Briata, P., Gherzi, R. and Ramos, A. (2012). KH domains with impaired nucleic acid binding as a tool for functional analysis. *Nucleic Acids Res* **40**, 6873–6886.

Horan, L., Yasuhara, J. C., Kohlstaedt, L. A. and Rio, D. C. (2015). Biochemical identification of new proteins involved in splicing repression at the Drosophila P-element exonic splicing silencer. *Genes Dev* **29**, 2298–2311.

Huber, W., von Heydebreck, A., Sültmann, H., Poustka, A. and Vingron, M. (2002). Variance stabilization applied to microarray data calibration and to the quantification of differential expression. *Bioinformatics* **18**, S96-104.

Hüttelmaier, S., Zenklusen, D., Lederer, M., Dictenberg, J., Lorenz, M., Meng, X. H., Bassell, G. J., Condeelis, J. and Singer, R. H. (2005). Spatial regulation of β-actin translation by Src-dependent phosphorylation of ZBP1. *Nature* **438**, 512–515.

Kammers, K., Cole, R. N., Tiengwe, C. and Ruczinski, I. (2015). Detecting significant changes in protein abundance. *EuPA Open Proteom* **7**, 11–19.

Karam Teixeira, F., Okuniewska, M., Malone, C. D., Coux, R. X., Rio, D. D. and Lehmann, R. (2017). piRNA-mediated regulation of transposon alternative splicing in the soma and germ line. *Nature* **552**, 268–272.

Kim, D., Langmead, B. and Salzberg, S. L. (2015). hisAt: a fast spliced aligner with low memory requirements. *Nat Methods* **12**, 357–362.

Lee, S. K., Xue, Y., Shen, W., Zhang, Y., Joo, Y., Ahmad, M., Chinen, M., Ding, Y., Ku, W. L., De, S., et al. (2018). Topoisomerase 3β interacts with RNAi machinery to promote heterochromatin formation and transcriptional silencing in Drosophila. *Nat Commun* **9**, 4946.

Lee, J. Y., Huang, N., Samuels, T. J. and Davis, I. (2025). Imp/IGF2BP and Syp/SYNCRIP temporal RNA interactomes uncover combinatorial networks of regulators of Drosophila brain development. *Sci Adv* **11**, eadr6682.

Lepelletier, L., Langlois, S., Kent, C. B., Welshhans, K., Morin, S., Bassell, G. J., Yam, P. T. and Charron, F. (2017). Sonic hedgehog guides axons via zipcode binding protein 1-mediated local translation. *J Neurosci* **37**, 1685–1695.

Leung, K. M., Van Horck, F. P. G., Lin, A. C., Allison, R., Standart, N. and Holt, C. E. (2006). Asymmetrical β-actin mRNA translation in growth cones mediates attractive turning to netrin-1. *Nat Neurosci* **9**, 1247–1256.

Liao, Y., Smyth, G. K. and Shi, W. (2014). Sequence analysis featureCounts: an efficient general purpose program for assigning sequence reads to genomic features. *Bioinformatics* **30**, 923–930.

Liu, H.-B., Muhammad, T., Guo, Y., Li, M.-J., Sha, Q.-Q., Zhang, C.-X., Liu, H., Zhao, S.-G., Zhao, H., Zhang, H., et al. (2019). RNA-Binding Protein IGF2BP2/IMP2 is a Critical Maternal Activator in Early Zygotic Genome Activation. *Adv Sci (Weinh)* **6**, 1900295.

927 **Love, M. I., Huber, W. and Anders, S.** (2014). Moderated estimation of fold change and
928 dispersion for RNA-seq data with DESeq2. *Genome Biol* **15**, 550.
929 **Luschnig, S., Bätz, T., Armbruster, K. and Krasnow, M. A.** (2006). serpentine and vermiform
930 encode matrix proteins with chitin binding and deacetylation domains that limit
931 tracheal tube length in Drosophila. *Current Biology* **16**, 186–194.
932 **Mancarella, C. and Scotlandi, K.** (2020). IGF2BP3 From Physiology to Cancer: Novel
933 Discoveries, Unsolved Issues, and Future Perspectives. *Front Cell Dev Biol* **7**, 363.
934 **M'Angale, G. P. and Staveley, B. E.** (2016). The Bcl-2 homologue Buffy rescues α-synuclein-
935 induced Parkinson disease-like phenotypes in Drosophila. *BMC Neurosci* **17**, 24.
936 **M'Angale, G. P., Lemieux, A., Liu, Y., Wang, S., Zinter, M., Alegre, G., Simkin, A., Budnik, V.,**
937 **Kelch, B. A. and Thomson, T.** (2025). Capsid transfer of the retrotransposon Copia
938 controls structural synaptic plasticity in Drosophila. *PLoS Biol* **23**, e3002983.
939 **Medioni, C., Ramialison, M., Ephrussi, A. and Besse, F.** (2014). Imp promotes axonal
940 remodeling by regulating profilin mRNA during brain development. *Current Biology* **24**,
941 793–800.
942 **Miyoshi, K., Tsukumo, H., Nagami, T., Siomi, H. and Siomi, M. C.** (2005). Slicer function of
943 Drosophila Argonautes and its involvement in RISC formation. *Genes Dev* **19**, 2837–
944 2848.
945 **Mohn, F., Sienski, G., Handler, D. and Brennecke, J.** (2014). The Rhino-Deadlock-Cutoff
946 complex licenses noncanonical transcription of dual-strand piRNA clusters in
947 Drosophila. *Cell* **157**, 1364–1379.
948 **Morin, X., Daneman, R., Zavortink, M. and Chia, W.** (2001). A protein trap strategy to detect
949 GFP-tagged proteins expressed from their endogenous loci in Drosophila. *Proc Natl*
950 *Acad Sci U S A* **98**, 15050–15055.
951 **Munro, T. P., Kwon, S., Schnapp, B. J. and St Johnston, D.** (2006). A repeated IMP-binding
952 motif controls oskar mRNA translation and anchoring independently of Drosophila
953 melanogaster IMP. *J Cell Biol* **172**, 577–588.
954 **Narbonne-Reveau, K., Lanet, E., Dillard, C., Foppolo, S., Chen, C.-H., Parrinello, H., phanie**
955 **Rialle, S., Sokol, N. S. and dric Maurange, C.** (2016). Neural stem cell-encoded temporal
956 patterning delineates an early window of malignant susceptibility in Drosophila. *Elife* **5**,
957 e13463.
958 **Nielsen, J., Cilius Nielsen, F., Kragh Jakobsen, R. and Christiansen, J.** (2000). The biphasic
959 expression of IMP/Vg1-RBP is conserved between vertebrates and Drosophila. *Mech*
960 *Dev* **96**, 129–132.
961 **Oleynikov, Y. and Singer, R. H.** (2003). Real-Time Visualization of ZBP1 Association with β-
962 Actin mRNA during Transcription and Localization. *Curr Biol* **13**, 199–207.
963 **Pan, F., Hüttelmaier, S., Singer, R. H. and Gu, W.** (2007). ZBP2 Facilitates Binding of ZBP1 to
964 β-Actin mRNA during Transcription. *Mol Cell Biol* **27**, 8340–8351.
965 **Pogorelcnik, R., Vaury, C., Pouchin, P., Jensen, S. and Brasset, E.** (2018). sRNAPipe: a Galaxy-
966 based pipeline for bioinformatic in-depth exploration of small RNAseq data. *Mob DNA*
967 **9**, 25.
968 **Prashad, S. and Gopal, P. P.** (2021). RNA-binding proteins in neurological development and
969 disease. *RNA Biol* **18**, 972–987.
970 **Rabinow, L., Nguyen-Huynh, A. T. and Birchler, J. A.** (1991). A trans-Acting Regulatory Gene
971 That Inversely Affects the Expression of the white, brown and scarlet Loci in Drosophila.
972 *Genetics* **129**, 463–480.

Rashpa, R., Vazquez-Pianzola, P., Colombo, M., Hernandez, G., Beuchle, D., Berger, F., Peischl, S., Bruggmann, R. and Suter, B. (2017). Cbp80 is needed for the expression of piRNA components and piRNAs. *PLoS One* **12**, e0181743.

Ren, F., Lin, Q., Gong, G., Du, X., Dan, H., Qin, W., Miao, R., Xiong, Y., Xiao, R., Li, X., et al. (2020). Igf2bp3 maintains maternal RNA stability and ensures early embryo development in zebrafish. *Commun Biol* **3**, 94.

Saito, K., Nishida, K. M., Mori, T., Kawamura, Y., Miyoshi, K., Nagami, T., Siomi, H. and Siomi, M. C. (2006). Specific association of Piwi with rasiRNAs derived from retrotransposon and heterochromatic regions in the Drosophila genome. *Genes Dev* **20**, 2214–2222.

Sasaki, Y., Welshhans, K., Wen, Z., Yao, J., Xu, M., Goshima, Y., Zheng, J. Q. and Bassell, G. J. (2010). Phosphorylation of zipcode binding protein 1 is required for brain-derived neurotrophic factor signaling of local β-actin synthesis and growth cone turning. *Journal of Neuroscience* **30**, 9349–9358.

Shoshkes, M., 1¤, C., Kahane, N., Oberman, F., Miloslavski, R., Sela-Donenfeld, D., Kalcheim, C. and Yisraeli, J. K. (2015). A Novel Role for VICKZ Proteins in Maintaining Epithelial Integrity during Embryogenesis. *PLoS One* **10**, e0136408.

Siebel, C. W., Kanaar, R. and Rio, D. C. (1994). Regulation of tissue-specific P-element pre-mRNA splicing requires the RNA-binding protein PSI. *Genes Dev* **8**, 1713–1725.

Siebel, C. W., Admon, A. and Rio, D. C. (1995). Soma-specific expression and cloning of PSI, a negative regulator of P element pre-mRNA splicing. *Genes Dev* **9**, 269–283.

Silva, J. C., Gorenstein, M. V., Li, G. Z., Vissers, J. P. C. and Geromanos, S. J. (2006). Absolute quantification of proteins by LCMSE: A virtue of parallel MS acquisition. *Molecular and Cellular Proteomics* **5**, 144–156.

Silver, J. D., Ritchie, M. E. and Smyth, G. K. (2009). Microarray background correction: Maximum likelihood estimation for the normal-exponential convolution. *Biostatistics* **10**, 352–363.

Uldry, A. C., Maciel-Dominguez, A., Jornod, M., Buchs, N., Braga-Lagache, S., Brodard, J., Jankovic, J., Bonadies, N. and Heller, M. (2022). Effect of Sample Transportation on the Proteome of Human Circulating Blood Extracellular Vesicles. *Int J Mol Sci* **23**, 4515.

Vazquez-Pianzola, P., Beuchle, D., Saro, G., Herna, G., Maldonado, G., Brunßen, D., Meister, P. and Suter, B. (2022). Female meiosis II and pronuclear fusion require the microtubule transport factor Bicaudal D. *Development* **149**, dev199944.

Vazquez-Pianzola, P. and Suter, B. (2012). Conservation of the RNA Transport Machineries and Their Coupling to Translation Control across Eukaryotes. *Comp Funct Genomics* **2012**, 287852.

Vazquez-Pianzola, P., Urlaub, H. and Suter, B. (2011). Pabp binds to the osk 3'UTR and specifically contributes to osk mRNA stability and oocyte accumulation. *Dev Biol* **357**, 404–418.

Vazquez-Pianzola, P., Adam, J., Haldemann, D., Hain, D., Urlaub, H. and Suter, B. (2014). Clathrin heavy chain plays multiple roles in polarizing the Drosophila oocyte downstream of Bic-D. *Development* **141**, 1915–1926.

Vazquez-Pianzola, P., Schaller, B., Colombo, M., Beuchle, D., Neuenschwander, S., Marcil, A., Bruggmann, R., Suter, B. and Emy Bruggmann, R. (2017). The mRNA transportome of the BicD/Egl transport machinery The mRNA transportome of the BicD/Egl transport machinery. *RNA Biol* **14**, 73–89.

1019 **Vijayakumar, J., Perrois, C., Heim, M., Bousset, L., Alberti, S. and Besse, F.** (2019). The
1020 prion-like domain of Drosophila Imp promotes axonal transport of RNP granules in vivo.
1021 *Nat Commun* **10**, 2593.
1022 **Wang, L., Wang, S. and Li, W.** (2012). RSeQC: Quality control of RNA-seq experiments.
1023 *Bioinformatics* **28**, 2184–2185.
1024 **Wu, T., Hu, E., Xu, S., Chen, M., Guo, P., Dai, Z., Feng, T., Zhou, L., Tang, W., Zhan, L., et al.**
1025 (2021). clusterProfiler 4.0: A universal enrichment tool for interpreting omics data.
1026 *Innovation (Camb)* **2**, 100141.
1027 **Xu, X., Shen, H. R., Zhang, J. R. and Li, X. L.** (2022). The role of insulin-like growth factor 2
1028 mRNA binding proteins in female reproductive pathophysiology. *Reproductive Biology*
1029 *and Endocrinology* **20**, 89.
1030 **Yaniv, K., Fainsod, A., Kalcheim, C. and Yisraeli, J. K.** (2003). The RNA-binding protein
1031 Vg1 RBP is required for cell migration during early neural development.
1032 *Development* **130**, 5649–5661.
1033

1034 # FIGURE LEGENDS

1035

1036 **Fig. 1. Imp forms part of the BicD/Egl complex and GO analysis of Imp interactors**
1037 **shows association with proteins involved in RNA metabolic pathways.**
1038 **(A)** Immunoprecipitation (IP) of wild-type (wt, used as mock IP control), Imp-GFP^{G080},
1039 and Egl-GFP expressing embryos with anti-GFP antibodies. The IP material was tested for
1040 the presence of BicD, Egl, Imp, and Pabp. 0.15% of the cytoplasmic extract used for each
1041 IP was loaded as an input control**. (B)** Imp weakly interacts with BicD but not with Egl in
1042 a yeast two-hybrid assay. Interaction test of BicD carboxy terminus (top, amino acids 534-
1043 782) and full-length Egl (lower) with different fragments of Imps in the activator domain
1044 (AD). *Drosophila Imp* produces 2 isoforms differing in the first N-terminal amino acids (18
1045 or 22 different amino acids at the N-term), described here as Imp1 and Imp2. Imp1 full-
1046 length (a), Imp1 amino terminus (amino acids 1-234) (b), Imp2 amino terminus (amino
1047 acids 1-242) (c), and IMP1/2 carboxy-terminal (amino acids 235-566, shared in both
1048 isoforms) (d) were tested. Egalitarian-AD and BicD full-length-AD were used as positive
1049 controls, respectively, and empty vector AD as a negative control. A weak but consistent
1050 interaction between the carboxy-terminal part of BicD and Imp1/2 carboxy-terminal was
1051 detected**. (C)** Embryo extracts from *Imp-GFP^{G080}*, *Imp-GFP^{Stop}* or *yw* were subjected to
1052 immunoprecipitation (IP) using anti-GFP antibodies. Additionally, *Imp-GFP^{G080}* extracts
1053 were subjected to IP with anti-GFP antibodies in the presence of RNase to detect direct
1054 interactors. The IP materials were directly analyzed by bulk mass spectrometry. GO
1055 analysis of the proteins found enriched in the *Imp-GFP^{G080}* IP compared to the mock IPs
1056 (performed with *yw* and *Imp-GFP^{Stop}* extracts). Proteins were selected based on a log2Fold
1057 Change >1 or were uniquely present in the *Imp-GFP ^{G080},* IP, with a padj <0.05. Simplified
1058 GO Terms identified with Cluster Profiler are shown. **(D)** Enrichment of selected proteins
1059 known to be involved in RNA transport in oogenesis and proteins known to be in complex
1060 with BicD and in Imp complexes are shown. The log2FoldChange enrichment between the
1061 peptides found in the *Imp-GFP^{G080}* IP and the mock control IP (*Imp-GFP^{Stop}*) and between
1062 the peptides found in the *Imp-GFP^{G080}* IP done in the absence and presence of RNase is
1063 shown together with the corresponding padj values of the enrichment.

1064

1065

1066 **Fig. 2. Co-recruitment of Imp and BicD to apically localizing *hairy (h)* RNA and Imp**
1067 **redundancy for endogenous mRNA apical localization. (A,a)** Immunostaining to reveal
1068 the distribution of Imp (**a**, red) following injection of *hSL1x3* transcripts (green) into wild-
1069 type embryos. The merged image is on the right. **(A,b)** Imp (magenta) and BicD (red)
1070 protein distribution in wild-type embryos injected with localizing *hSL1x3* RNA (green).
1071 Imp and BicD are co-recruited to apically localizing *hSL1x3* RNA in this case bearing a
1072 poly-A tail (A_{71}) that stabilizes the RNA. **(A,c)** Immunostaining of *Imp-GFP*^{G080} embryos
1073 with anti-BicD antibodies (red). GFP signal is shown in green, and the merged image is
1074 seen on the right. Both proteins colocalize apically of the nuclei, although they also display
1075 a strong basal accumulation. **(A,d)** Distribution of Imp-GFP following injection with *h*
1076 transcripts into *Imp-GFP*^{G080} embryos, Imp-GFP (green) is recruited to *hSL1x3* localized
1077 transcripts (red). The merged image is on the right. **(B-C).** Pre-injection of antibodies
1078 against Imp blocks apical localization of injected transcripts. **(B)** Distribution of injected
1079 (*ftz* (red) and *h* (green)) transcripts after pre-injection with anti-GFP (as control) or
1080 antibodies against Imp. Imp antibodies block apical colocalization and lead to the
1081 accumulation of injected RNA in the basal cytoplasm. **(B')** Percentage of embryos
1082 displaying strong (black bars), weak (grey bars), or no localization (white bars) of injected
1083 *h* and *ftz* transcripts from the experiment shown in **B**. More embryos showed unlocalized
1084 RNAs upon injection with anti-Imp antibodies. Antibodies were injected 9-10 min before
1085 injection of a mixture of *h* and *ftz* RNAs. Embryos were fixed 6 min after RNA injection.
1086 **(**Distribution of staining intensity (Strong, Weak, None apical RNA localization) differed
1087 significantly between the two groups (Fisher's exact test, 2×3 contingency table: $\chi^2(2) =$
1088 9.57, $p = 0.0083$, **$p < 0.01$). **B")** Similar experiment as in **B**, but a mixture of *hSL1x3* and
1089 *grk t*ranscripts was injected and embryos were fixed 9-12 min after RNA injection.
1090 Percentage of embryos displaying strong (black bars), weak (grey bars) or no localization
1091 (white bars) of the injected transcripts after injection of anti-GFP or anti-Imp antibodies
1092 into wild-type embryos. Upon pre-injection with anti-Imp antibodies, apical localization of
1093 injected transcripts was affected to a greater extent than upon injection with anti-GFP
1094 antibodies. Statistical significance was assessed using Fisher's exact test on a 2×3
1095 contingency table ($\chi^2(2) = 9.74$, $p = 0.0077$, **$p < 0.01$). **(C)** Percentage of embryos
1096 displaying strong (black bars), weak (grey bars), or no localization (white bars) of injected
1097 *h* transcripts after pre-injection of anti-GFP antibodies into wild-type or *Imp-GFP*^{G080}
1098 expressing embryos. Antibody was injected 10-17 min before RNA injection, and embryos
1099 were fixed 6 min later. 30 % of *Imp-GFP*^{G080} embryos showed unlocalized *h* RNA

1100 compared with only 2 % observed in wild-type embryos. Distribution of staining intensity
1101 (Strong, Weak, No) differed significantly between groups (Fisher's exact test on a 2×3
1102 contingency table: $\chi^2(2) = 14.14$, $p = 0.00085$, ***$p < 0.001$). **(C')** Examples of *Imp-*
1103 *GFP*^{G080} embryos pre-injected with anti-GFP antibodies before injection with *h* RNA (red).
1104 Examples scored as strong, weak, and no *h* localization are shown. **(D)** *In*
1105 *situ* hybridization to whole-mount wild-type (a, d), *Imp*^{2} (b, e), and *Imp*^{8} (c, f) embryos
1106 using digoxigenin-labeled *ftz* (a-c) or *h* (d-f) anti-sense RNA probes (red signals). The
1107 embryos are also stained with Hoechst (blue) to visualize the DNA. No defects in apical
1108 RNA localization of pair-rule transcripts were observed in embryos devoid of
1109 maternal *Imp.* The same results were obtained with the *Imp*^{7} allele (not shown).
1110
1111 **Fig. 3. Transcriptome profile of embryos lacking maternal *Imp.*** Total RNA sequencing
1112 was performed in triplicates on embryos aged 0-4 hours (A-B) and 0-8 hours (C-D) derived
1113 from the induction of *Imp*^{2} and *Imp*^{8} germline clones (GLCs), alongside control wild-type
1114 embryos (yw). Heat maps display the top differentially expressed (DE) genes (A, C) or only
1115 the top upregulated genes (B, D) in the mutants compared to wild-type embryos. Selected
1116 cutoffs are indicated. Both *Imp* mutant embryos cluster closely together in the heat maps.
1117
1118 **Fig. 4. Gene Ontology Analysis (GO) of deregulated RNAs in *Imp* mutants reveals**
1119 **functional links to observed phenotypes. (A-B)** GO analysis was performed on the list of
1120 genes found to be significantly (Padj < 0.02) differentially expressed in both *Imp*^{8} and *Imp*^{2}
1121 mutants in the 0-4 h and 0-8 h old collections, compared to controls. The GO analysis was
1122 conducted separately for downregulated (A) and upregulated (B) genes. Cutoff for
1123 upregulated genes: log2FoldChange > 0. Cutoff for downregulated genes: log2FoldChange
1124 < 0 in 0-4 h old embryos and < -0.04 in 0-8 h old embryos. **(C)** mRNA *in situ* hybridization
1125 against *Osiris9 (Osi9)* mRNA (red), a gene expressed in the tracheal system. **(C')** Embryos
1126 immunostained for the chitin deacetylase Serpentine (Serp) protein, a marker of the tracheal
1127 lumen (Hansen et al., 2004). *Imp* mutant embryos display abnormally branched trachea and
1128 a smaller body size. Embryos were counterstained with Hoechst to visualize the nuclei.
1129
1130 **Fig. 5. Identification of RNAs present in Imp-RNP complexes**. **(A)** Venn diagram
1131 showing the overlap between the genes found enriched in *Imp*-GFP IPs compared to the
1132 mock control IPs and those found enriched in the *Imp*-GFP IPs compared to the input

1133 RNAs. A cutoff of log2FoldChange > 0 and Padj < 0.05 was used for this graph. A high
1134 degree of overlap was observed. **(B)** Heat map illustrating the top 55 differentially
1135 expressed (DE) genes with the highest absolute log2FoldChange difference between *Imp*-
1136 GFP and the mock IPs (Padj < 0.05). The heat map reveals similar expression patterns
1137 between the input and mock control IPs (*Imp-GFP*^{Stop}) compared to the *Imp*::GFP IPs. **(C)**
1138 GO enrichment analysis of *Imp*-associated RNAs. The RNAs selected as enriched using
1139 the two different controls depicted in the Venn diagram in **(A)** are shown.
1140
1141 **Fig. 6. Transposable element (TE) mRNAs and ncRNAs are upregulated in *Imp***
1142 **mutant embryos, and they also associate with Imp**. **(A)** Percentage of RNA biotypes
1143 among the genes found to be either upregulated or downregulated in both *Imp* mutants
1144 compared to control embryos. **(B)** RNAs found to be differentially expressed between *Imp*^{2}
1145 and *Imp*^{8} mutants on one side, and control embryos in the 0-4 h collections were specifically
1146 mapped to TEs. Volcano plots are shown. **(B')** Same as **(B)**, but in 0-8 h old embryos. **(C)**
1147 Percentage of RNA biotypes observed among genes found enriched in the *Imp*-GFP IP
1148 compared to the two different controls described in Fig. 5 (input and mock IP). The
1149 percentage of biotypes among RNAs not enriched in the IPs is also shown as a control.
1150 ncRNAs and TE RNAs are the most enriched RNAs in Imp-GFP pull-downs. **(D)** Volcano
1151 plot showing the RNAs pulled down with Imp-GFP specifically mapped to TEs.
1152
1153 **Fig. 7. Copia protein is upregulated in *Imp* mutant embryos and at NMJs with reduced**
1154 ***Imp* levels**. Embryos lacking maternal *Imp* (*Imp*^{7} GLCs) and wild-type embryos were
1155 subjected to immunofluorescence staining using anti-Copia antibodies (green signal). DNA
1156 stained with Hoechst is shown in blue. Stage 12 and stage 14 embryos are shown. In wild-
1157 type embryos, the Copia signal remains at background levels, similar to staining with only
1158 the secondary antibodies. In contrast, *Imp* mutant embryos show clear and specific
1159 expression of Copia in individual cells and cell clusters. **(B)** Copia protein was detected by
1160 Western blot, too. Anti-BicD was used as a loading control. Imp protein is absent in *Imp*^{7}
1161 mutants. Copia is expressed in different bands (indicated by arrows), which may represent
1162 various proteolytically cleaved fragments with a main band around 50 KDa corresponding
1163 to the Gag protein. **(C)** Control and *Imp* RNAi expressing larval NMJs stained for Horse
1164 Radish Peroxidase (HRP) and Disc Large (DLG) to trace the motor neurons and the
1165 postsynaptic machinery, respectively. Knockdown of *Imp* causes a reduction in bouton
1166 numbers. **(C')** Quantification of bouton numbers. **(D)** Knockdown of *Imp* using either the

1167 pan-neuronal driver *elav*-GAL4 or the motor neuron-specific driver *C380*-GAL4 causes a
1168 reduction in lifespan. **(E)** Representative confocal images of NMJs stained to detect Copia
1169 Gag (green), HRP (red, motoneuron marker), and Dlg (blue, postsynaptic marker) in wild-
1170 type larvae (C380-Gal4/CantonS) and upon knocking down (KD) *Imp* in the presynaptic
1171 compartment with C380-Gal4 RNAi. **(E')** *Imp* KD causes an increase of α-Copia Gag
1172 signal at larval NMJs compared to wild-type NMJs.
1173
1174 **Fig. 8. *Imp* associates with proteins involved in TE silencing.** The log2FoldChange
1175 enrichment of selected proteins, known to be involved in RNA silencing pathways, is
1176 shown for different versions of Imp-GFP proteins compared to the mock controls. The
1177 corresponding padj values of the enrichment are also depicted. **(A)** Enrichment between the
1178 peptides found in the *Imp-GFP*^{G080} IPs over the ones found in the control IPs (*Imp-GFP*^{Stop}
1179 *IP*) (left panel) or the *Imp-GFP*^{G080} IPs done in the absence and presence of RNase are
1180 shown (right panel). **(B)** Enrichments between the peptides found in the *Imp-GFP*^{G080} IPs
1181 and the KH mutant versions of Imp-GFP (Imp-GFPKH3-4 and Imp-GFPKH1-2), compared
1182 to the mock IPs (*Imp-GFP*^{Stop} *IP*), are shown. Data from A and B represent different
1183 experiments, and pull-downs were performed in biological triplicates.
1184
1185 **Fig. 9. *Imp* is required to maintain Piwi localization in the germline during oogenesis**
1186 **and for transcriptional silencing by position-effect variegation (PEV) in the soma. (A)**
1187 Piwi presence in stage 6 and 8 egg chambers was monitored by acquiring z-stack images.
1188 Piwi was localized to nurse cell nuclei in most wild-type egg chambers in two independent
1189 analyses (96.8%, n=30; 100%, n=25). In *Imp*-mutant GLCs, Piwi failed to localize in most
1190 nurse cell nuclei. Specifically, 84% of *Imp*^{8} GLCs (n=25), 70.8% of *Imp*^{2}, and 67.7% of
1191 *Imp*^{7} GLC egg chambers (n=31) that did not express *Imp* in the germline, showed nurse cell
1192 nuclei where Piwi was not enriched, indicating that *Imp* is required to maintain nuclear
1193 Piwi during these stages in the germline. In these *Imp* germline mutant egg chambers Piwi
1194 still shows normal localization to the Imp-expressing follicle cell nuclei. **(B)** Ovarioles
1195 devoid of *Imp* in the germline and wild-type ovarioles were stained for Ago1 (red) and Imp
1196 (green). Ago1 localization seems not affected in *Imp* mutant egg chambers. **(C)**
1197 Representative images of eye pigmentation observed in the indicated genetic backgrounds.
1198 The *wm4h* white line reporter in the pericentromeric X chromosome region was used. *Imp*^{7}
1199 and the *Imp*^{H44} and *Imp*^{H149} excision lines generated by mobilization of a different P-
1200 element were all defective in transcriptional silencing by PEV, similar to *piwi* mutants. **(C')**

Eye pigment quantification for the indicated genotypes was measured by absorbance at A480 nm.

Table 1.

Leading_Protein	GN	Razor + unique peptides	Sequence coverage [%]	OnOff imp2 vs yw onIn	OnOff imp8 vs yw onIn	iTop3 log2FC yw - imp2	iTop3 log2FC yw - imp8	iTop3 EB_adjpVal yw - imp2	iTop3 EB_adjpVal yw - imp8
sp|Q9VCK2|GILT3_DROME	GILT3	4	27.3	imp2	imp8	-6.9168821	-6.6131717	0.00085918	0.00122111
sp|Q9V466|NU107_DROME	Nup107	3	58.1	imp2	imp8	-6.8731124	-6.8065267	0.00016683	0.00010254
tr|Q8T3M6|Q8T3M6_DROME	l(2)k14505	2	68.1	imp2	imp8	-6.6700332	-5.0280688	0.00090922	0.04017607
tr|X2J7U0|X2J7U0_DROME	piwi	3	48.9	imp2	imp8	-6.6494654	-6.758602	9.2055E-05	0.00016165
tr|M9PFW8|M9PFW8_DROME	Apl	2	55.6	imp2	imp8	-6.3288662	-6.8998502	0.00027405	0.00016126
tr|B5RJE2|B5RJE2_DROME	CG31759-RC	2	43.1	imp2	imp8	-5.7441196	-6.7972454	0.00708043	0.01433944
tr|Q5K600|Q5K600_DROME	**env**	**9**	**24.2**	**imp2**	**imp8**	**-5.7241751**	**-6.4680114**	**0.00085918**	**0.00010254**
tr|M9ND27|M9ND27_DROME	TotM	2	22.1	imp2	imp8	-5.5483355	-5.5484832	0.00288595	0.0024462
tr|Q0PQ30|Q0PQ30_DROME	Klp61F	3	50.9	imp2	imp8	-5.3935639	-6.3955052	0.00085918	0.00028428
tr|A0A126GUZ1|A0A126GUZ1_DROME	pre-mod(mdg4)-V	2	13.4	imp2	imp8	-4.9430511	-1.4721161	0.0029427	0.12082997
tr|O01350|O01350_DROME	**gag**	**6**	**19.1**	**imp2**	**imp8**	**-4.8399795**	**-3.2956569**	**0.14913184**	**0.3246185**
tr|O96828|O96828_DROME	Psi	2	30.4	imp2	imp8	-4.6419875	-6.6219878	0.01164512	0.00061907
tr|Q7JWN2|Q7JWN2_DROME	BcDNA:RE25177	2	14.5	imp2	imp8	-4.5622276	-5.8737987	0.01151427	0.04632044
tr|Q8I7Q1|Q8I7Q1_DROME	**ORF**	**24**	**11.6**	**imp2**	**imp8**	**-4.4142745**	**-5.5475568**	**0.03106931**	**0.00286508**
tr|Q6IL18|Q6IL18_DROME	Dmel\CG43085	6	28.6	imp2	imp8	-4.258992	-4.8566626	0.01164512	0.01850379
sp|Q9VKQ6|SMG8_DROME	CG6729	8	11	imp2	imp8	-4.0986713	-3.8310926	0.00341247	0.00061907
sp|Q9VHH7|ADAL_DROME	Ada	6	24.3	imp2	imp8	-3.929745	-2.2803383	0.00116747	0.15392334
tr|A0A0B4LGA7|A0A0B4LGA7_DROME	gbb	5	16.9	imp2	imp8	-3.7389145	-4.5745524	0.13042456	0.0357959
tr|A1ZAU3|A1ZAU3_DROME	nw	8	25.5	imp2	imp8	-3.5958544	-5.1012024	0.07176396	0.0076637
tr|A9UNH6|A9UNH6_DROME	Nep6	7	19.1	imp2	imp8	-3.5424653	-2.3473998	0.01195632	0.02765291
tr|Q9VH79|Q9VH79_DROME	Rpt3R	7	45.2	imp2	imp8	-3.4398044	-3.143097	0.01920338	0.00274083
tr|Q9VA54|Q9VA54_DROME	Rpt6R	2	35.3	imp2	imp8	-3.4157029	-3.0087144	0.13576066	0.1946401
tr|Q8SYU6|Q8SYU6_DROME	NimC4	4	28.2	imp2	imp8	-3.2323438	-4.7666313	0.0576223	0.00043939
tr|Q8T3T8|Q8T3T8_DROME	ORF1	2	7.9	imp2	imp8	-3.0260626	-4.115249	0.01164512	0.00254699
tr|M9PFH0|M9PFH0_DROME	Wbp2	3	26.1	imp2	imp8	-2.8398692	-2.4870331	0.12116968	0.38773839
tr|B7Z0J4|B7Z0J4_DROME	CG9288	3	53.8	imp2	imp8	-2.6640149	-3.8887337	0.03217661	0.00254354
tr|Q9VI65|Q9VI65_DROME	Dmel\CG10068	2	11.1	imp2	imp8	-2.2847174	-1.1270004	0.29526555	0.19834486
sp|Q9VHG4|RENR_DROME	ATP6AP2	4	19.1			-2.1615219	-2.3834103	0.01290078	0.0076637
tr|Q9W0N1|Q9W0N1_DROME	hng3	5	21.3			-2.1381652	-3.3840958	0.02589408	0.02531551
sp|P91679|PEPT1_DROME	yin	12	27.2			-2.137624	-1.6661389	0.00225798	0.02452972

Table 1. **Transposable Element–Encoded Proteins Are Derepressed in *Imp* Mutants.** Top 30 up-regulated proteins in *Imp* mutant embryos. Embryos collected 0–4 hours after egg laying from wild-type (*yw*) and *Imp*-depleted backgrounds—generated using germline clones (GLCs) of the Imp^2 and *Imp8* alleles—were analyzed by mass spectrometry. The 30 proteins with the highest $\log_2$ fold change in both *Imp* mutants compared to wild-type

samples are shown. Proteins were selected based on a p-value cutoff of 0.05 or if they were exclusively detected in one condition but not the other (as indicated in the "OnOff" column, which specifies the condition in which the protein was detected). TE encoded proteins are highlighted in bold.

1218 # SUPPLEMENTARY FIGURE LEGENDS

1219

1220 **Fig. S1. Imp forms part of the BicD/Egl complex and the interaction is stabilized by**
1221 **the presence of RNA. (A-B)** Immunoprecipitation (IP) of total embryo extracts was done
1222 with the indicated antibodies. The IP material was resolved by SDS-PAGE and stained with
1223 Coomassie Blue **(A)** or analyzed by Western blot to detect the indicated proteins **(B)**. **(A)**
1224 Anti-BicD antibodies 4C2 (lane 2) and 1B11 (lane 3), which recognize different epitopes,
1225 were used for the IPs. Anti-Cdk7 antibody (unrelated control protein, lane 4) and protein G
1226 beads alone (lane 1) were used as controls for nonspecific binding. The gel area containing
1227 Pabp, Imp, BicD, and Egl is shown; the bands containing these proteins are indicated by
1228 arrowheads**. (A´)** Magnification of the gel region where Pabp and Imp were identified. **(B)**
1229 IPs performed with anti-BicD 4C2 (lanes 2 and 3), anti-BicD 1B11 (lanes 4 and 5), anti-
1230 Pabp (lane 7), beads alone (lane 8), and a control monoclonal antibody against a murine
1231 protein (lane 9). 0.15% of the cytoplasmic extract used for each IP was loaded as an input
1232 control (lanes 1 and 6). The IPs were performed in the presence (+, lanes 3 and 5) or absence
1233 (-, lanes 2, 4, 7, 8, and 9) of RNase A. These figures were partially published in (Vazquez-
1234 Pianzola et al., 2011) and are reproduced in this report since Imp was identified by mass
1235 spectrometry on the same band where Pabp was detected.

1236

1237 **Fig. S2. Structure and expression of the *Imp-GFP* genes. (A**) Sequence of the RA protein
1238 isoform predicted to be generated from the *Imp-GFP*^{G080} chromosome, and the mutant
1239 version produced via CRISPR-Cas9 mutagenesis of the same chromosome, referred to in
1240 the text as the *Imp-GFP*^{Stop} line. Both alleles were sequenced. **(B-B')** Input and IP samples
1241 were loaded, and Imp fusion proteins were detected using anti-GFP antibodies. Control
1242 extract, not expressing GFP was prepared from *yw* embryos. 1% of the input and 2.5% **(B)**
1243 and 6% **(B')** of the IP material were loaded. The fusion proteins were not detected in the
1244 input samples due to their high dilution. However, specific bands corresponding to the
1245 expected molecular weight of the fusion proteins were detected in the IP samples.
1246 The heavy and light chains of the monoclonal antibody, also recognized by the secondary
1247 anti-mouse antibody, are indicated.

1248

1249 **Fig. S3**. **Identification of *Imp*-associated proteins.** Embryo extracts from *Imp*-GFP^{G080}
1250 (expressing full-length *Imp*-GFP) and control extracts used for mock IPs - Imp-GFP^{Stop}

1251 (expressing a truncated version of Imp internally tagged with GFP) and *yw* (not expressing
1252 any GFP) - were subjected to immunoprecipitation (IP) using anti-GFP antibodies.
1253 Additionally, *Imp*-GFP^{G080} extracts were subjected to IP with anti-GFP antibodies in the
1254 presence of RNase to detect RNA-independent interactors. The IP materials were directly
1255 analyzed by bulk mass spectrometry. **(A, B)** Top enriched proteins showing the highest
1256 log2FoldChange between the *Imp*-GFP pull-downs and the control mock pull-downs. **(C)**
1257 Top enriched proteins in the *Imp*-GFP pull-downs conducted in the absence vs. presence
1258 of RNase. A cutoff of padj < 0.05 was also applied. Pull-downs were performed in
1259 biological triplicates.
1260
1261 **Fig. S4. GO analysis of Imp interactors.**
1262 Embryo extracts from *Imp-GFP^{G080}*, *Imp-GFP^{Stop}* or *yw* were subjected to
1263 immunoprecipitation (IP) using anti-GFP antibodies. Additionally, *Imp-GFP^{G080}* extracts
1264 were subjected to IP with anti-GFP antibodies in the presence of RNase to detect direct
1265 interactors. The IP materials were directly analyzed by bulk mass spectrometry. The top 30
1266 GO terms (A) and Simplified GO Terms (B-D), identify with Cluster profiler, are depicted.
1267 **(A)** GO analysis of the proteins enriched in the *Imp-GFP^{G080}* IPs compared to the mock IPs
1268 (performed with *yw* and *Imp-GFP^{Stop}* extracts). Interacting proteins were selected based on
1269 a log2Fold Change >1 or were uniquely present in the *Imp-GFP^{G080}* IPs, with a padj <0.05.
1270 **(B)** GO analysis of proteins associated with Imp via RNA (i.e., their interaction was lost in
1271 the presence of RNase). These proteins were preselected as in **(A)** but showed a reduced
1272 association with Imp in the presence of RNase. **(C)** GO analysis of proteins either enriched
1273 (log2Fold Change >1) in the *Imp-GFP^{G080}* IPs performed in the presence of RNase
1274 (compared to the one performed in the absence of RNase) or that did not show changes (no
1275 significant padj value). The proteins are also enriched (log2Fold Change >1) compared to
1276 the mock *Imp-GFP^{Stop}* IP (padj <0.05 for both). **(D)** GO analysis of proteins enriched
1277 (log2Fold Change >1) in the *Imp-GFP^{G080}* IP performed in the presence of RNase compared
1278 to the one performed in the absence of RNase. These proteins are also enriched (log2Fold
1279 Change >1) compared to the mock *Imp-GFP^{Stop}* IP (padj <0.05 for both).
1280
1281 **Fig. S5. Embryos lacking maternal *Imp* arrest in early development, exhibiting**
1282 **anterior defects and defective dorsal closure. (A)** The diagrams show the *Imp* gene
1283 structure and the alternatively spliced isoforms. Exons are depicted as boxes, introns as
1284 lines. Protein-coding exons are marked in orange. The deletions and insertions identified

1285 in the *Imp*^{2}, *Imp*^{8}, and *Imp*^{7} alleles are depicted in green, red, and blue, respectively. **(B)**
1286 Cuticle preparations of embryos devoid of maternal *Imp* (derived from *Imp*^{2}, *Imp*^{7}, or *Imp*^{8}
1287 germline clones) and *Imp*$^{+}$ controls (*yw*). **(C)** Embryos derived from *Imp*^{8} GLCs and wild-
1288 type embryos were stained with Hoechst to visualize nuclear DNA to assess embryo
1289 morphology.
1290
1291 **Fig. S6. Nuclear RNA export of piRNA precursors and production of piRNAs**
1292 **mapping to deregulated TEs are not impaired in embryos devoid of *Imp*. (A-B)** Wild-
1293 type and *Imp7* mutant ovaries generated by GLC induction were stained for Imp (green).
1294 **(A)** The ovarioles were additionally stained for Lamin (blue) and piRNA precursor
1295 transcripts from clusters 42AB (red) and 20A (white). Egg chamber stages 8 and 9 are
1296 shown for the different genotypes. **(B)** The ovaries were also stained for Lamin (red) and
1297 *flamenco* (*flam*) locus precursor RNAs. Egg chambers are shown in two different planes:
1298 one focusing on the nurse cells and oocyte to show the reduction of the Imp signal in the
1299 oocyte observed in clones devoid of Imp in the germline, and the other focusing on the
1300 follicle cells to show the presence of *Imp* mutant somatic clones marked within the yellow
1301 line. Although the precursor signals were not quantified, no visual differences were
1302 observed between the different genotypes. **(C)** Small RNAs purified from *Imp*$^{+}$ (*yw*)
1303 embryos and embryos lacking maternal Imp (by induction of *Imp8* and *Imp2* GLCs) were
1304 quantified by sequencing. The small RNAs were mapped to TE RNAs. The experiment was
1305 performed in biological triplicates. No significant difference in the amount of small RNAs
1306 mapping to TEs was observed between the mutants and the controls. The mean read counts
1307 mapping to TE sequences are shown for the different genotypes. **(D)** Mapping of piRNAs
1308 to specific TEs. The mean read counts of piRNAs mapping to different TE sequences are
1309 shown. **(E)** The Ping-Pong cycle is not clearly affected in *Imp* mutants since the percentage
1310 of sense and antisense piRNA pairs with a 10-nt overlap, relative to the total piRNA pairs,
1311 does not show a clear difference between *Imp*$^{+}$ and *Imp* mutant samples. Only piRNAs for
1312 which the sum of overlaps across all samples is 10 or more are shown.
1313
1314 **Fig. S7. Embryos lacking maternal *Imp* do not show abnormal Piwi, Hp1, or H3 lysine**
1315 **9 trimethylation staining signals.** Maternal *Imp*-depleted and *Imp*$^{+}$embryos were
1316 immunostained for Hp1 (green) and for histone H3 lysine 9 trimethylation (H3K9me3, red)
1317 **(A),** or for Piwi protein (red) **(B).** The embryos were also counterstained with Hoechst to
1318 visualize the DNA (blue).

1319

1320

1321 **Fig. S8. *Imp* loss in transcriptional silencing of different *white* reporters by position-**
1322 **effect variegation (PEV) (A)** Representative images of eye pigmentation observed in the
1323 indicated genetic backgrounds. The 118E-10 (IV) *white* reporter line in the centric
1324 heterochromatin and the 39C-12 (IV) reporter in the 4th chromosome were used. The *Imp*
1325 mutant lines, Imp^{7}, Imp^{H44}, and Imp^{H14}, as well as the *piwi* mutant, $piwi^{2}$, were tested for
1326 their capacity to silence the variegating *white* gene. Imp^{H44} and Imp^{H14} are excision lines
1327 generated by the mobilization of a different P-element than the one used to generate the
1328 Imp^{7} allele. **(B)** Eye pigment quantification for the indicated genotypes was measured by
1329 absorbance at A480 nm.
1330 None of the tested alleles showed an effect on the 4th chromosome reporter expression.
1331 Although Imp^{7} shows a significant de-repression of transcriptional silencing by PEV on the
1332 heterochromatin 118E-10 (IV) reporter compared to the *yw* and w^{118} controls, neither the
1333 other *Imp* mutant alleles nor $piwi^{2}$ showed this difference. This suggests that the defective
1334 transcriptional silencing by PEV of this particular *white* reporter could be due to a different
1335 genetic background in the Imp^{7} mutant.

Figure 1

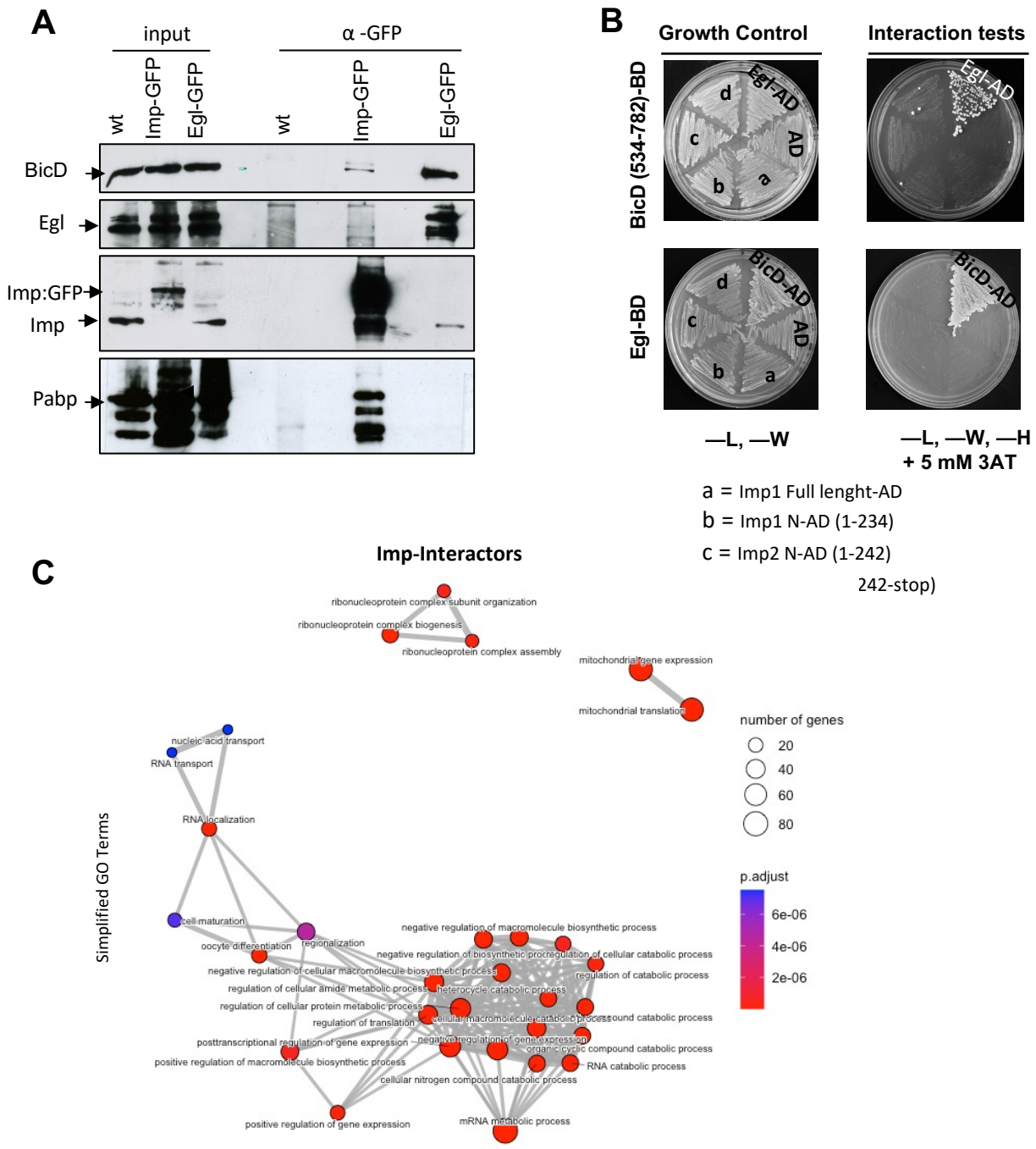
A
input
α -GFP
wt
Imp-GFP
Egl-GFP
wt
Imp-GFP
Egl-GFP
BicD
Egl
Imp:GFP
Imp
Pabp
B
Growth Control
Interaction tests
BicD (534-782)-BD
Egl-BD
Egl-AD
AD
BicD-AD
a
b
c
d
—L, —W
—L, —W, —H
+ 5 mM 3AT
a = Imp1 Full lenght-AD
b = Imp1 N-AD (1-234)
c = Imp2 N-AD (1-242)
242-stop)
C
Imp-Interactors
ribonucleoprotein complex subunit organization
ribonucleoprotein complex biogenesis
ribonucleoprotein complex assembly
mitochondrial gene expression
mitochondrial translation
nucleic acid transport
RNA transport
RNA localization
cell maturation
oocyte differentiation
regionalization
negative regulation of macromolecule biosynthetic process
negative regulation of biosynthetic process
regulation of cellular catabolic process
negative regulation of cellular macromolecule biosynthetic process
regulation of catabolic process
regulation of cellular amide metabolic process
heterocycle catabolic process
regulation of cellular protein metabolic process
regulation of translation
posttranscriptional regulation of gene expression
negative regulation of gene expression
organic cyclic compound catabolic process
positive regulation of macromolecule biosynthetic process
RNA catabolic process
cellular nitrogen compound catabolic process
positive regulation of gene expression
mRNA metabolic process
Simplified GO Terms
number of genes
20
40
60
80
p.adjust
6e-06
4e-06
2e-06
D
Imp Interactors
Proteins known to interact with BicD or involved in RNA localization
Imp-GFP^G080 IP vs Imp-GFP^Stop IP
Imp-GFP^G080 IP vs Imp-GFP^G080 (+RNase) IP
p-adj
sqd 5.6e-07
Hrb27C 5.6e-07
Imp 5.61e-07
Cbp80 2.4e-06
Fmr1 8.72e-07
pAbp 5.6e-07
egl 8.6e-06
Dhc64C 2.7e-05
polo 5.5e-06
stau 1.5e-05
EGFP 9.8e-05
BicD-RA 1.0e-03
Dlic 2.8e-04
Chc NaN
Gene Name (GN)
iLFQ log2Fold Change
p-adj
sqd 3.08e-07
Hrb27C 3.3e-07
Imp 9.2e-06
Cbp80 8.0e-07
Fmr1 7.2e-02
pAbp 4.1e-07
egl 8.7e-05
Dhc64C 2.3e-03
polo 1.9e-02
stau 7.9e-05
EGFP 2.8e-05
BicD-RA 3.6e-05
Dlic 1.0e-01
Chc 4.9e-05
Gene Name (GN)
iLFQ log2Fold Change

Figure 2

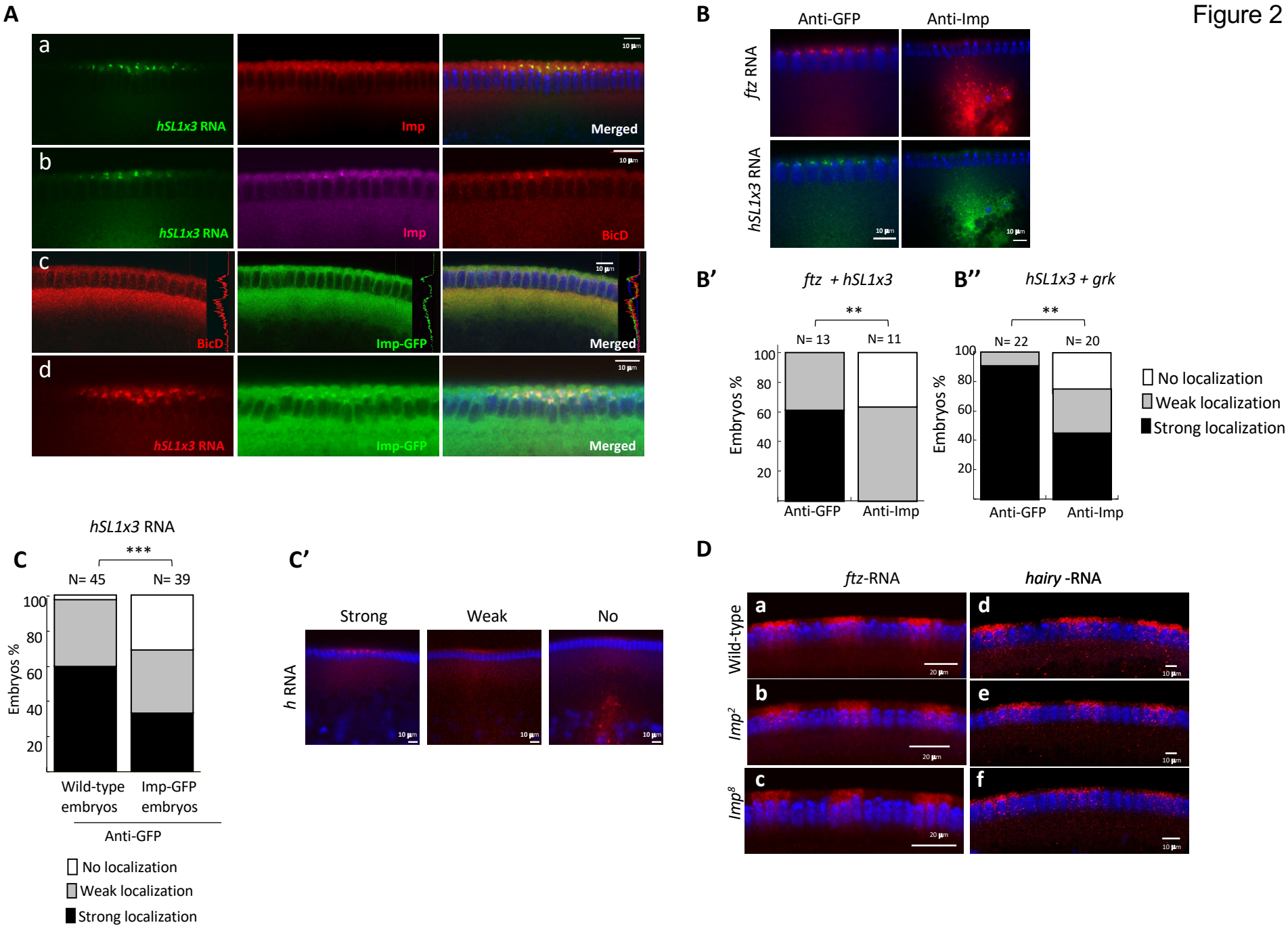
A
a
hSL1x3 RNA
Imp
Merged
b
hSL1x3 RNA
Imp
BicD
c
BicD
Imp-GFP
Merged
d
hSL1x3 RNA
Imp-GFP
Merged
B
Anti-GFP
Anti-Imp
ftz RNA
hSL1x3 RNA
B'
ftz + hSL1x3
**
N= 13
N= 11
Embryos %
Anti-GFP
Anti-Imp
B''
hSL1x3 + grk
**
N= 22
N= 20
Embryos %
Anti-GFP
Anti-Imp
No localization
Weak localization
Strong localization
C
hSL1x3 RNA
***
N= 45
N= 39
Embryos %
Wild-type embryos
Imp-GFP embryos
Anti-GFP
No localization
Weak localization
Strong localization
C'
Strong
Weak
No
h RNA
D
ftz-RNA
hairy -RNA
Wild-type
Imp2
Imp8

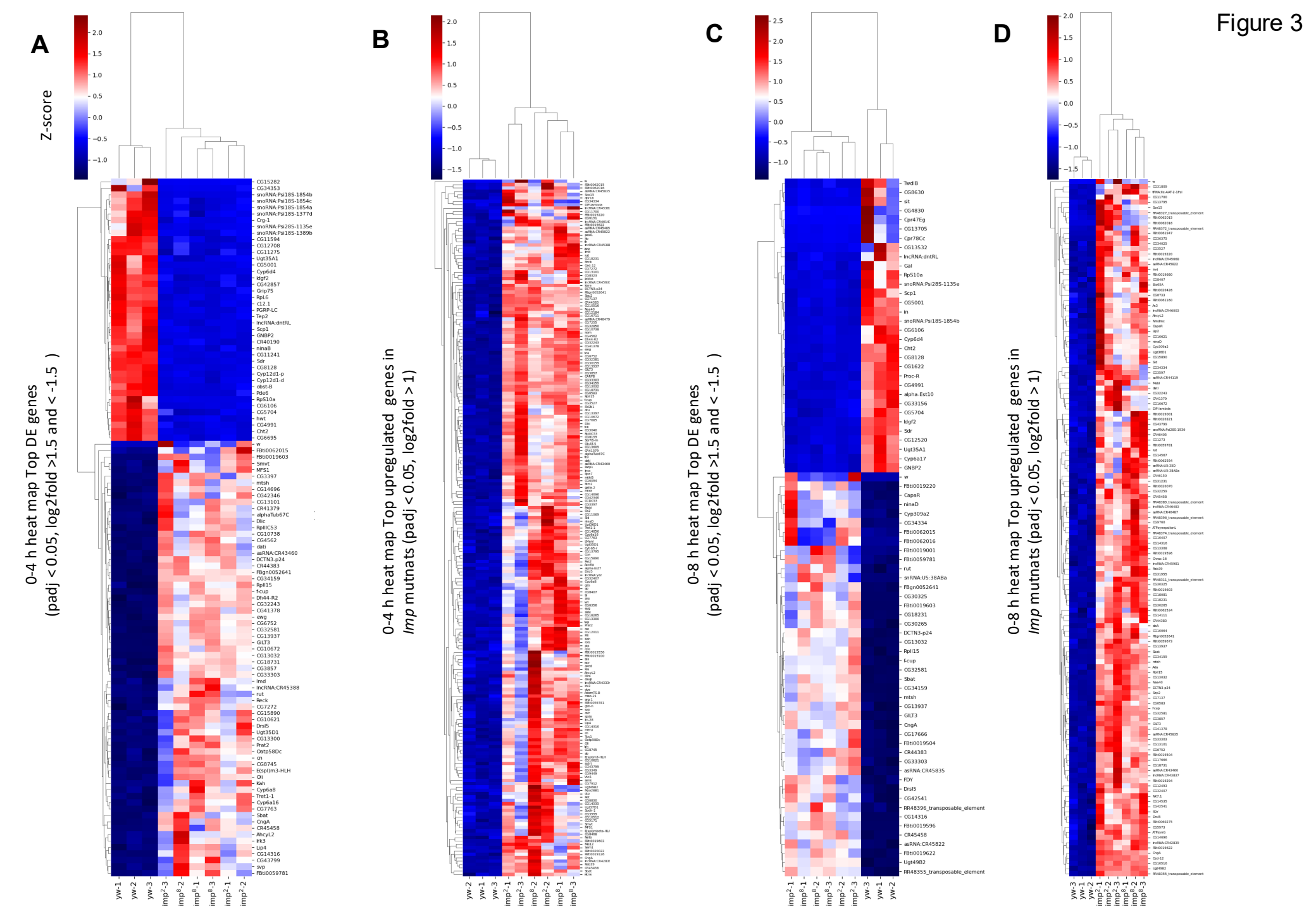
Figure 3
A
Z-score
0-4 h heat map Top DE genes
(padj < 0.05, log2fold >1.5 and < -1.5)
B
0-4 h heat map Top upregulated genes in
Imp mutnats (padj < 0.05, log2fold > 1)
C
0-8 h heat map Top DE genes
(padj < 0.05, log2fold >1.5 and < -1.5)
D
0-8 h heat map Top upregulated genes in
Imp mutnats (padj < 0.05, log2fold > 1)

Figure 4

A

Down at 0-4 h
(Repressed in the absense of *Imp*)

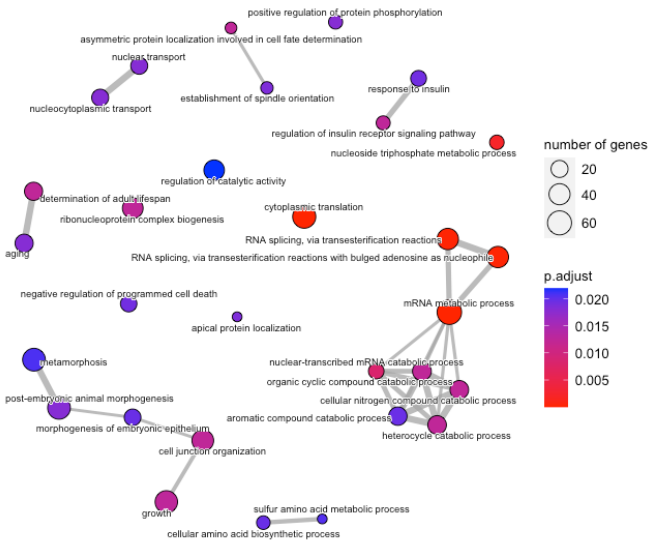

Down at 0-8 h
(Repressed in the absense of *Imp*)

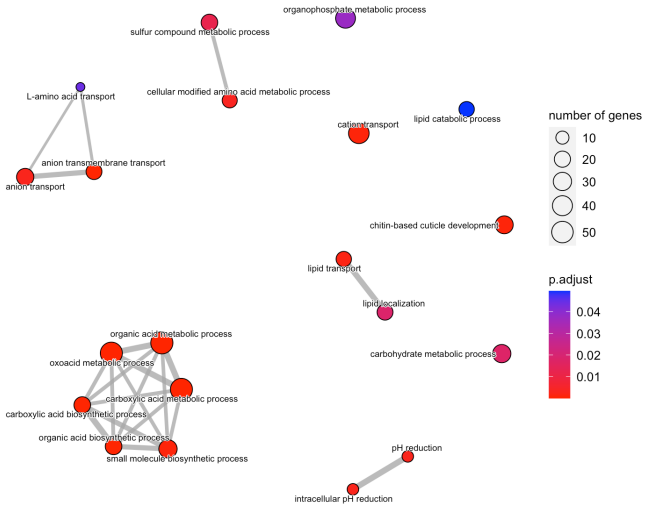

B

Up at 0-4 h
(De-repressed in the absense of *Imp*)

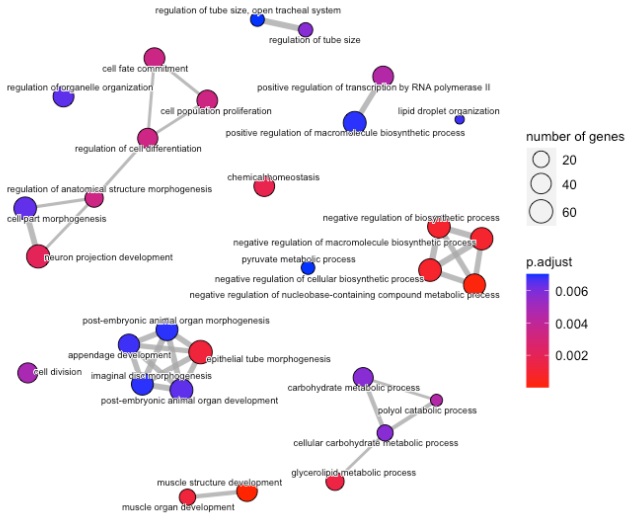

Up at 0-8 h
(De-repressed in the absense of *Imp*)

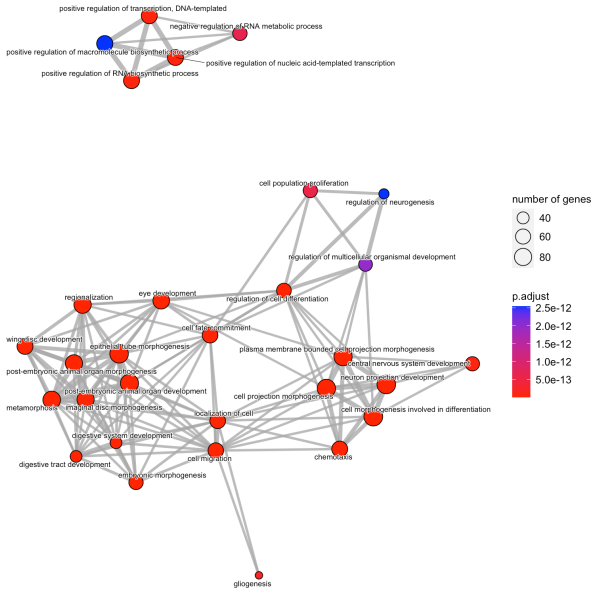

C

Osi9 mRNA DNA

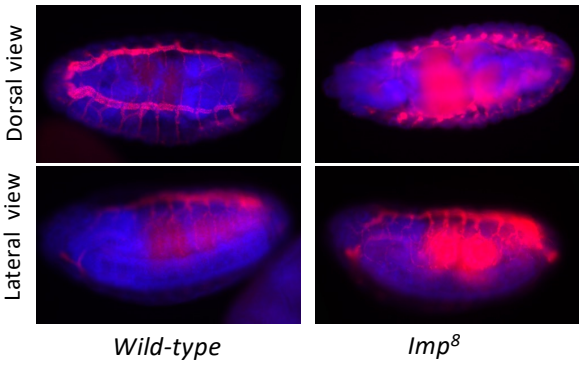

C'

Serp protein DNA

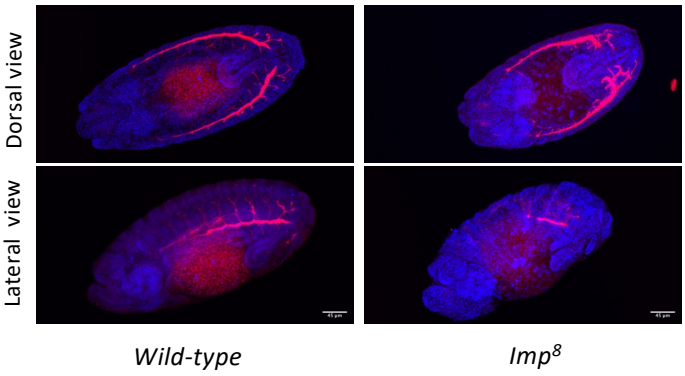

Figure 5

A

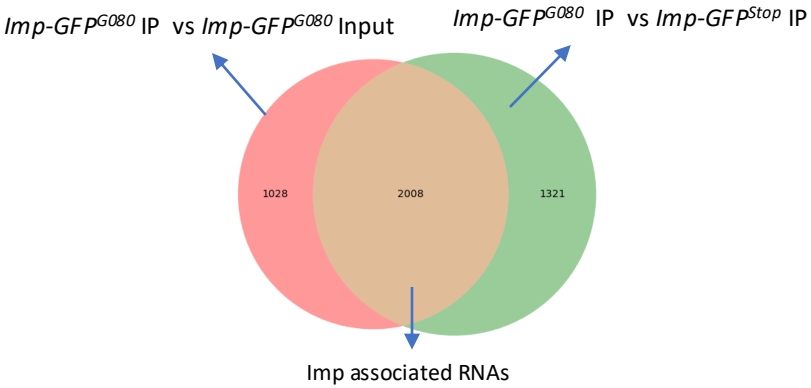
Imp-GFP^G080 IP vs Imp-GFP^G080 Input
Imp-GFP^G080 IP vs Imp-GFP^Stop IP
1028
2008
1321
Imp associated RNAs

B

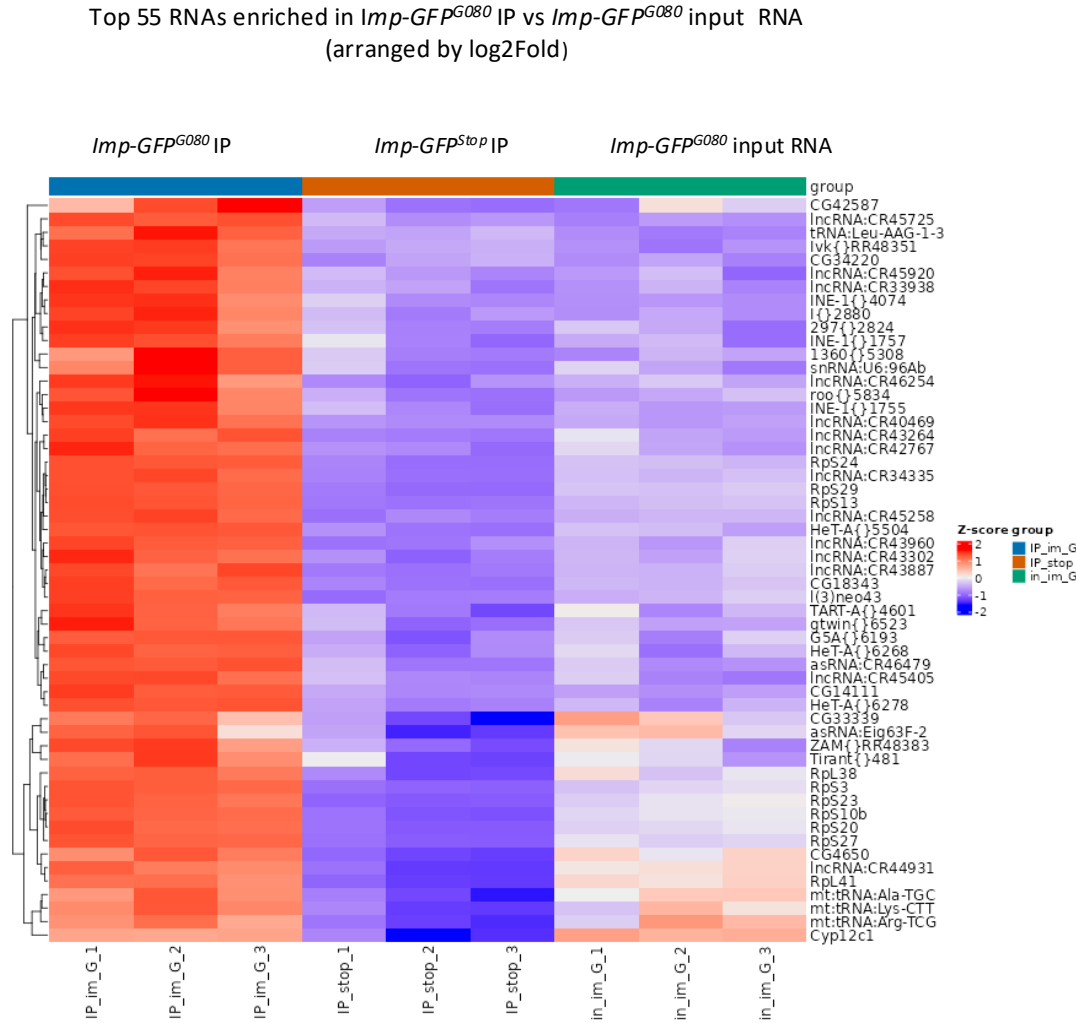
Top 55 RNAs enriched in Imp-GFP^G080 IP vs Imp-GFP^G080 input RNA
(arranged by log2Fold)
Imp-GFP^G080 IP
Imp-GFP^Stop IP
Imp-GFP^G080 input RNA
group
CG42587
lncRNA:CR45725
tRNA:Leu-AAG-1-3
lvk{}RR48351
CG34220
lncRNA:CR45920
lncRNA:CR33938
INE-1{}4074
l{}2880
297{}2824
INE-1{}1757
1360{}5308
snRNA:U6-96Ab
lncRNA:CR46254
roo{}5834
INE-1{}1755
lncRNA:CR40469
lncRNA:CR43264
lncRNA:CR42767
RpS24
lncRNA:CR34335
RpS29
RpS13
lncRNA:CR45258
HeT-A{}5504
lncRNA:CR43960
lncRNA:CR43302
lncRNA:CR43887
CG18343
l(3)neo43
TART-A{}4601
qtwin{}6523
G5A{}6193
HeT-A{}6268
asRNA:CR46479
lncRNA:CR45405
CG14111
HeT-A{}6278
CG33339
asRNA:Eig63F-2
ZAM{}RR48383
Tirant{}481
RpL38
RpS3
RpS23
RpS10b
RpS20
RpS27
CG4650
lncRNA:CR44931
RpL41
mt:tRNA:Ala-TGC
mt:tRNA:Lys-CTT
mt:tRNA:Arg-TCG
Cyp12c1
IP_im_G_1
IP_im_G_2
IP_im_G_3
IP_stop_1
IP_stop_2
IP_stop_3
in_im_G_1
in_im_G_2
in_im_G_3
Z-score
2
1
0
-1
-2
group
IP_im_G
IP_stop
in_im_G

C

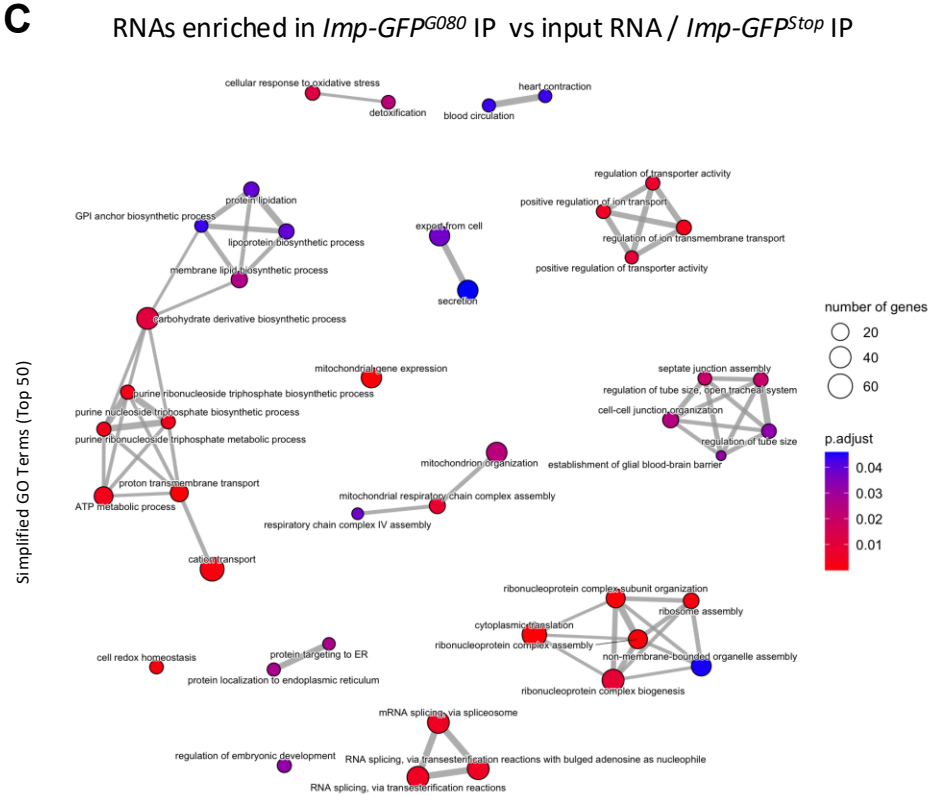
RNAs enriched in Imp-GFP^G080 IP vs input RNA / Imp-GFP^Stop IP
Simplified GO Terms (Top 50)
cellular response to oxidative stress
detoxification
heart contraction
blood circulation
protein lipidation
GPI anchor biosynthetic process
lipoprotein biosynthetic process
membrane lipid biosynthetic process
carbohydrate derivative biosynthetic process
export from cell
secretion
regulation of transporter activity
positive regulation of ion transport
regulation of ion transmembrane transport
positive regulation of transporter activity
mitochondrial gene expression
purine ribonucleoside triphosphate biosynthetic process
purine nucleoside triphosphate biosynthetic process
purine ribonucleoside triphosphate metabolic process
proton transmembrane transport
ATP metabolic process
cation transport
septate junction assembly
regulation of tube size, open tracheal system
cell-cell junction organization
regulation of tube size
establishment of glial blood-brain barrier
mitochondrion organization
mitochondrial respiratory chain complex assembly
respiratory chain complex IV assembly
ribonucleoprotein complex subunit organization
ribosome assembly
cytoplasmic translation
ribonucleoprotein complex assembly
non-membrane-bounded organelle assembly
ribonucleoprotein complex biogenesis
cell redox homeostasis
protein targeting to ER
protein localization to endoplasmic reticulum
mRNA splicing, via spliceosome
regulation of embryonic development
RNA splicing, via transesterification reactions with bulged adenosine as nucleophile
RNA splicing, via transesterification reactions
number of genes
20
40
60
p.adjust
0.04
0.03
0.02
0.01

Figure 6

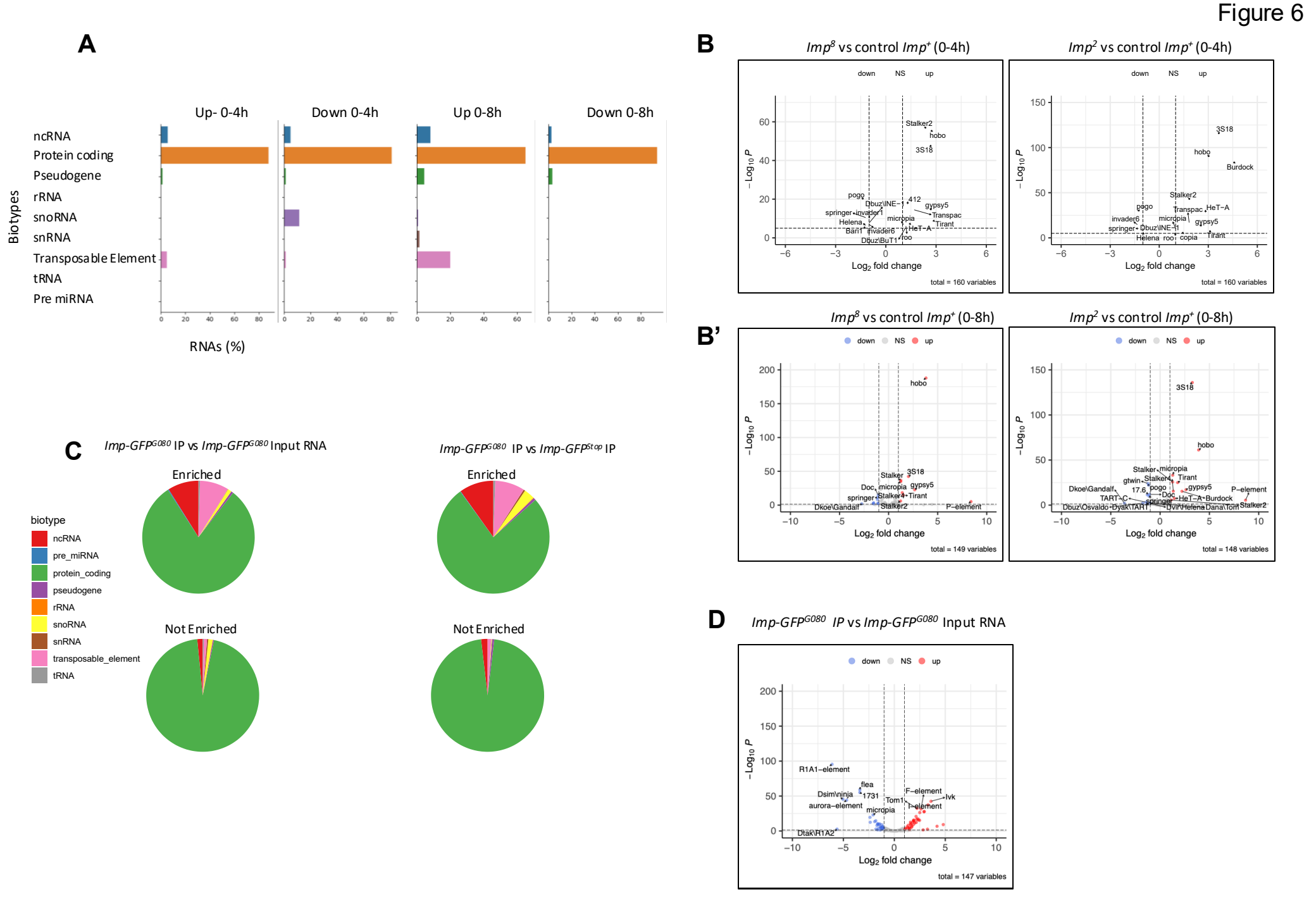
A
Up- 0-4h
Down 0-4h
Up 0-8h
Down 0-8h
Biotypes
ncRNA
Protein coding
Pseudogene
rRNA
snoRNA
snRNA
Transposable Element
tRNA
Pre miRNA
RNAs (%)
B
Imp8 vs control Imp+ (0-4h)
Imp2 vs control Imp+ (0-4h)
down
NS
up
Log2 fold change
total = 160 variables
B'
Imp8 vs control Imp+ (0-8h)
Imp2 vs control Imp+ (0-8h)
total = 149 variables
total = 148 variables
C
Imp-GFPG080 IP vs Imp-GFPG080 Input RNA
Imp-GFPG080 IP vs Imp-GFPStop IP
Enriched
Not Enriched
biotype
ncRNA
pre_miRNA
protein_coding
pseudogene
rRNA
snoRNA
snRNA
transposable_element
tRNA
D
Imp-GFPG080 IP vs Imp-GFPG080 Input RNA
total = 147 variables

Figure 7

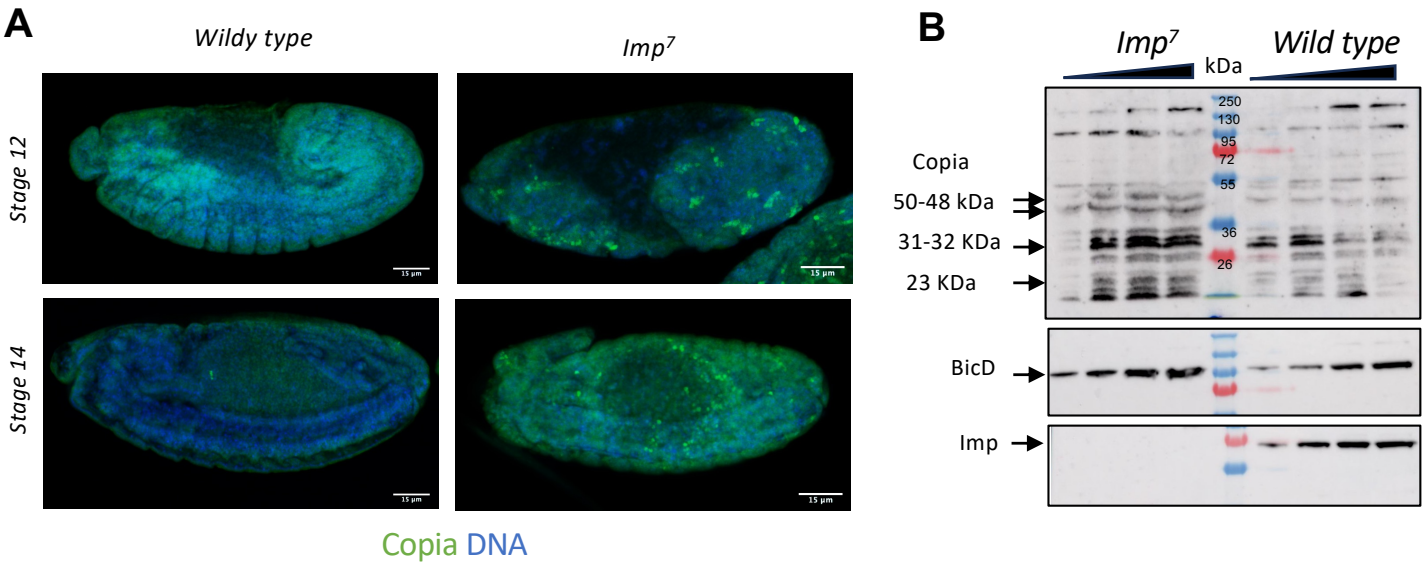
A
Wildy type
Imp7
Stage 12
Stage 14
Copia DNA
B
Imp7
Wild type
kDa
250
130
95
72
55
36
26
Copia
50-48 kDa
31-32 KDa
23 KDa
BicD
Imp

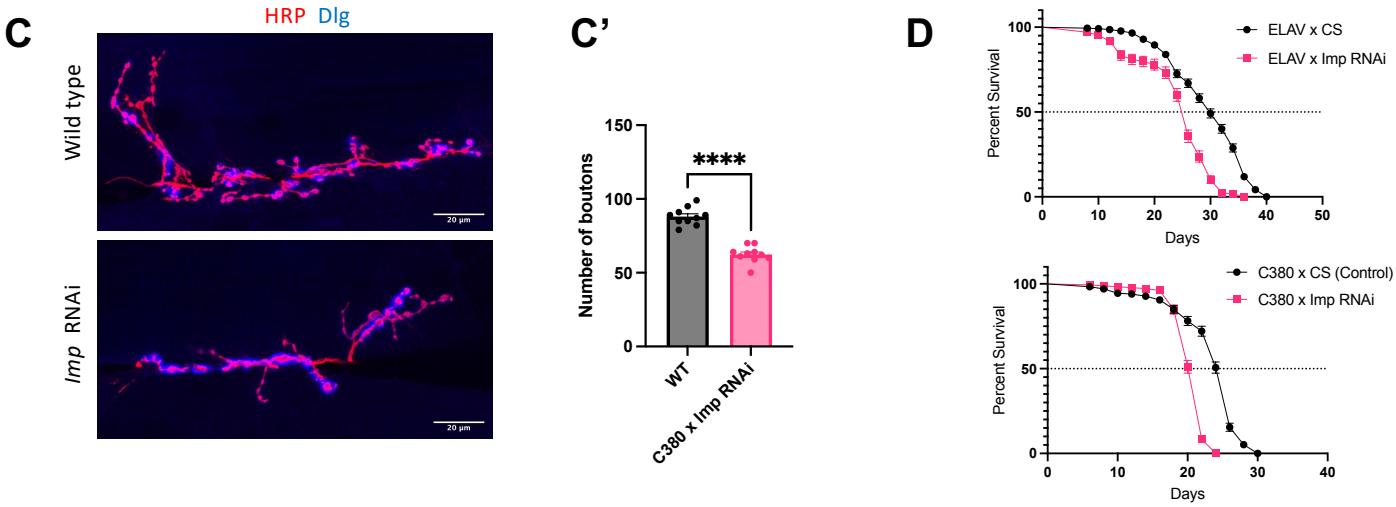
C
HRP Dlg
Wild type
Imp RNAi
C'
Number of boutons
****
WT
C380 x Imp RNAi
D
Percent Survival
Days
ELAV x CS
ELAV x Imp RNAi
C380 x CS (Control)
C380 x Imp RNAi

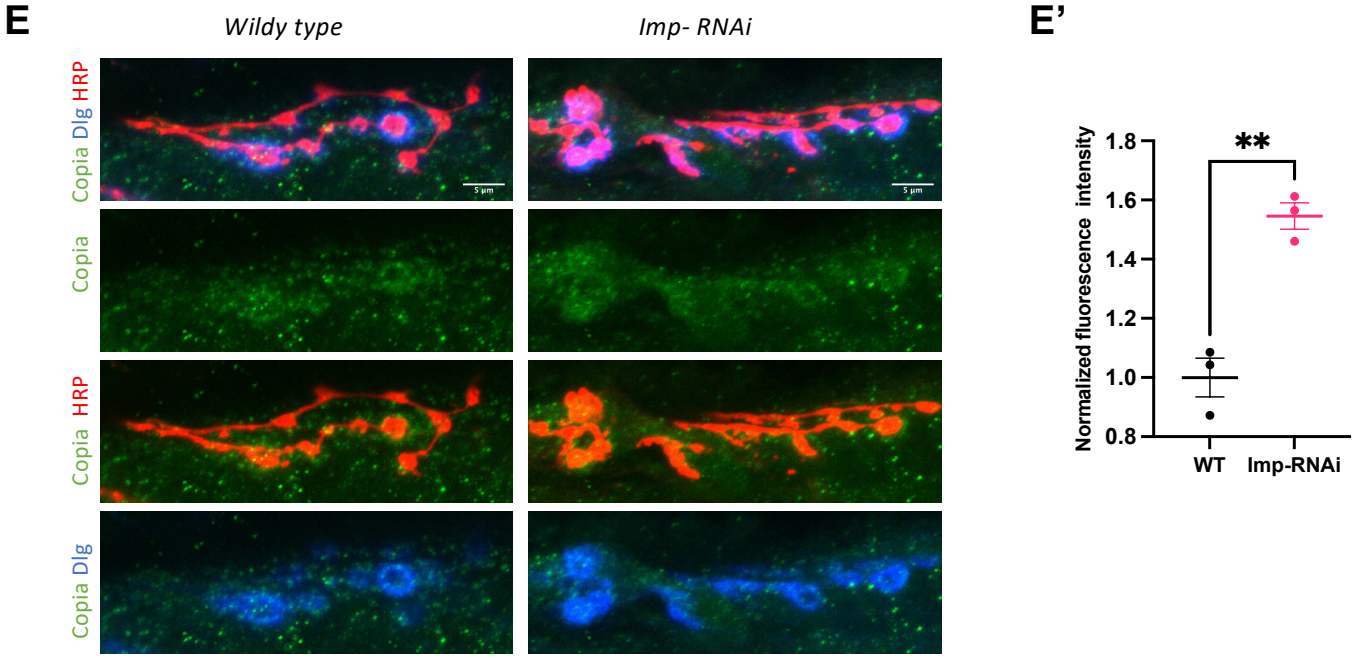
E
Wildy type
Imp- RNAi
Copia Dlg HRP
Copia
Copia HRP
Copia Dlg
E'
Normalized fluorescence intensity
**
WT
Imp-RNAi

Figure 8

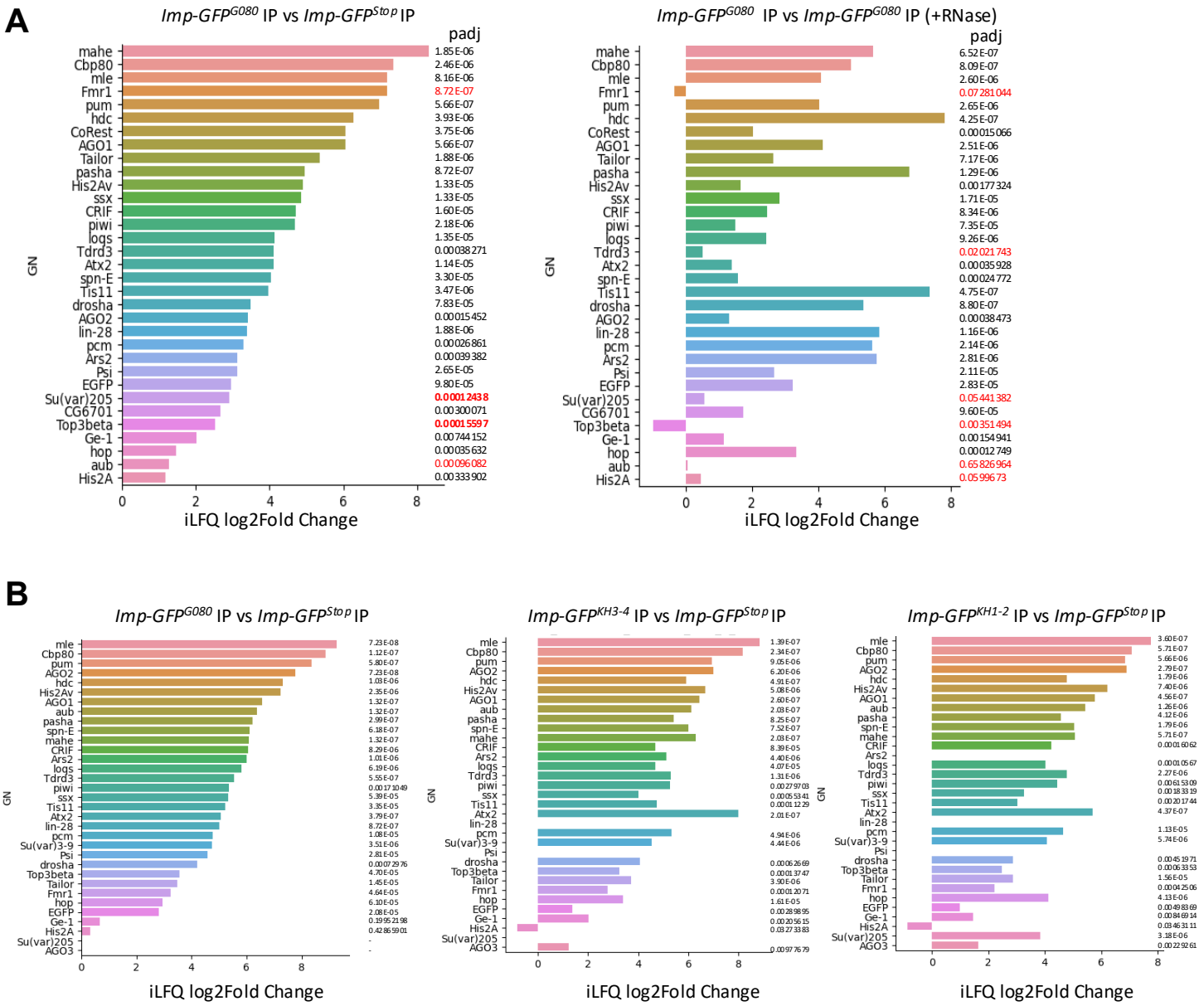
A
Imp-GFPG080 IP vs Imp-GFPStop IP
padj
mahe 1.85E-06
Cbp80 2.46E-06
mle 8.16E-06
Fmr1 8.72E-07
pum 5.66E-07
hdc 3.93E-06
CoRest 3.75E-06
AGO1 5.66E-07
Tailor 1.88E-06
pasha 8.72E-07
His2Av 1.33E-05
ssx 1.33E-05
CRIF 1.60E-05
piwi 2.18E-06
logs 1.35E-05
Tdrd3 0.00038271
Atx2 1.14E-05
spn-E 3.30E-05
Tis11 3.47E-06
drosha 7.83E-05
AGO2 0.00015452
lin-28 1.88E-06
pcm 0.00026861
Ars2 0.00039382
Psi 2.65E-05
EGFP 9.80E-05
Su(var)205 0.00012438
CG6701 0.00300071
Top3beta 0.00015597
Ge-1 0.00744152
hop 0.00035632
aub 0.00096082
His2A 0.00333902
GN
iLFQ log2Fold Change
Imp-GFPG080 IP vs Imp-GFPG080 IP (+RNase)
padj
mahe 6.52E-07
Cbp80 8.09E-07
mle 2.60E-06
Fmr1 0.07281044
pum 2.65E-06
hdc 4.25E-07
CoRest 0.00015066
AGO1 2.51E-06
Tailor 7.17E-06
pasha 1.29E-06
His2Av 0.00177324
ssx 1.71E-05
CRIF 8.34E-06
piwi 7.35E-05
logs 9.26E-06
Tdrd3 0.02021743
Atx2 0.00035928
spn-E 0.00024772
Tis11 4.75E-07
drosha 8.80E-07
AGO2 0.00038473
lin-28 1.16E-06
pcm 2.14E-06
Ars2 2.81E-06
Psi 2.11E-05
EGFP 2.83E-05
Su(var)205 0.05441382
CG6701 9.60E-05
Top3beta 0.00351494
Ge-1 0.00154941
hop 0.00012749
aub 0.65826964
His2A 0.05996 73
GN
iLFQ log2Fold Change
B
Imp-GFPG080 IP vs Imp-GFPStop IP
mle 7.23E-08
Cbp80 1.12E-07
pum 5.80E-07
AGO2 7.23E-08
hdc 1.03E-06
His2Av 2.35E-06
AGO1 1.32E-07
aub 1.32E-07
pasha 2.99E-07
spn-E 6.18E-07
mahe 1.32E-07
CRIF 8.29E-06
Ars2 1.01E-06
logs 6.19E-06
Tdrd3 5.55E-07
piwi 0.00173049
ssx 5.39E-05
Tis11 3.35E-05
Atx2 3.79E-07
lin-28 8.72E-07
pcm 1.08E-05
Su(var)3-9 3.51E-06
Psi 2.81E-05
drosha 0.00072976
Top3beta 4.70E-05
Tailor 1.45E-05
Fmr1 4.64E-05
hop 6.10E-05
EGFP 2.08E-05
Ge-1 0.19952198
His2A 0.42865901
Su(var)205 -
AGO3 -
GN
iLFQ log2Fold Change
Imp-GFPKH3-4 IP vs Imp-GFPStop IP
mle 1.39E-07
Cbp80 2.34E-07
pum 9.05E-06
AGO2 6.20E-06
hdc 4.91E-07
His2Av 5.08E-06
AGO1 2.60E-07
aub 2.03E-07
pasha 8.25E-07
spn-E 7.52E-07
mahe 2.03E-07
CRIF 8.39E-05
Ars2 4.40E-06
logs 4.07E-05
Tdrd3 1.31E-06
piwi 0.00279703
ssx 0.00055341
Tis11 0.00012229
Atx2 2.01E-07
lin-28
pcm 4.94E-06
Su(var)3-9 4.44E-06
Psi
drosha 0.00062669
Top3beta 0.00013747
Tailor 3.90E-06
Fmr1 0.00012071
hop 1.61E-05
EGFP 0.00289895
Ge-1 0.00205615
His2A 0.03273383
Su(var)205
AGO3 0.00976779
GN
iLFQ log2Fold Change
Imp-GFPKH1-2 IP vs Imp-GFPStop IP
mle 3.60E-07
Cbp80 5.71E-07
pum 5.66E-06
AGO2 2.79E-07
hdc 1.79E-06
His2Av 7.40E-06
AGO1 4.56E-07
aub 1.26E-06
pasha 4.12E-06
spn-E 1.79E-06
mahe 5.71E-07
CRIF 0.00016062
Ars2
logs 0.00010567
Tdrd3 2.27E-06
piwi 0.00615309
ssx 0.00183319
Tis11 0.00201744
Atx2 4.37E-07
lin-28
pcm 1.13E-05
Su(var)3-9 5.74E-06
Psi
drosha 0.00451971
Top3beta 0.00063353
Tailor 1.56E-05
Fmr1 0.00042506
hop 4.13E-06
EGFP 0.00493869
Ge-1 0.00846914
His2A 0.03463111
Su(var)205 3.18E-06
AGO3 0.00229261
GN
iLFQ log2Fold Change

Figure 9

A

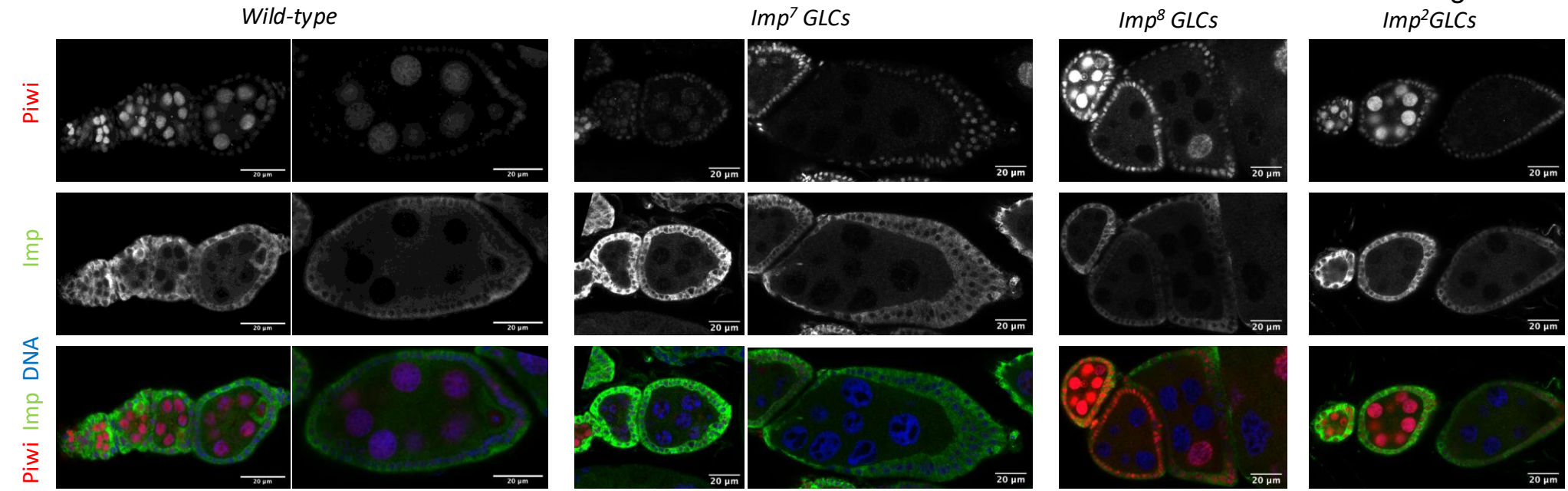

B

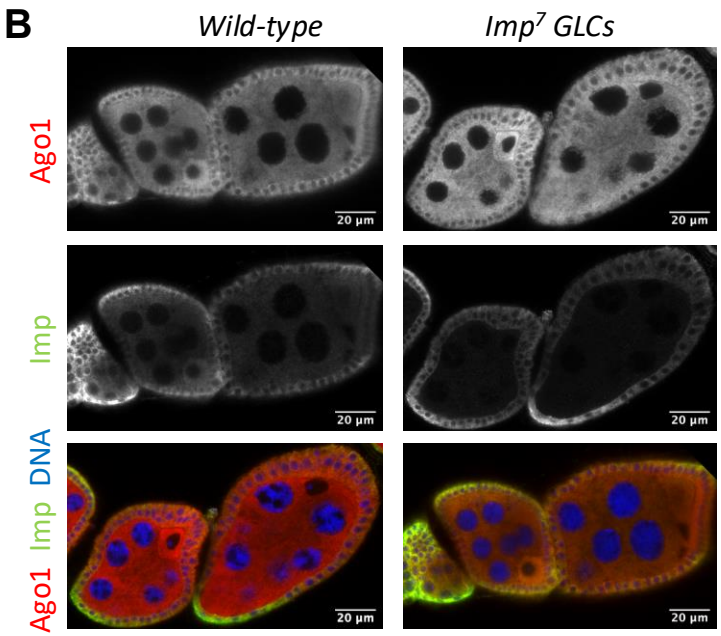

C

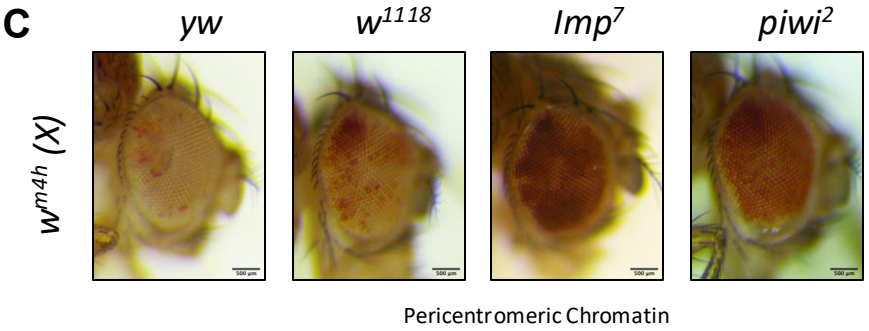

C'

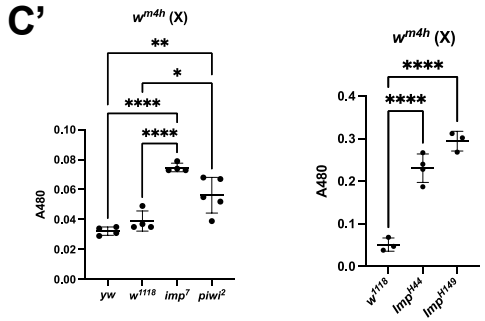

Figure S1

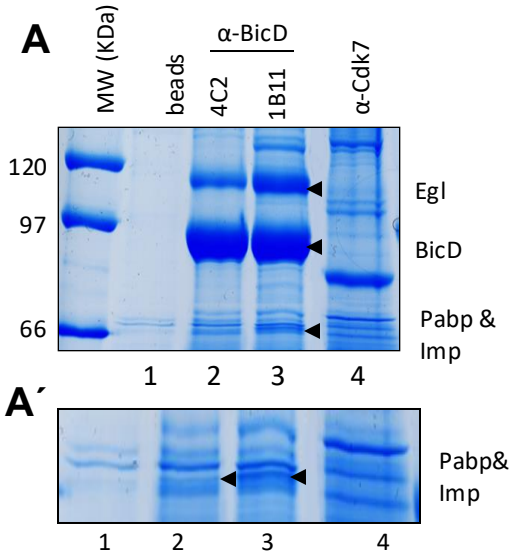
A
MW (KDa)
beads
α-BicD
4C2
1B11
α-Cdk7
120
97
66
Egl
BicD
Pabp &
Imp
1
2
3
4
A´
Pabp&
Imp
1
2
3
4

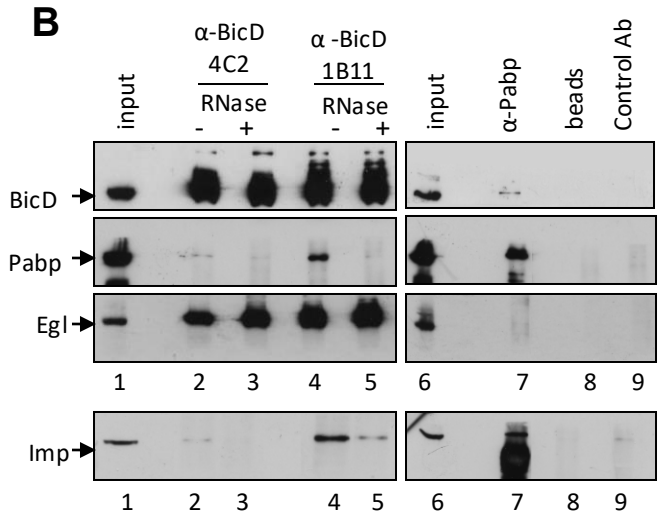
B
input
α-BicD
4C2
RNase
-
+
α -BicD
1B11
RNase
-
+
input
α-Pabp
beads
Control Ab
BicD
Pabp
Egl
Imp
1
2
3
4
5
6
7
8
9

Figure S2

A

Imp-GFP^{G080} (RA isoform)

MHSNNNSSRLNNNISNNYYQ QKQSLIRYLDR (GFP) AAVGLNGVE FEGSKLHAEQLDKNQRRSQR NQRNPYPGMPGPGRQADFPL
RILVQSEMVGAIIGRQGSTI RTITQQSRARVDVHRKENVG SLEKSITIYGNPENCTNACK GMVFNTSMPFPSCQSFAMSK TPASVVPPVFPNDLQETTYL
YIPNNAVGAIIGTRGSHIRS IMRFSNASLKIAPLDADKPL DQQTERKVTIVGTPEGQWKA QYMIFEKMREEGFMCGTDDV RLTVELLVASSQVGRIIGKG
GQNVRELQRVTGSVIKLPEH ALAPPSGGDEETPVHIIGLF YSVQSAQRRIRAMMLSTNPP PITKKQKAAKEQLQQQQQSL
AGAASSGSQQQQPQSPSQQQ ALPPQLHHQPVSSASSSSTP PAHHQQQASTAATSHQLQQQ QPSPPPPGNATAAAAQQQQQ LASSQQ*

Imp-GFP^{Stop} (RA isoform) = (Imp $^{1-31}$-GFP- Imp$^{32-95}$-Stop- XX^{18aa})

MHSNNNSSRLNNNISNNYYQ QKQSLIRYLDR(GFP)AAVGLNGVE FEGSKLHAEQLDKNQRRSQR NQRNPYPGMPGPGRQADFPL
RILVQSEMVGAIIG**Q**HHQDDHTTEPCSRRRPS*

B

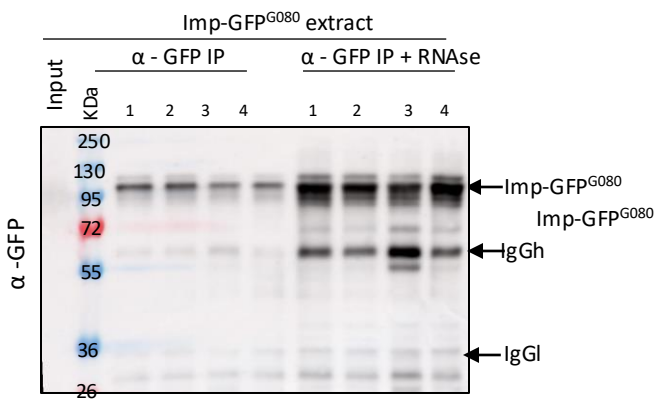

B'

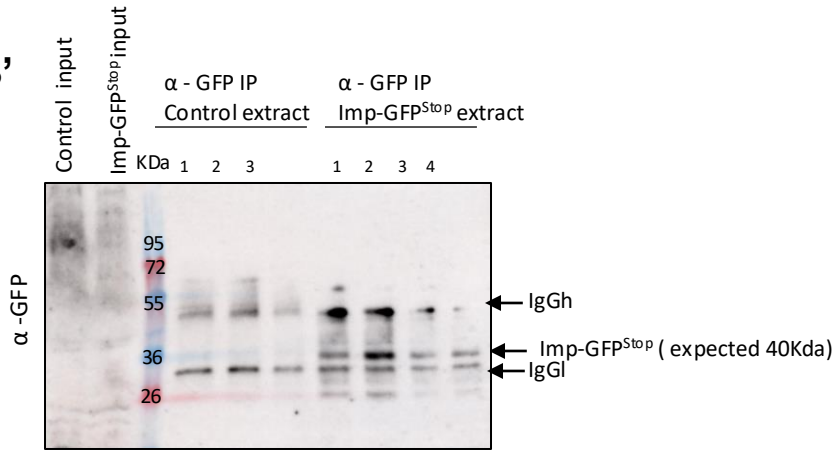

Figure S3

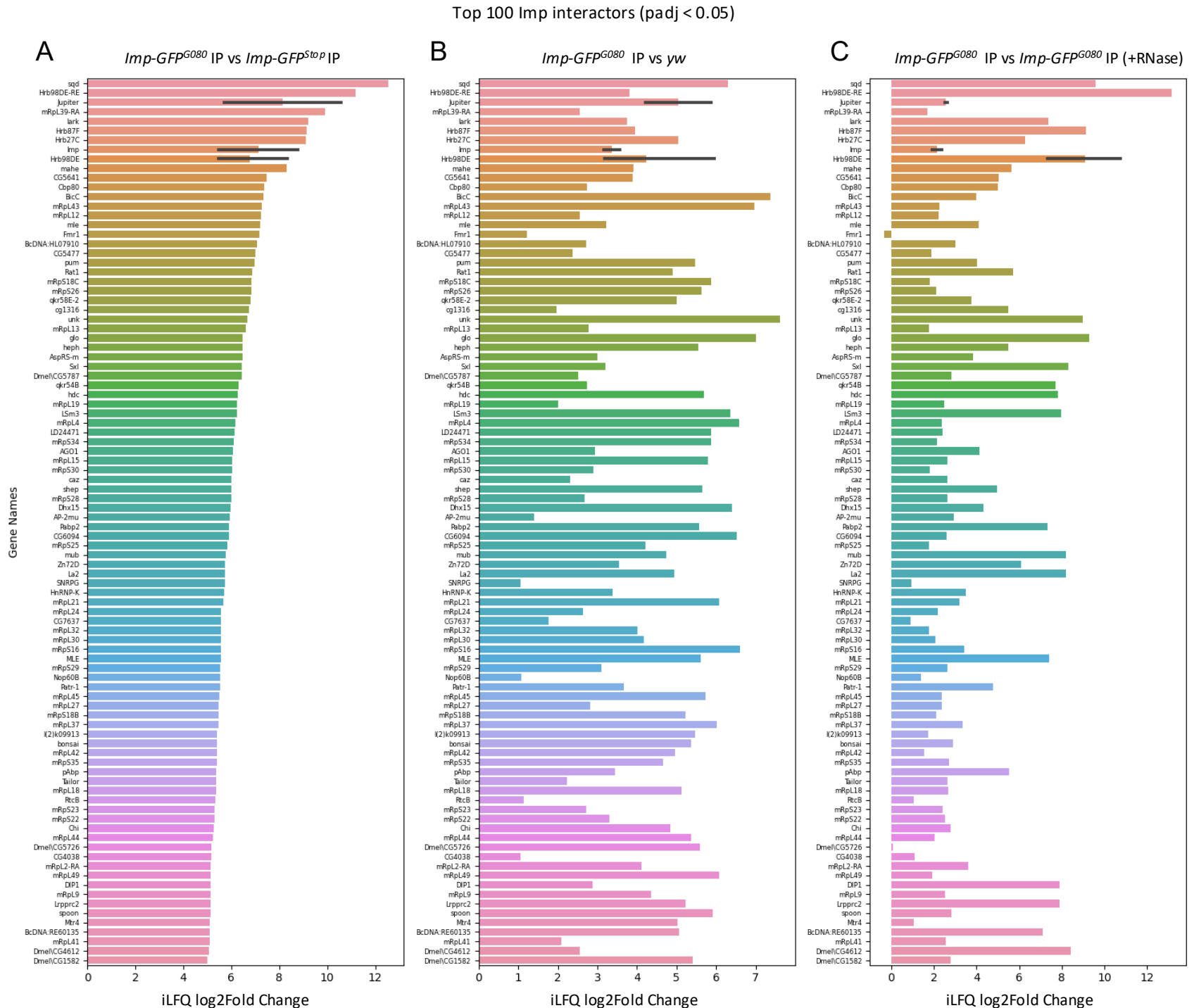
Top 100 Imp interactors (padj < 0.05)
A
Imp-GFP^G080 IP vs Imp-GFP^Stop IP
B
Imp-GFP^G080 IP vs yw
C
Imp-GFP^G080 IP vs Imp-GFP^G080 IP (+RNase)
Gene Names
iLFQ log2Fold Change
iLFQ log2Fold Change
iLFQ log2Fold Change

Figure S4

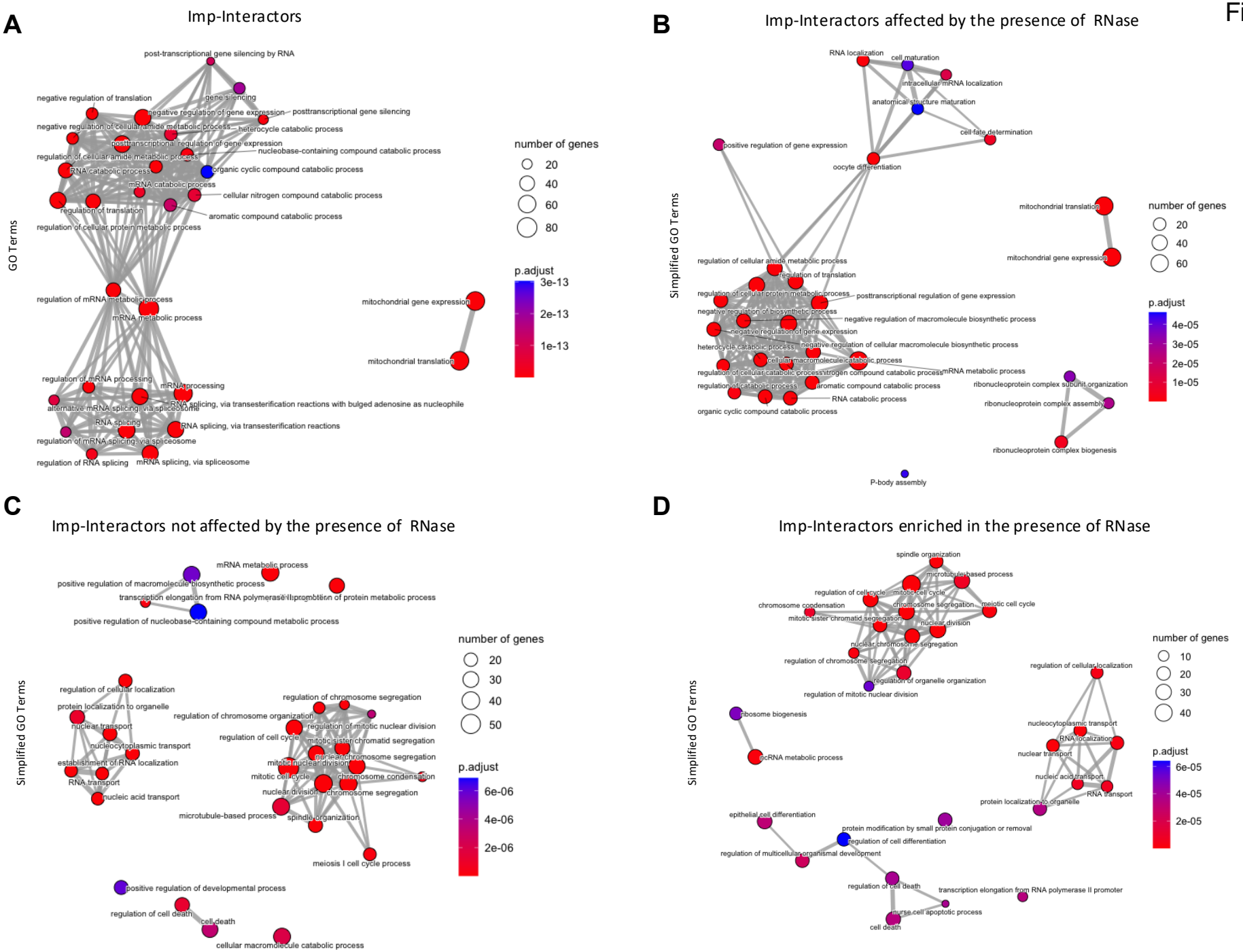
A
Imp-Interactors
GO Terms
post-transcriptional gene silencing by RNA
gene silencing
negative regulation of translation
negative regulation of gene expression
posttranscriptional gene silencing
negative regulation of cellular amide metabolic process
heterocycle catabolic process
posttranscriptional regulation of gene expression
nucleobase-containing compound catabolic process
regulation of cellular amide metabolic process
RNA catabolic process
organic cyclic compound catabolic process
mRNA catabolic process
cellular nitrogen compound catabolic process
regulation of translation
aromatic compound catabolic process
regulation of cellular protein metabolic process
regulation of mRNA metabolic process
mRNA metabolic process
mitochondrial gene expression
mitochondrial translation
regulation of mRNA processing
mRNA processing
alternative mRNA splicing, via spliceosome
RNA splicing, via transesterification reactions with bulged adenosine as nucleophile
RNA splicing
RNA splicing, via transesterification reactions
regulation of mRNA splicing, via spliceosome
regulation of RNA splicing
mRNA splicing, via spliceosome
number of genes
20
40
60
80
p.adjust
3e-13
2e-13
1e-13
B
Imp-Interactors affected by the presence of RNase
Simplified GO Terms
RNA localization
cell maturation
intracellular mRNA localization
anatomical structure maturation
cell fate determination
positive regulation of gene expression
oocyte differentiation
mitochondrial translation
mitochondrial gene expression
regulation of cellular amide metabolic process
regulation of translation
regulation of cellular protein metabolic process
posttranscriptional regulation of gene expression
negative regulation of biosynthetic process
negative regulation of macromolecule biosynthetic process
negative regulation of gene expression
heterocycle catabolic process
negative regulation of cellular macromolecule biosynthetic process
cellular macromolecule catabolic process
regulation of cellular catabolic process
nitrogen compound catabolic process
mRNA metabolic process
regulation of catabolic process
aromatic compound catabolic process
RNA catabolic process
organic cyclic compound catabolic process
ribonucleoprotein complex subunit organization
ribonucleoprotein complex assembly
ribonucleoprotein complex biogenesis
P-body assembly
number of genes
20
40
60
p.adjust
4e-05
3e-05
2e-05
1e-05
C
Imp-Interactors not affected by the presence of RNase
Simplified GO Terms
mRNA metabolic process
positive regulation of macromolecule biosynthetic process
transcription elongation from RNA polymerase II promoter
positive regulation of nucleobase-containing compound metabolic process
regulation of cellular localization
protein localization to organelle
nuclear transport
nucleocytoplasmic transport
establishment of RNA localization
RNA transport
nucleic acid transport
regulation of chromosome segregation
regulation of chromosome organization
regulation of mitotic nuclear division
regulation of cell cycle
mitotic sister chromatid segregation
nuclear chromosome segregation
mitotic nuclear division
mitotic cell cycle
chromosome condensation
nuclear division
chromosome segregation
microtubule-based process
spindle organization
meiosis I cell cycle process
positive regulation of developmental process
regulation of cell death
cell death
cellular macromolecule catabolic process
number of genes
20
30
40
50
p.adjust
6e-06
4e-06
2e-06
D
Imp-Interactors enriched in the presence of RNase
Simplified GO Terms
spindle organization
microtubulebased process
regulation of cellcycle
mitotic cell cycle
chromosome condensation
chromosome segregation
meiotic cell cycle
mitotic sister chromatid segregation
nuclear division
nuclear chromosome segregation
regulation of chromosome segregation
regulation of organelle organization
regulation of mitotic nuclear division
regulation of cellular localization
ribosome biogenesis
nucleocytoplasmic transport
RNA localization
nuclear transport
ncRNA metabolic process
nucleic acid transport
RNA transport
protein localization to organelle
epithelial cell differentiation
protein modification by small protein conjugation or removal
regulation of cell differentiation
regulation of multicellular organismal development
regulation of cell death
transcription elongation from RNA polymerase II promoter
nurse cell apoptotic process
cell death
number of genes
10
20
30
40
p.adjust
6e-05
4e-05
2e-05

Figure S5

A

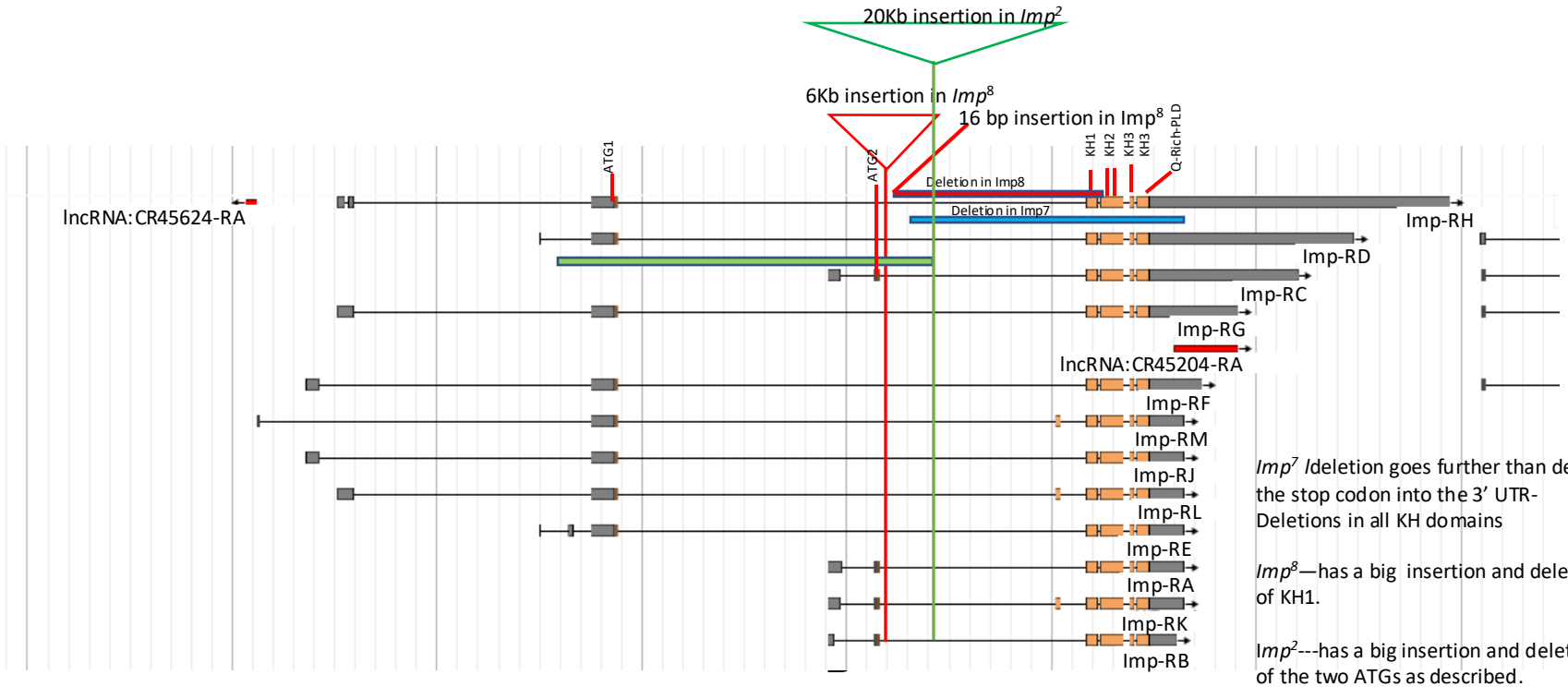

Imp^7 *I*deletion goes further than described after the stop codon into the 3' UTR-Deletions in all KH domains

Imp^8—has a big insertion and deletion of KH1.

Imp^2---has a big insertion and deletions of the two ATGs as described.

B

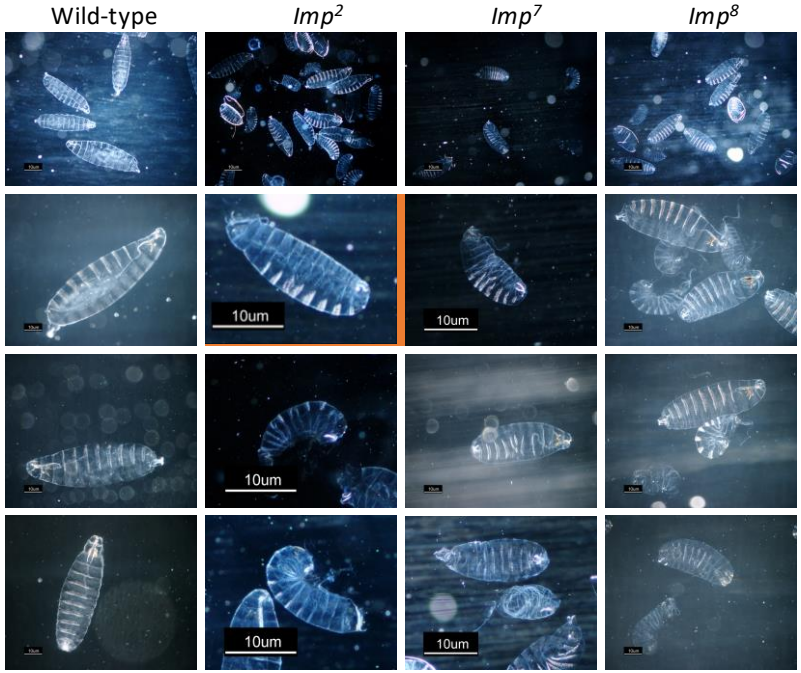

C

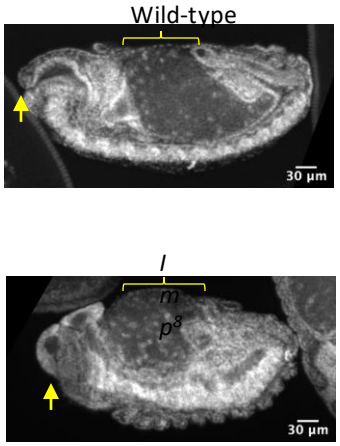

Figure S6

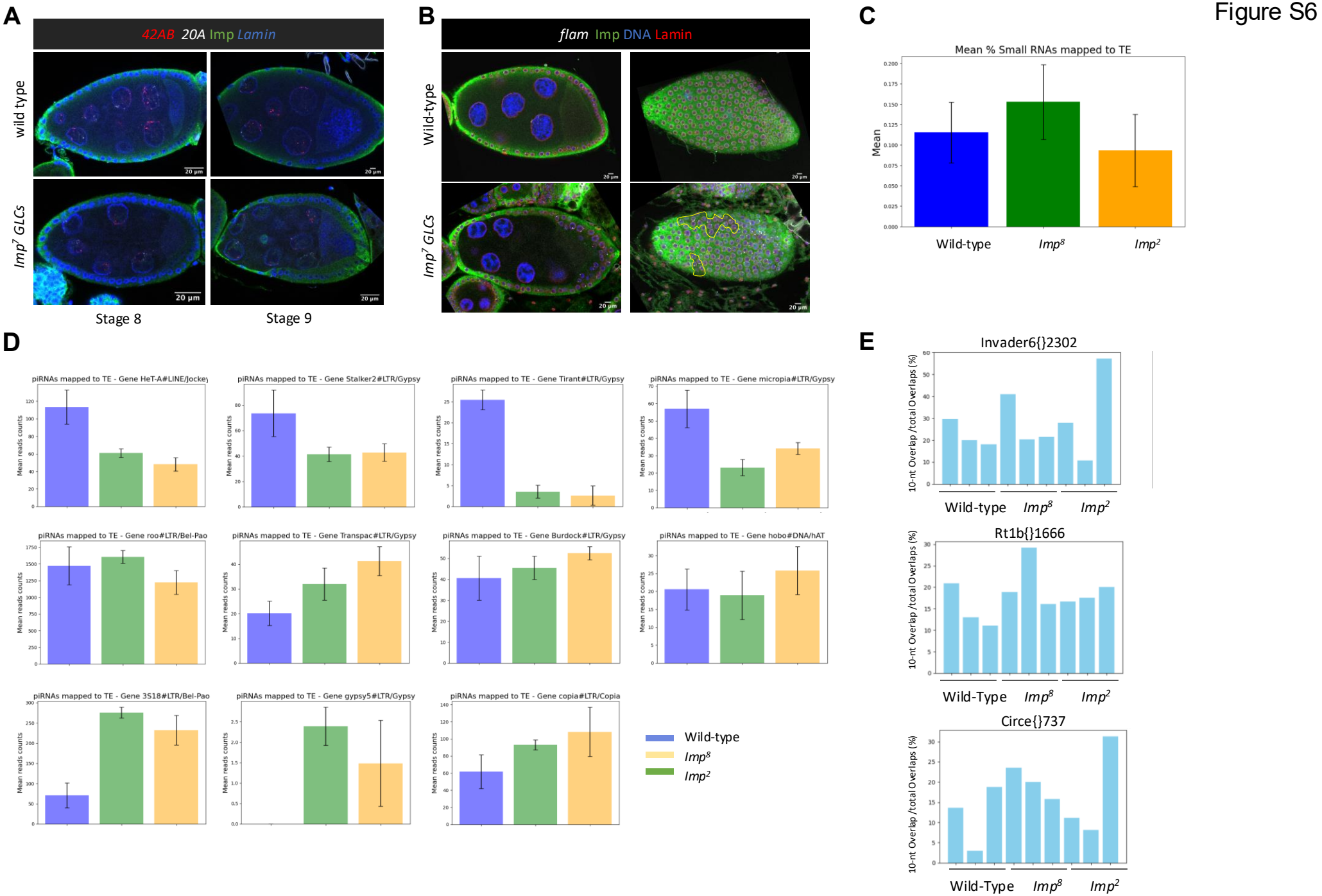
A
42AB 20A Imp Lamin
wild type
Imp7 GLCs
20 µm
Stage 8
Stage 9
B
flam Imp DNA Lamin
Wild-type
Imp7 GLCs
20 µm
C
Mean % Small RNAs mapped to TE
Mean
Wild-type
Imp8
Imp2
D
piRNAs mapped to TE - Gene HeT-A#LINE/Jockey
piRNAs mapped to TE - Gene Stalker2#LTR/Gypsy
piRNAs mapped to TE - Gene Tirant#LTR/Gypsy
piRNAs mapped to TE - Gene micropia#LTR/Gypsy
piRNAs mapped to TE - Gene roo#LTR/Bel-Pao
piRNAs mapped to TE - Gene Transpac#LTR/Gypsy
piRNAs mapped to TE - Gene Burdock#LTR/Gypsy
piRNAs mapped to TE - Gene hobo#DNA/hAT
piRNAs mapped to TE - Gene 3S18#LTR/Bel-Pao
piRNAs mapped to TE - Gene gypsy5#LTR/Gypsy
piRNAs mapped to TE - Gene copia#LTR/Copia
Mean reads counts
Wild-type
Imp8
Imp2
E
Invader6{}2302
Rt1b{}1666
Circe{}737
10-nt Overlap /total Overlaps (%)
Wild-type
Wild-Type
Imp8
Imp2

Figure S7

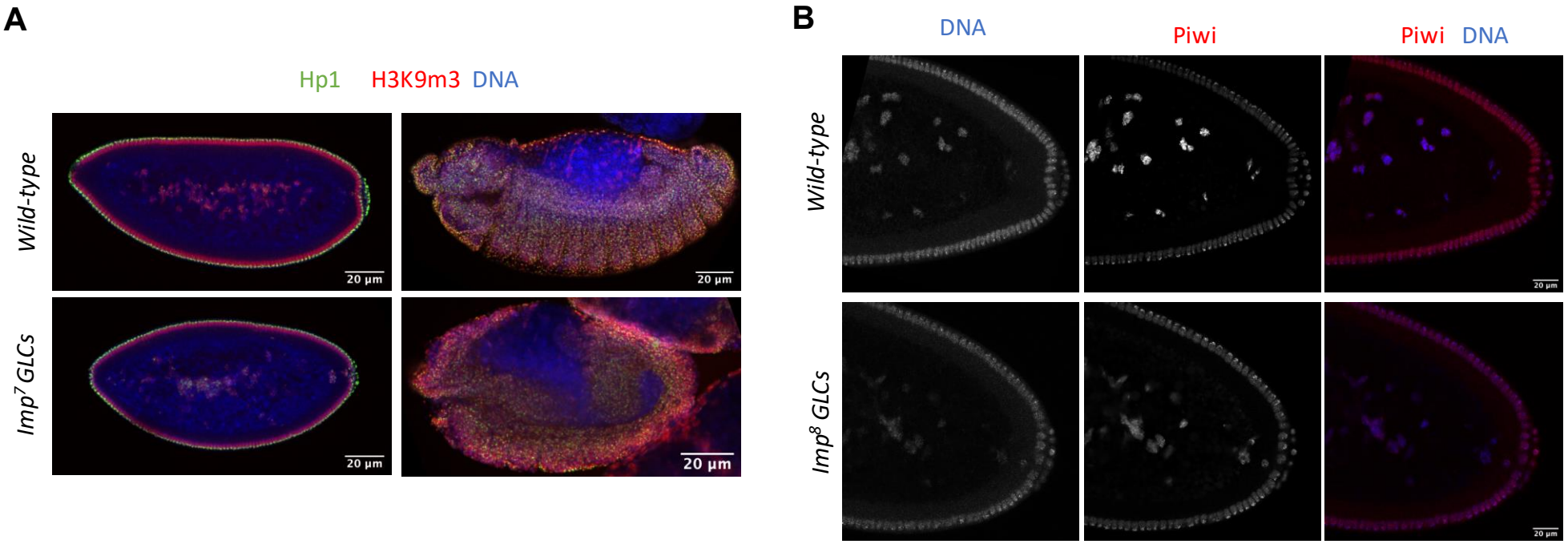
A
Hp1
H3K9m3
DNA
Wild-type
Imp7 GLCs
20 µm
B
DNA
Piwi
Piwi DNA
Wild-type
Imp8 GLCs

Figure S8

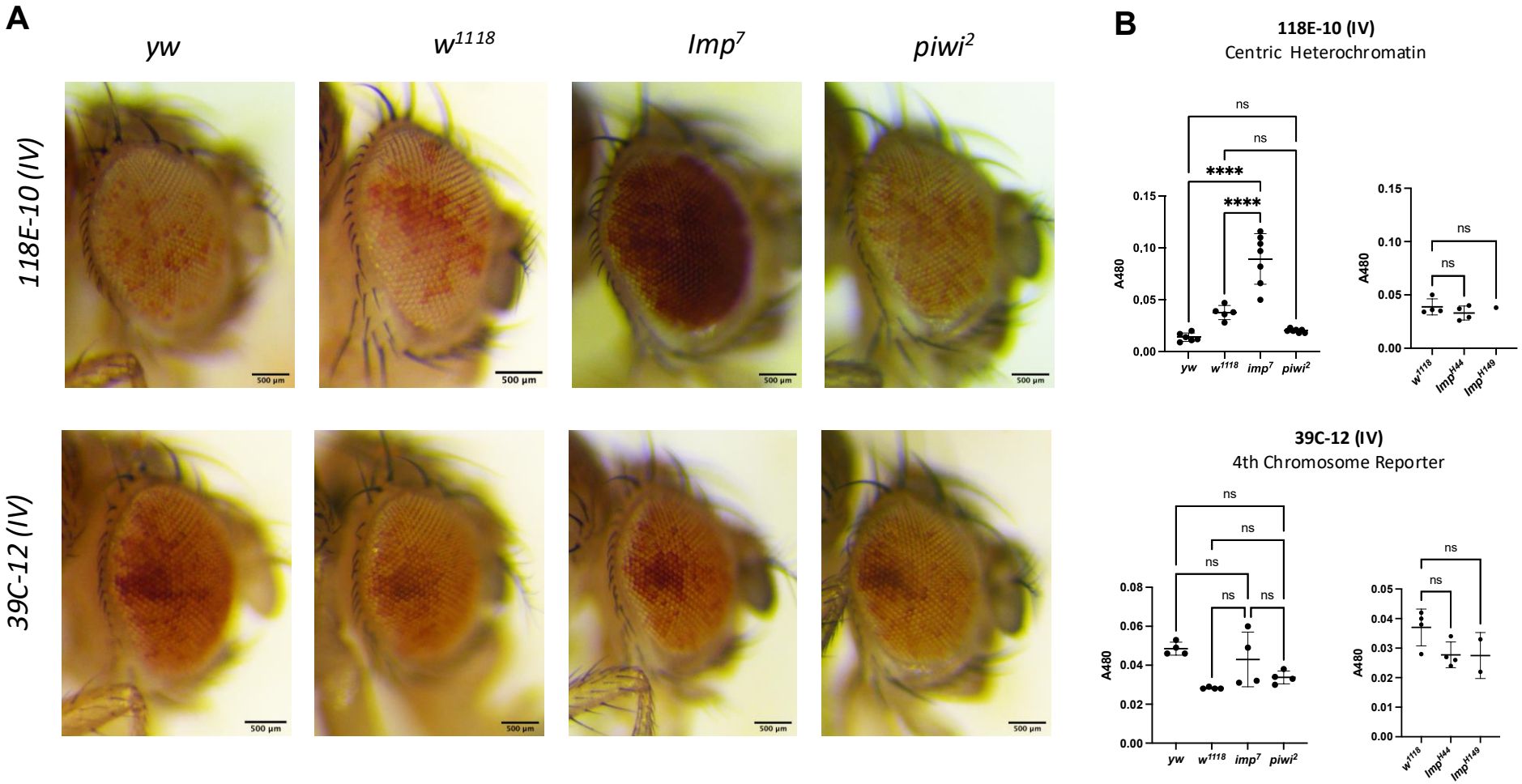
A
yw
w1118
Imp7
piwi2
118E-10 (IV)
39C-12 (IV)
500 µm
B
118E-10 (IV)
Centric Heterochromatin
ns
****
A480
0.15
0.10
0.05
0.00
yw
w1118
imp7
piwi2
Imp H44
Imp H149
39C-12 (IV)
4th Chromosome Reporter
0.08
0.06
0.04
0.02
0.01
0.03